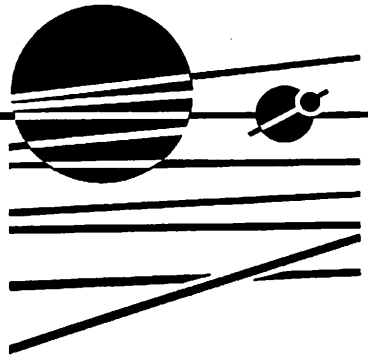

Lunar and Planetary Laboratory
Department of Planetary Sciences

Chiricahua Mountains

Planetary Geology Field Practicum
PTYS 594a
May 2-4, 2003

The University of Arizona
Tucson, Arizona

Editor's note

I don't have too much to say, since I did not plan this trip. However, I would like to say thanks to the authors who contributed to this booklet for converting your handouts into PDF format for me. It helped me greatly in assembling the final product. Thank you also for limiting your handouts in length so it was economical to have them printed by someone other than me.

I hope that the electronic copy of this book will be handy for people in the future, which will make the trouble of assembling everything in electronic form worthwhile, despite the added time it took me to work through Adobe Acrobat's painfully unintuitive interface. Please feel free to let me know what you think or to offer suggestions for improving the field guides in the future, both in terms of form and efficiency for everyone involved. For this semester, I'm pleased with how things went. Enjoy!

Sincerely,

Curtis S. Cooper, ed.

Contents

PTYS 594a,

PLANETARY FIELD GEOLOGY PRACTICUM

Itinerary, Willcox Playa and Chiricahua Mountains 2 May-4 May 2003

H. J. Melosh, 935 Gould/Simpson, 621-2806

We will assemble at 7:30 am on Friday, 2 May from the LPL loading dock off Warren Street. in two vans and two pickup trucks. Try to be at LPL by 7:30 am to get the vans and pickups loaded. Please be sure that you have had breakfast beforehand, have ice for the coolers, etc. before we are scheduled to leave: Breakfast and ice runs just before departure have caused long delays in the past!

Our approximate itinerary is:

Friday, 2 May:

8:00 am	Distribute handouts, Depart LPL, turn right on Second St. to Campbell. Make a right and proceed South via Kino to I-10. Turn East on I-10 toward El Paso.
9:30 am	Stop at rest stop in Texas Canyon where **Mandy Proctor** will inform us about Spheroidal Weathering. **Jason Barnes** will introduce us to the granitic rocks of Southeastern Arizona.
10:00 am	Continue East on I-10 to Rte 191. Exit and drive South to railroad crossing of Willcox Playa. ***CHECK THAT PLAYA SURFACE IS DRY***! If dry, proceed onto playa.
11:00 pm	Don hats and sunscreen. **Janie Radebaugh** will tell us about the shorelines of ancient Lake Cochise. **Dave O'Brien** will discuss the age of the playa and estimate the probability of finding meteorites here. **Dante Lauretta**, recent veteran of the Antarctic Meteorite Collection team will collaborate with veteran Arizona Meteorite Hunter **David Kring** to lead us on a Playa Meteorite Hunt using metal detectors and geological common sense. This expedition will include lunch and an excursion across the playa. **Fred Ciesla** will chime in occasionally on the importance of chondrites and give us a longer dissertation on Robotic Searches for Meteorites as we trudge wearily back to the vans. During this time **Gareth Collins** will demonstrate the use of a Gravimeter. As we proceed, he will instruct small groups of students in how to make a gravimeter measurement.
3:30 pm	After documenting the numerous new meteorites we expect to find, return to the vehicles and return to I-10. Proceed East. Drive to Willcox, then take exit to Rte 186 and drive South toward the Chiricahua National Monument.
4:15 pm	Exit at Kansas Settlement Road and proceed south for 3 miles, stop at the clay dune outcrop on the E shore of Lake Willcox. **Joe Spitale** will describe the planetary significance of these humble features.
4:45 pm	Return to Rte 186 and proceed South. Stop at the Dos Cabezas Dike. **Pete Lanagan** will describe the use of a Magnetometer and show the distinctive signature of the dike by this method.
6:00 pm	Depart Dos Cabezas Dike and proceed South on Rte 186. We will make several stops for gravity measurements along the road.
7:00 pm	Make camp at the Group Campground at the Chiricahua National Monument.

Saturday, 3 May:

7:30 am Break Camp, drive up the monument road toward the Echo Canyon overlook. Stop at Organ Pipe rocks, where **Terry Hurford** will acquaint us with the reason for all the magnificent holes apparent in the rocks, after which **John Keller** will give us a personal introduction to some of the agents of this destruction: lichens and endolithic organisms.

9:00 am Arrive at the Echo Canyon overlook. From this magnificent viewpoint, **Ross Beyers** and **Abby Sheffer** will discuss the mechanics of Ash Flow Tuffs and the geology of the Turkey Creek Caldera that produced them. Peter **Lanagan** will discuss the mechanics of silicic volcanism and **Brandon Preblich** will tell us where all those cracks in the rock came from.

12:00 noon Lunch at the Sugarloaf overlook. After lunch, **Jonathan Fortney** will acquaint us with a new use for all these rock columns: Paleoseismology! **Carl Hergenrother** will then describe the the Great Sonoran Earthquake of 1887.

2:00 pm Leave the Sugarloaf overlook and return to the Monument Headquarters. Approximately 1 mile past the ranger station, turn South on Pinery Canyon Road. Proceed to the summit at Onion Saddle. Continue SE on FR 42. This is a good dirt road that winds along the rim of the Turkey Creek Caldera. **Abby Sheffer** will describe the geologic history of this feature as we proceed downward past Paradise to Portal, AZ. Continue East to NM Rte 80, turn North, then again East on NM Rte 9 to Animas, NM. In Animas, proceed North on Nm Rte 38. This road crosses the bed and Eastern shorelines of glacial Lake Animas, where **Rachel Mastrapa** will tell us about the history of the lake.

4:00 pm Continue North to I-10, drive East to Lordsburg, NM where we will take the first exit and proceed to NM Rte 70. Drive NW on Rte 70 to Duncan, AZ, where we will continue NW on Rte 75 to the intersection with Rte 78. Turn East on Rte 78 and proceed up the Mogollon Rim toward Mule Creek. We will stop briefly at the overlook near the summit, but then proceed to our camp site in the Gila National Forest.

6:00 pm Make Camp in the Gila National Forest. **Carl Hergenrother** will guide us in the contemplation of the heavens in this high and, hopefully, clear spot.

Sunday, 4 May:

8:00 am Break camp, return West on Rte 78, and stop at the overlook near the summit. **Mike Bland** and **Gwen Bart** will describe the forces that led to this grand escarpment and **Matt Pasek** will describe the enormous Mogollon Volcanic field just to the East of us.

9:00 am Continue down Rte 78 to its junction with Rte 75 and Rte 191. Proceed North on Rte 191 to the overlook of the Great Pit of the Morenci-Clifton copper mine.

10:30 am **Celinda Kelsey** will tell us why this pit is of economic value and of how such Porphry Copper deposits are related to silicic volcanism.

11:00 am Leave the Morenci-Clifton mine and return South on Rte 191. Continue to the intersection with Rte. 78 and turn West through Safford. Exit on Rte. 366 and climb the flank of the Pinaleno Mountain range. We plan to stop near Turkey Flat, where **John Weirich** will describe Basin and Range extension and detachment faulting. This will be our lunch stop

1:00 pm Return to Safford and drive NW on Rte 70 to Globe. Just short of Globe turn South on Rte 77 and proceed toward Winkleman.

3:30 pm Stop at mile marker 153 to observe the El Capitan landslide. **Jim Richardson** will guide us in our study of this enormous rockfall.

4:15 pm Continue South on Rte 77 Mammoth. Here we will divert onto River Road, on the East side of the San Pedro valley and drive about 8 miles South to a Diatomite deposit (and fossil locality), where **Curtis Cooper** will describe the story that lies hidden in these apparently lifeless rocks.

5:00 pm Return to Mammoth on River road, then proceed South on Rte 77 to Oracle Road in Tucson

6:00 pm Return to LPL, unpack, clean vans, go home.

Primary Drivers: Barnes, Lanagan, Fortney, Beyers

Student Participants:

R. Beyers
G. Bart
F. Ciesla
J. Fortney
T. Hurford
C. Kelsey
M. Mastrapa
M. Pasek
M. Procter
J. Richardson
J. Spitale
B. Yanites
J. Barnes
M. Bland
C. Cooper
C. Hergenrother
J. Keller
P. Lanagan
D. O'Brien
B. Preblish
J. Radebaugh
A. Sheffer
J. Weirich

Faculty Participants:

G. Collins
D. Lauretta
A. Showman
D. Kring
J. Melosh

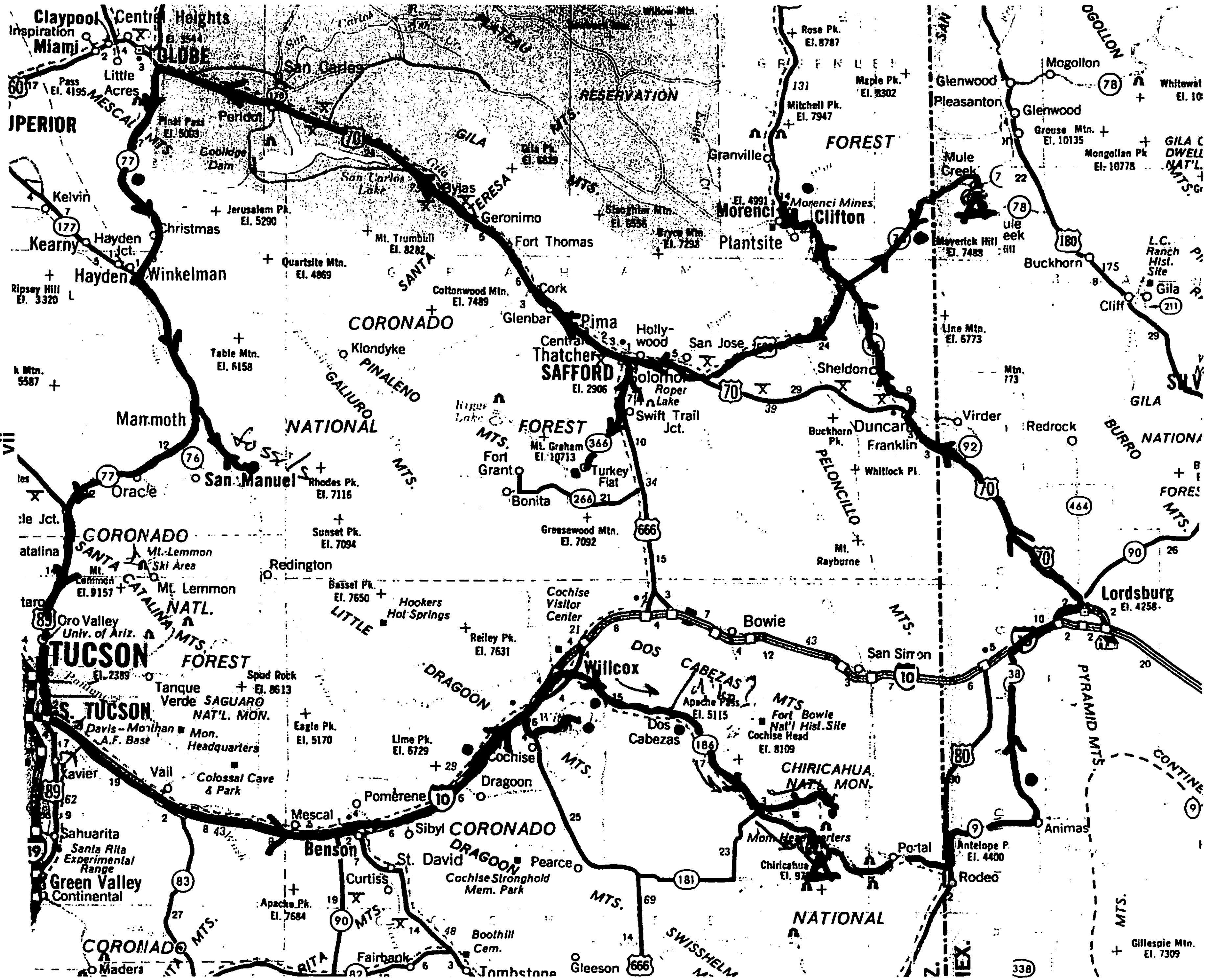
Claypool
Inspiration
Miami
Central Heights
GLOBE
Little Acres
SUPERIOR
Pass El. 4195
MESCAL MTS.
Kelvin
Kearny
Hayden Jct.
Hayden
Winkelman
Christmas
Ripsey Hill El. 3320
Peridot
Coolidge Dam
San Carlos
San Carlos Lake
RESERVATION
GILA MTS.
Bylas
SANTA TERESA MTS.
Geronimo
Fort Thomas
Jerusalem Pk. El. 5290
Mt. Trumbull El. 8282
Quartsite Mtn. El. 4869
Cottonwood Mtn. El. 7489
Cork
Glenbar
Pima
Central
Thatcher
SAFFORD
El. 2906
Hollywood
San Jose
Solomon
Roper Lake
Swift Trail Jct.
Table Mtn. El. 6158
CORONADO
Klondyke
GALIURO
PINALENO
NATIONAL
FOREST
MTS.
Mt. Graham El. 10713
Fort Grant
Turkey Flat
Bonita
Greasewood Mtn. El. 7092
Mammoth
San Manuel
Rhodes Pk. El. 7116
Oracle
Sunset Pk. El. 7094
Redington
CORONADO
Mt. Lemmon Ski Area
Mt. Lemmon
SANTA CATALINA MTS.
NATL.
FOREST
Oro Valley
Univ. of Ariz.
TUCSON
El. 2389
S. TUCSON
Davis-Monthan A.F. Base
Tanque Verde
SAGUARO NAT'L. MON.
Mon. Headquarters
Spud Rock El. 8613
Bassel Pk. El. 7650
LITTLE
Hookers Hot Springs
Reiley Pk. El. 7631
Eagle Pk. El. 5170
Lime Pk. El. 6729
DRAGOON
Cochise Visitor Center
Willcox
DOS CABEZAS MTS.
Apache Pass El. 5115
Dos Cabezas
Fort Bowie Nat'l Hist. Site
Cochise Head El. 8109
CHIRICAHUA NAT'L. MON.
Cochise
Dragoon
Pomerene
Mescal
Benson
Sibyl
CORONADO
St. David
DRAGOON
Pearce
Cochise Stronghold Mem. Park
Vail
Colossal Cave & Park
Xavier
Sahuarita
Santa Rita Experimental Range
Green Valley
Continental
Curtiss
Apache Pk. El. 7684
Fairbank
Boothill Cem.
Tombstone
CORONADO
Madera
Gleeson
SWISSHELM
NATIONAL
Chiricahua
Portal
Antelope P. El. 4400
Rodeo
Animas
Bowie
San Simon
Lordsburg
El. 4258
PYRAMID MTS.
CONTINE
Gillespie Mtn. El. 7309
PELONCILLO
Mt. Rayburne
Buckhorn Pk.
Duncan
Franklin
Whitlock Pl.
Sheldon
Morenci
El. 4991
Morenci Mines
Clifton
Plantsite
Granville
Rose Pk. El. 8787
Maple Pk. El. 8302
Mitchell Pk. El. 7947
FOREST
GREENLEE
GRAHAM
Slaughter Mtn. El. 6556
Bryce Mtn. El. 7298
Line Mtn. El. 6773
Virder
Redrock
Maverick Hill El. 7488
Mule Creek
Glenwood
Pleasanton
Mogollon
MOGOLLON
Whitewat
Grouse Mtn. El. 10135
Mongollon Pk El. 10778
GILA CLIFF DWELL NAT'L.
Buckhorn
L.C. Ranch Hist. Site
Cliff
Gila
GILA
BURRO
NATIONAL
FORES
MTS.
IEX.
Z.

Era	Period	Epoch	Millions of years ago
Cenozoic	Quaternary	Holocene	0.01
		Pleistocene	1.8
	Tertiary	Pliocene	5.3
		Miocene	23.8
		Oligocene	33.7
		Eocene	54.8
		Paleocene	65.0
Mesozoic		Cretaceous	144
		Jurassic	206
		Triassic	248
Paleozoic		Permian	290
	Carboniferous	Pennsylvanian	323
		Mississippian	354
		Devonian	417
		Silurian	443
		Ordovician	490
		Cambrian	540
Proterozoic			2500
Archean			3800
Hadean			4500

Eon	Era	Millions of years ago
Phanerozoic	Cenozoic	65
	Mesozoic	248
	Paleozoic	540
Proterozoic	Late	900
	Middle	1600
	Early	2500
Archean	Late	3000
	Middle	3400
	Early	3800
Hadean		4500
Precambrian		

By Don Thieme,
Notes for
Physical Geology

Measuring the Gravity of the Situation

Gareth Collins and Pete Lanagan

Gravity Surveying

The gravitational acceleration over the surface of a planet is not constant. It varies from place to place because of differences in altitude, distance away from the axis of rotation (latitude), Earth tides and the density of the underlying rock. *Gravity surveying* is based on the idea that, if the strength of gravity can be measured accurately enough, and if all other effects can be corrected for, a map of sub-surface density variations can be determined.

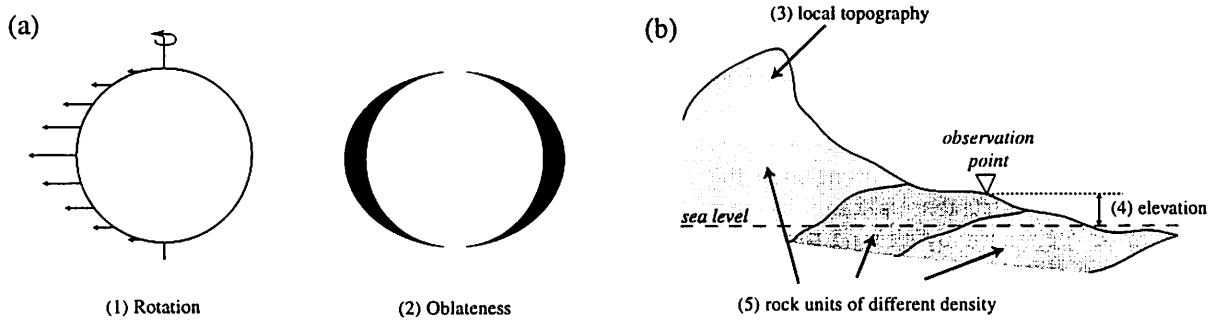

Figure 1: Factors that influence the gravitational field strength at a point on the surface of a planet - (a) global factors; (b) local factors.

The central concept in gravity surveying is the idea of a causative body, which is a sub-surface rock unit with differing density to its surroundings. Examples might be an impact crater, a salt dome, an igneous intrusion, a buried river valley, the root of a mountain range, or, on a smaller scale, a buried mine, ore deposit, or natural cavity. A causative body represents a sub-surface zone of anomalous mass and causes a localized perturbation in the gravitational field strength, called a *gravity anomaly*. Accurately determining the shape and magnitude of a gravity anomaly may be used to constrain the extent and nature of a causative body.

Measuring Gravity

Measuring acceleration sounds simple enough; however, the accuracy required for gravity surveying makes matters quite complicated. Variations in gravity caused by local density variations are less than one part in 10^5 of Earth's mean gravitational acceleration (that's ~100 μm^{-2} compared with 9.8 ms^{-2}). In fact, an accuracy of one part in 10^8 is sometimes desired. Consequently, terrestrial gravity anomalies are measured in *gravity units* (gu; 1 gu = 1 $\mu m/s^2$), or the cgs equivalent, *milligals* (named after Galileo; 1 mgal = 10^{-3} cm/s^2 = 10 gu). To measure an absolute value of gravity to this accuracy requires complex apparatus and a lengthy period of observation (a fascinating subject in its own right, see Nettleton (1976)). Thus, in gravity surveying we generally measure *relative* changes in gravity.

Measurements of the vertical component of gravity are made in the field using a *gravimeter* (or *gravity meter*). Gravimeters are, basically, spring balances carrying a constant mass. Variations in the weight of the mass are caused by variations in gravitational acceleration. Hooke's law can be used to relate these variations in gravity to varying extensions in the spring, provided the stiffness of the spring is known. The problem is that the extension in the spring must be known to within one part in 10^8! This issue is overcome in modern instruments by employing an additional force that amplifies the extension in the spring (see figure 2) and by using "zero-length" springs, which are very expensive pre-tensioned springs that have the peculiar property that the restoring force is proportional to the length of the spring, not the extension. Thus, a portable instrument can be fashioned with a very sensitive response over a wide range.

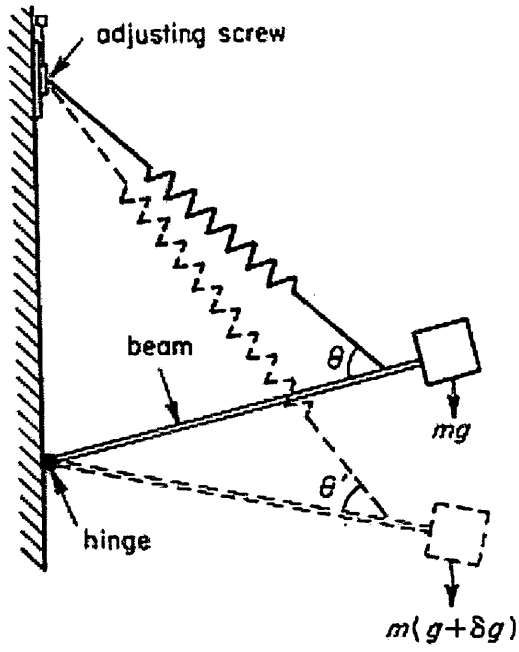

Figure 2: A schematic of the internal workings of a LaCoste and Romberg gravimeter (From Keary and Brooks, 1984). A mass on the end of a beam is supported by a spring. The moment supporting the mass is proportional to the extension in the spring and the sine of the angle θ. Thus, if gravity increases, the angle θ decreases and the extension in the spring is amplified. The instrument is read by restoring the beam to the horizontal by altering the vertical location of the spring attachment using the adjusting screw.

To correct for all the factors influencing the local gravitational field strength, except the causative body under investigation, and obtain a final gravity value accurate to within 1 gu, the gravimeter must be read to a precision of ± 0.1 gu, the latitude of the observation point must be known to ± 10 m, and the elevation must be known to ± 1 cm! To account for instrumental drift the time of the reading must also be recorded (see the following section).

Extracting Useful Information From a Gravity Survey

The process of filtering out parts of the measured gravity anomaly that are not associated with the causative body under investigation is known as *gravity reduction*, or *reduction to the geoid* as this is the most common reference datum. In general, gravity data reduction comprises a series of corrections that remove the dependence of gravity on a particular variable. The factors that have to be corrected for are global, temporal, regional and local - the table summarizes the correction terms and their importance.

Gravity varies on a global scale because of the non-spherical shape of the Earth and because the centripetal acceleration at a point on the surface of the Earth, caused by the Earth's rotation, decreases with distance from the rotation axis. The net effect of these factors is that surface gravity decreases from the equator to the pole by about 0.05 ms^{-2} (5 gals).

Scale	Name	Factors	Magnitude	Importance
Global	Latitude	Rotation and oblateness of Earth	~O.3 - 8 gu / km north-south, depending on latitude	Important if large changes in latitude
Temporal	Instrument Drift	Anelasticity of spring and/or temperature changes		Depends on gravimeter
	Earth Tides	Sun and Moon's gravitational influence on the Earth	Max. amplitude of 3 gu	Only in high precision surveying
Regional	Regional Trend	Rock density variations on scale larger than survey	?	Depends on regional geology
Local	Free-Air (FAC)	Decrease in gravity with elevation	~3 gu / m elevation	Very important
	Bouguer (BC)	Accounts for rock mass between observation point and datum	~1 gu / m elevation (for rock density = 2.67 g/cc)	Very important
	Terrain (TC)	Accounts for local topography	< 10 gu in flat areas	Very important in areas with large topographic variation

Temporal changes in gravity measurements may be due to the subtle but observable gravitational influence of the Sun and the Moon, and instrumental drift. Instrument drift is a shortcoming of all gravimeters that refers to the gradual change in a reading with time resulting from the imperfect elasticity of the springs. It is corrected for by making repeated readings at a fixed location at regular intervals and by assuming linear drift between these times.

Gravimeters with a precision of ± O.1 gu are sensitive to the change in gravity associated with a change in elevation of just 30 cm. Hence, the most important corrections in the reduction procedure remove the effect of elevation. These corrections are made in three parts (see figure 3). First the *Free-Air Correction* corrects for the decrease in gravity with height. For observation points above the datum this term is positive, because the datum is closer to the Earth's center of mass. Second, the *Bouguer Correction* accounts for the gravitational effect of the rock present between the observation point and the datum. For observation points above the datum, this term is negative as the downward pull of this rock unit is being removed. The Bouguer correction assumes that the rock unit extends to infinity in all directions. In regions of subtle topographic variations this approximation is fine; however, in locations of undulating topography a final correction must be made - the *Terrain Correction.* The terrain correction is applied by dividing the area surrounding the observation point into compartments. The relief within these zones is averaged to give a mean difference in elevation between the compartment and the observation point. The gravitational effect of each compartment is then determined by reference to a formula for the gravitational effect of a sector of a vertical cylinder at its axis. The terrain correction is always positive as may be appreciated from figure 3c. The lightly shaded regions form part of the Bouguer correction slab although they do not consist of rock. For these regions, the Bouguer correction has over-compensated (removed the downward pull of too much mass); hence, their effect must be restored by a positive correction. The darkly shaded region, on the other hand, represents a volume of rock not considered by the Bouguer correction but whose influence is to reduce the gravity at the observation point (upward pull). Hence, the terrain correction for this unit must also be positive.

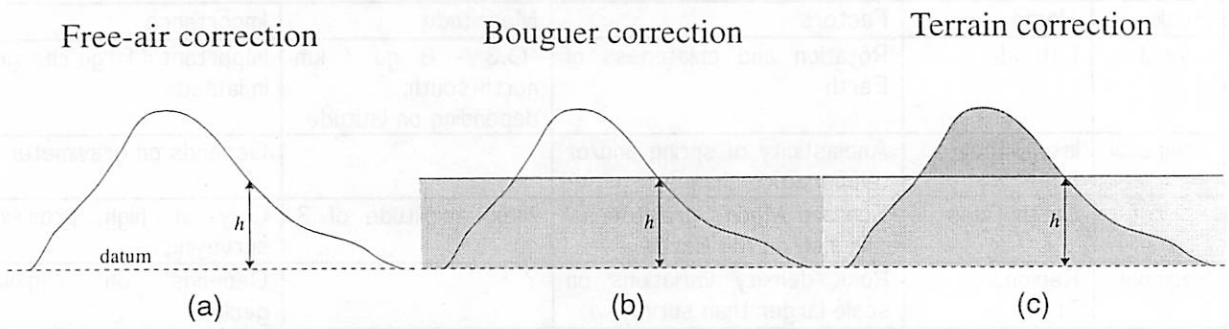

Figure 3: Illustration of the three components of the combined elevation correction (a) the free-air correction; (b) the Bouguer correction; and (c) the terrain correction.

The departure of a corrected gravity value from the theoretical value of gravity at that latitude is called the gravity anomaly. The type of anomaly depends on the corrections that have been applied. If only the free-air correction has been applied the anomaly is known as the *free-air anomaly*, if the Bouguer correction and terrain correction have also been applied the anomaly is known as the *Bouguer anomaly*. The free-air anomaly is zero if there is no topography above the reduction datum and if there are no horizontal variations in rock density below the datum. The Bouguer anomaly should be zero if the density of the rocks is everywhere homogeneous at any given depth below the datum. Thus, provided the rock densities used in the Bouguer and terrain corrections are accurate, any non-zero Bouguer anomaly indicates a sub-surface density perturbation.

Bouguer anomalies are often characterized by a broad, gently varying regional anomaly on which may be superposed a shorter wavelength local anomaly. If the local feature is the causative body of interest the regional trend must be removed by some form of graphical or analytical filtering.

Interpretation of Gravity Anomalies

The interpretation of any potential field anomaly (gravity, magnetic and electrical) is ambiguous because the anomaly could be caused by an infinite number of possible sources. For example, buried concentric spheres of the same mass but different densities and diameters will give the same anomaly. When interpreting gravity anomalies it is therefore important to decrease ambiguity by using all available external constraints on the causative body. Thus, where possible, gravity surveys should be combined with geological observations, borehole analysis and other, complementary, geophysical studies.

Direct interpretation of the gravity anomaly can provide estimates on the depth, thickness and mass excess of the causative body, from the amplitude and extent of the anomaly. For a more accurate determination of the size and shape of the causative body, indirect interpretation methods are employed, using modeling software. Typically, the user generates a simple, plausible, 2 or 3-D geological model, for which a theoretical gravity anomaly is computed. The theoretical and observed anomalies are then compared and the simple model is refined until the best agreement between the anomalies is reached.

So, what's the point? Applications of Gravity Surveying

Gravity surveys have many applications in geophysics on a range of scales. On the planetary scale, gravity studies have been used to study the shape and crustal thickness of planets, to delineate large scale features such as mantle upwellings, mid-ocean ridges, etc., and more recently to monitor large scale movements in the Earth's interior. On a regional scale, gravity surveys have been used to search for impact craters, reveal the state of isostatic compensation of a feature, prospect for hydrocarbon deposits and investigate the shape and extent of igneous intrusions and buried sedimentary basins. On the smallest scale micro-gravity studies are becoming a powerful tool in the location of sub-surface voids, ore deposits and groundwater movement.

Case Study: Are the Chiricahuas Isostatically Compensated?

To provide a feel for gravity surveying, on the field trip we will be crossing over the Chiricahua Mountains and taking gravity readings along the way. The question we will be attempting to answer is: are the Chiricahuas isostatically compensated? In other words, is the topography of the Chiricahua Mountains supported by the strength of the rock it is made of (isostatically uncompensated)? Or, is it supported by density contrasts between it and the surrounding rock (compensated)? That is, do the Chiricahua Mountains have a low-density root beneath them? (For those of you who don't know what isostatic compensation is - don't worry, you'll learn all about it in Jay's class!)

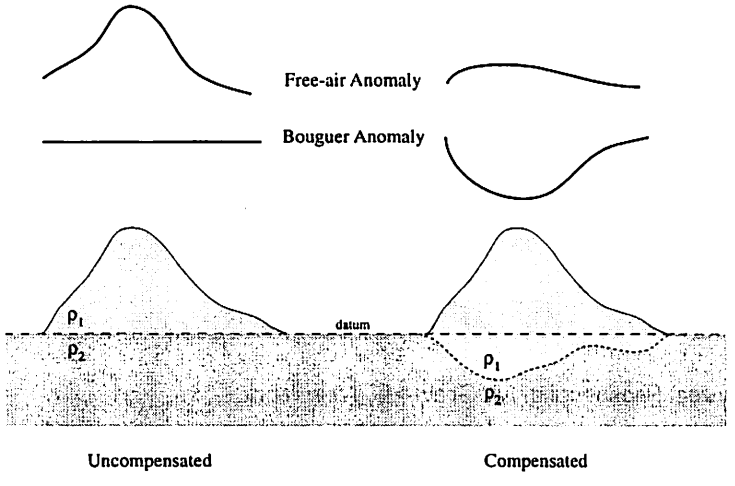

Figure 4: Gravity anomalies over isostatically compensated and uncompensated mountains.

A simple way of assessing the degree of compensation of a geologic feature is to look at the free-air anomaly and the Bouguer anomaly (see figure 4). If a positive geologic feature like a mountain range is totally uncompensated, the free-air anomaly will be positive and the Bouguer anomaly will be zero, because the observed gravity anomaly is due entirely to the topography of the feature (the mass above the datum). If, on the other hand, the mountain range is totally compensated, the free-air anomaly should be close to zero and the Bouguer anomaly will be negative, indicating that beneath the mountains and below the datum, there is a rock unit of lower density than its surroundings.

So that we could put the (an) answer in this handout, and because the data reduction cannot be done "on the fly", Pete, Joe and I went out a few weeks ago and collected some gravity data over the route we will be following. Figure 5 shows the observed anomaly after various corrections have been applied. (Note the importance of the correction terms!)

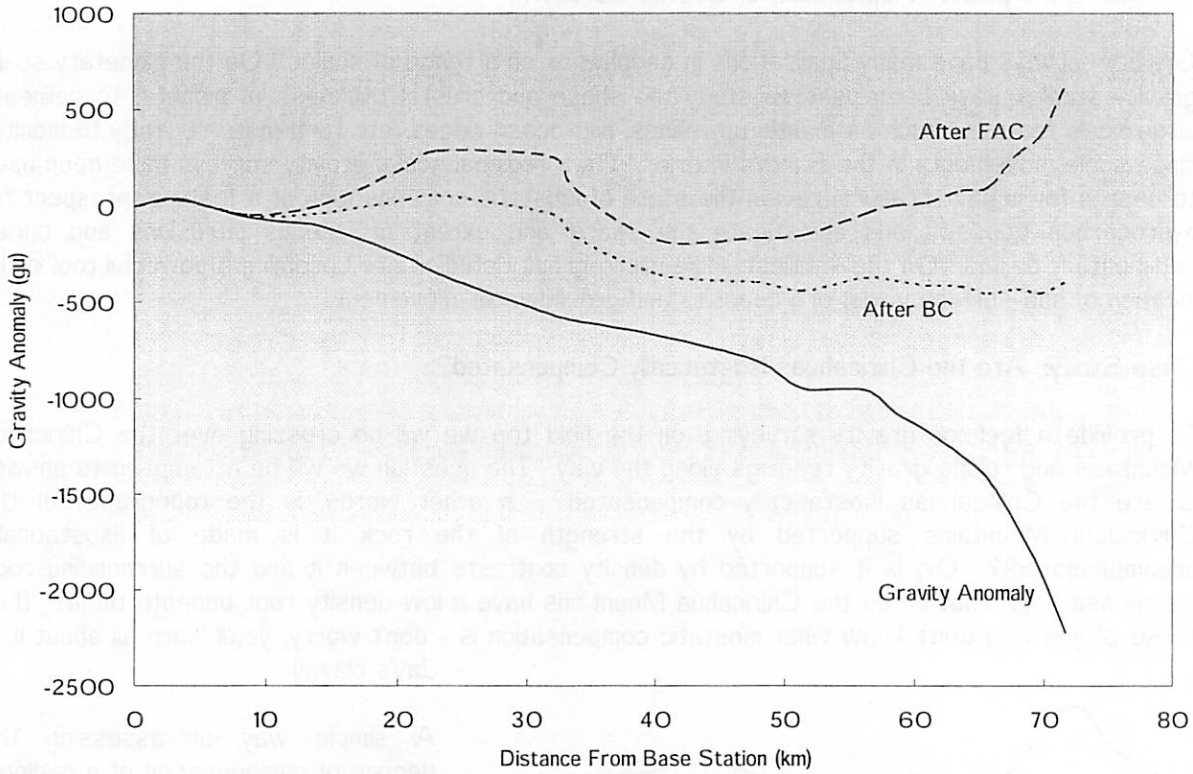

Figure 5: Gravity anomaly over the Chiricahua Mountain Range, relative to base station in Wilcox, at various stages of the data reduction process. Solid curve is the anomaly after the latitude correction and instrument drift correction. Large dashed curve is the anomaly after the free-air correction. Small dashed curve is the anomaly after the Bouguer correction is applied (without the terrain correction).

References and Further Reading

Keary, P. and Brooks, M., 1984, An Introduction to Geophysical Exploration, Blackwell Scientific Publications.

Dobrin, M. B., 1960, Introduction to Geophysical Prospecting, McGraw-Hill, New York.

Cordell, Lindrith, Keller, G.R., and Hildenbrand, T.G., 1982, Bouguer gravity map of the Rio Grande Rift, Colorado, New Mexico,and Texas: U.S. Geological Survey Geophysical Investigations Series Map GP-949, scale 1:1,000,000

Hittleman, A.D., Dater, D., Buhmann, R., and Racey, S., 1994,Gravity CD-ROM and Users's Manual (1994 Edition): National Oceanic and Atmospheric Administration, National Geophysical Data Center, Boulder, Colorado

Nettleton, L. L., 1976, Gravity and Magnetics in Oil Exploration, Mc-Graw-Hill, New York.

Plouff, Donald, 1977, Preliminary documentation for a FORTRAN program to compute gravity terrain corrections based on topography digitized on a geographic grid: U.S. Geological Survey Open File Report 77-535, 45 p.

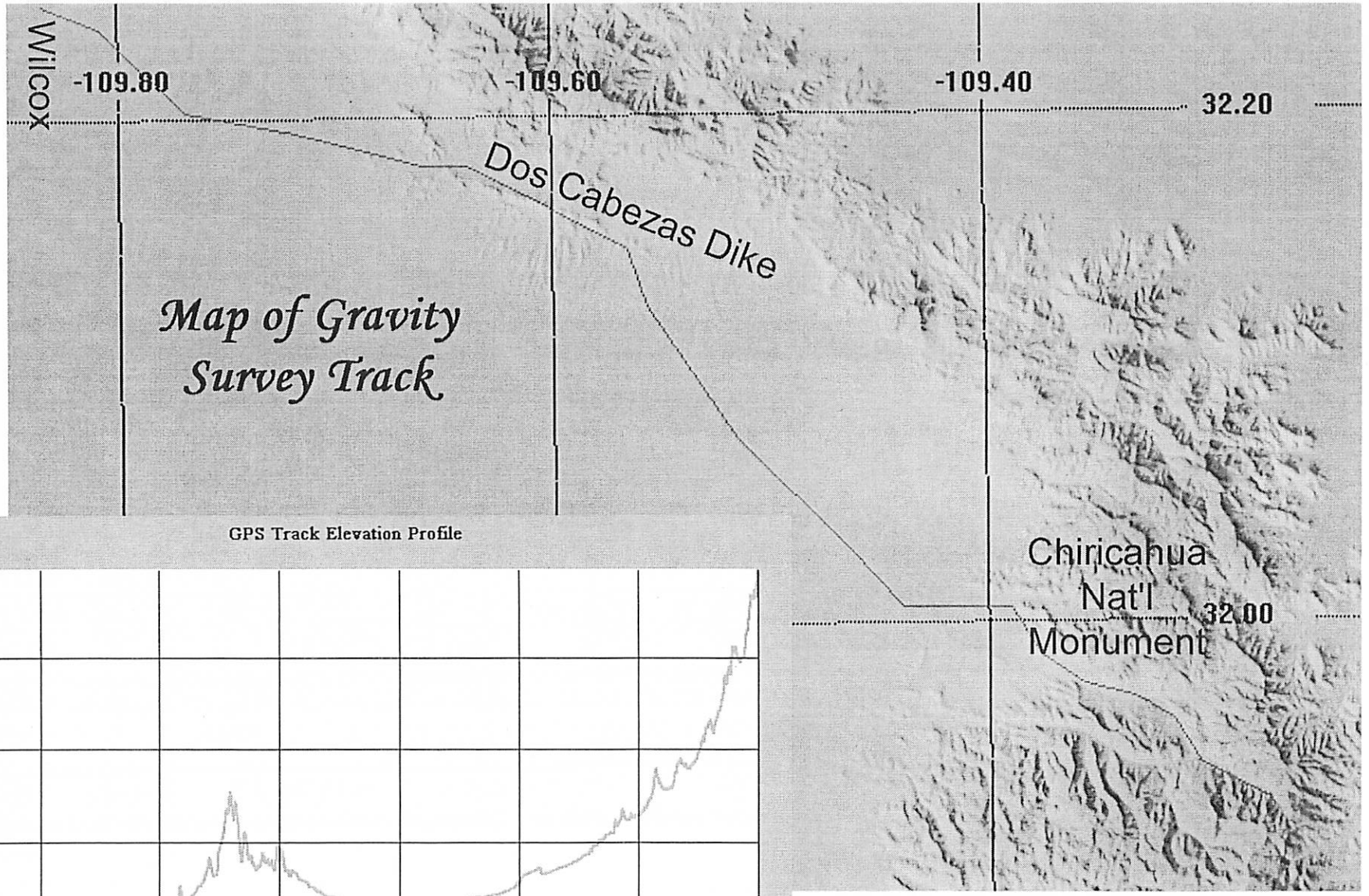
Wilcox
-109.80
-109.60
-109.40
32.20
Dos Cabezas Dike
Map of Gravity
Survey Track
Chiricahua
Nat'l
Monument
32.00

GPS Track Elevation Profile
Elevation
(meters)
2000
1800
1600
1400
10
20
30
40
50
60
Distance (kilometers)

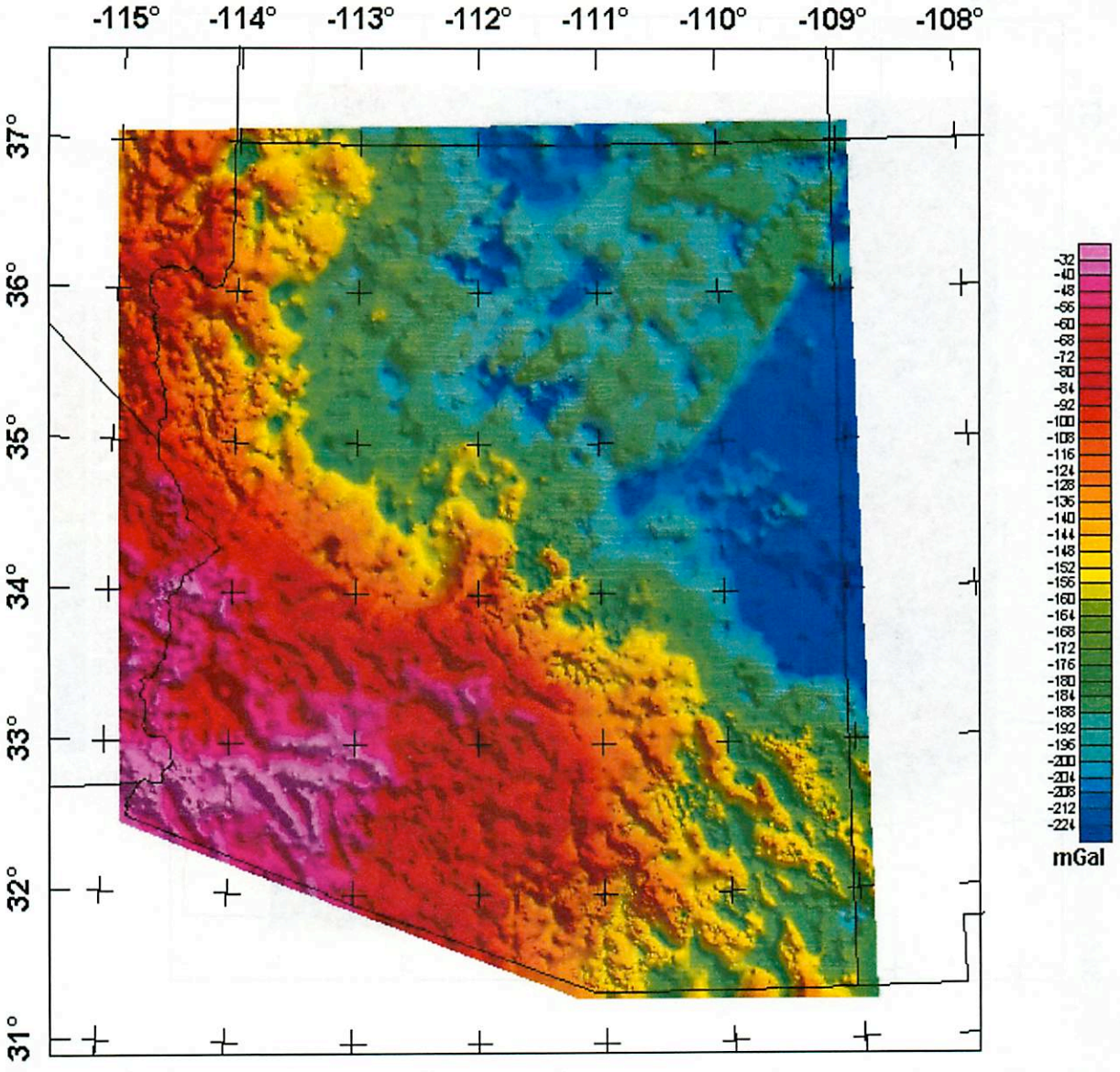

Figure 6. Complete-Bouguer gravity anomaly map of Arizona (from *U.S. Department of the Interior, U.S. Geological Survey.* This page is <URL: http://greenwood.cr.usgs.gov/pub/open-file-reports/ofr-01-0081/html/az_boug.htm>). Grid was compiled using data from 42,707 gravity stations in and adjacent to the state of Arizona. These data were extracted from the gravity data base maintained by the National Geophysical Data Center (from Department of Defense unclassified data) (Hittleman and others, 1994) and augmented with data from the USGS and from several university theses and dissertations. Observed gravity relative to the IGSN-71 datum were reduced to the Bouguer anomaly using the 1967 gravity formula (Cordell and others, 1982) and a reduction density of 2.67 g/cc. Terrain corrections were calculated radially outward from each station to a distance of 167 km using a method developed by Plouff (1977). The data were converted to a 500 m grid using minimum curvature techniques and are displayed with an illumination from the Northeast.

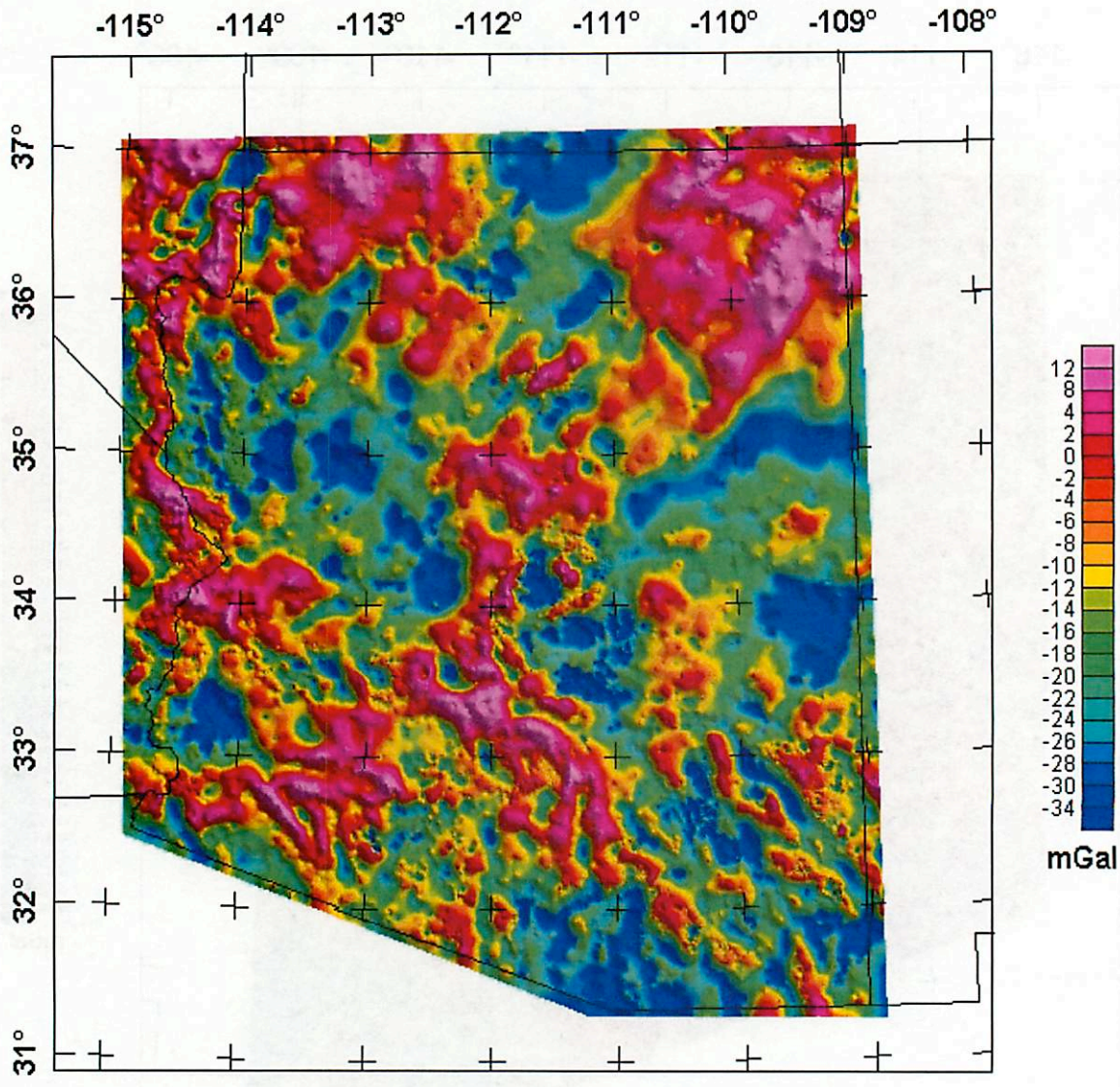

Figure 7. Isostatic residual gravity anomaly map of Arizona (from *U.S. Department of the Interior, U.S. Geological Survey.* This page is <URL: http://greenwood.cr.usgs.gov/pub/open-file-reports/ofr-01-0081/html/az_iso.htm>). The colors on this isostatic residual gravity map reflect variations in the Earth's gravity field caused primarily by lateral variations in density in the rocks that make up the upper part of the Earth's crust. An isostatic residual gravity grid was derived from Bouguer and free-air gravity anomaly data. This grid was created by removing from the Bouguer gravity grid a model of the gravity expression caused by deficiencies in mass (compensating mass) that supports topographic loads. The calculation of the isostatic model used averaged digital topography, a crustal thickness of 30 km, a crustal density of 2.67 g/cc, and a density contrast between the crust and upper mantle of 0.40 g/cc. The anomalies and patterns on the map reveal details of subsurface geology including the location of buried faults, sedimentary basins, plutons, uplifted basement rocks, etc. Positive anomalies (red colors) delineate rocks denser than the surrounding rocks. Negative anomalies (blue colors) delineate rocks less dense than the surrounding rocks. The displayed grid has an illumination from the Northeast.

Spheroidal Weathering in Texas Canyon:

Another Beating of a Spherical Horse

Mandy Proctor

Spheroidal Weathering: A chemical and mechanical process involving acid rain, which results in rocks becoming rounded over time. Weathering processes affect the corners and edges of a rock causing them to be worn away over time. Later, the spheroidal weathering will cause layers to fall off the rock.

The Chemical Process:

- Rain falls through the atmosphere, dissolving CO_2 as it heads toward the surface. This combination creates a weak carbonic acid.

$$H_2O + CO_2 \rightarrow H_2CO_3$$

- The carbonic acid is ionized into hydrogen and bicarbonate ions.

$$H_2CO_3 \rightarrow H^+ + (HCO_3)^-$$

- Hydrogen ions are very small and can easily invade the minerals and disrupt the crystal structure. One example is the decomposition of potassium feldspar shown below,

$$2KAlSi_3O_8 + 2H^+ + H_2O \rightarrow 2K^+ + Al_2Si_2O_5(OH)_4 + 4SiO_2$$

- The result of this decomposition is potassium ion, kaolinite and quartz. The kaolinite is a clay that can easily be weathered away.

- The process above is for the decomposition of K-spar, common in granites. The Fe-Mg minerals in Basalt can also undergo a similar process which will make kaolinite.

The Mechanical Process:

- The decomposition can only occur on the surface of the rock. The edges and corners of a cubic rock are more vulnerable to attack (Figure 1) because they have the most exposed surface area.

- The wearing away of the corners and edges of the rock will eventually lead to a spherically shaped rock (Figure 3).

- Once the boulder becomes rounded, the weathering process results in layers falling off the boulder, like peeling an onion (Figure 2).

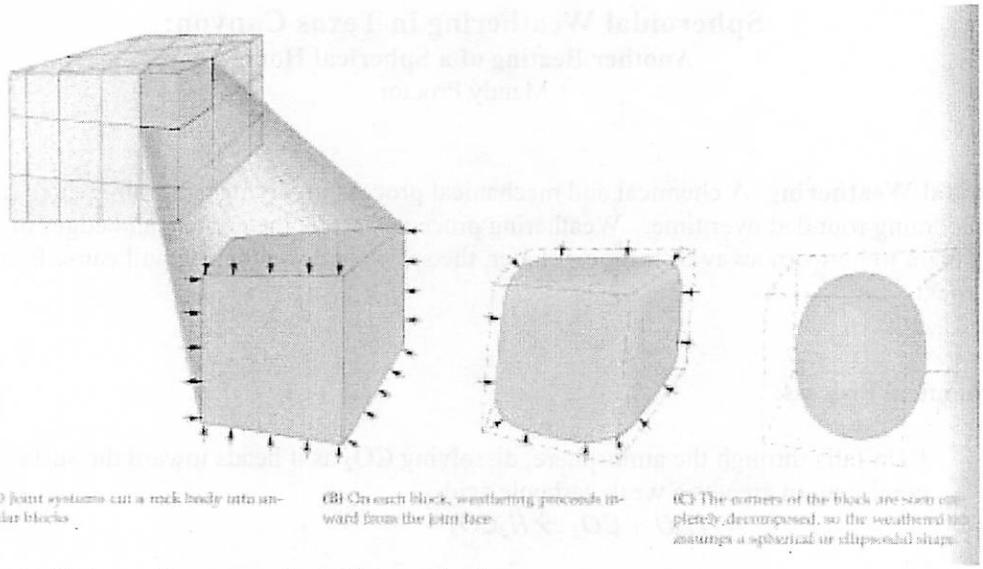

Figure 1: Cartoon showing spheroidal weathering process.

Figure 2: Onion like peeling of formed sphere.

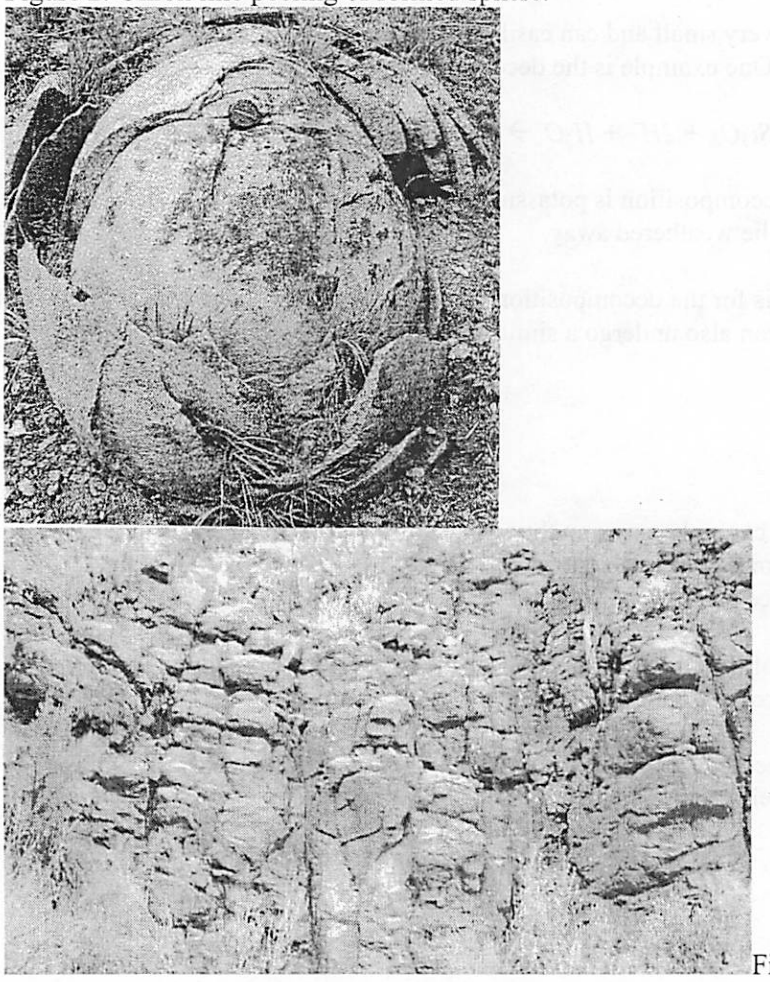

Figure 3: Spheroidal weathering in basalt.

Remote Sensing and the Planetary Connection:

- In what kinds of environments would spheroidal weathering exist? Could these effects exist elsewhere in the Solar System?
  - Must have water precipitation.
  - Need to create acidic rainfall onto the surface.
  - Could this possibly exist on Mars?
    - So far only talked about spheroidal weathering of granites. Which are not present on Mars.
    - Can have spheroidal weathering of basalts, so this process may be present on Mars (Figure 3).

- Can we detect spheroidal weathering on Mars? (Figure 4)
  - With MOC you can detect objects ~ 5 km in diameter, so right now we do not have the resolution to detect these boulders on Mars
  - With HiRISE we will be able to see 0.3 meters per pixel, so we will have to wait until 2006 when HiRISE arrives at Mars.

References:

Beyer, Ross (2001). Spheroidal Weathering in Texas Canyon, AZ. Southern New Mexico LPL Field Trip. May 2001.

Hurford, Terry (2002). Remote Sensing of Spheroidal Weathering: Detecting a Dead Horse. Beach Processes LPL Field Trip. April 2002.

Press, Frank & Raymond Siever. (1997) Understanding Earth.

http://www.geocities.com/bccrockclub/files/Basalt-spher.htm

The figure below has images of Texan Canyon with 1 meter per pixel resolution. Would we be able to see the spheroidal weathering with the MOC resolution? What about with HiRISE?

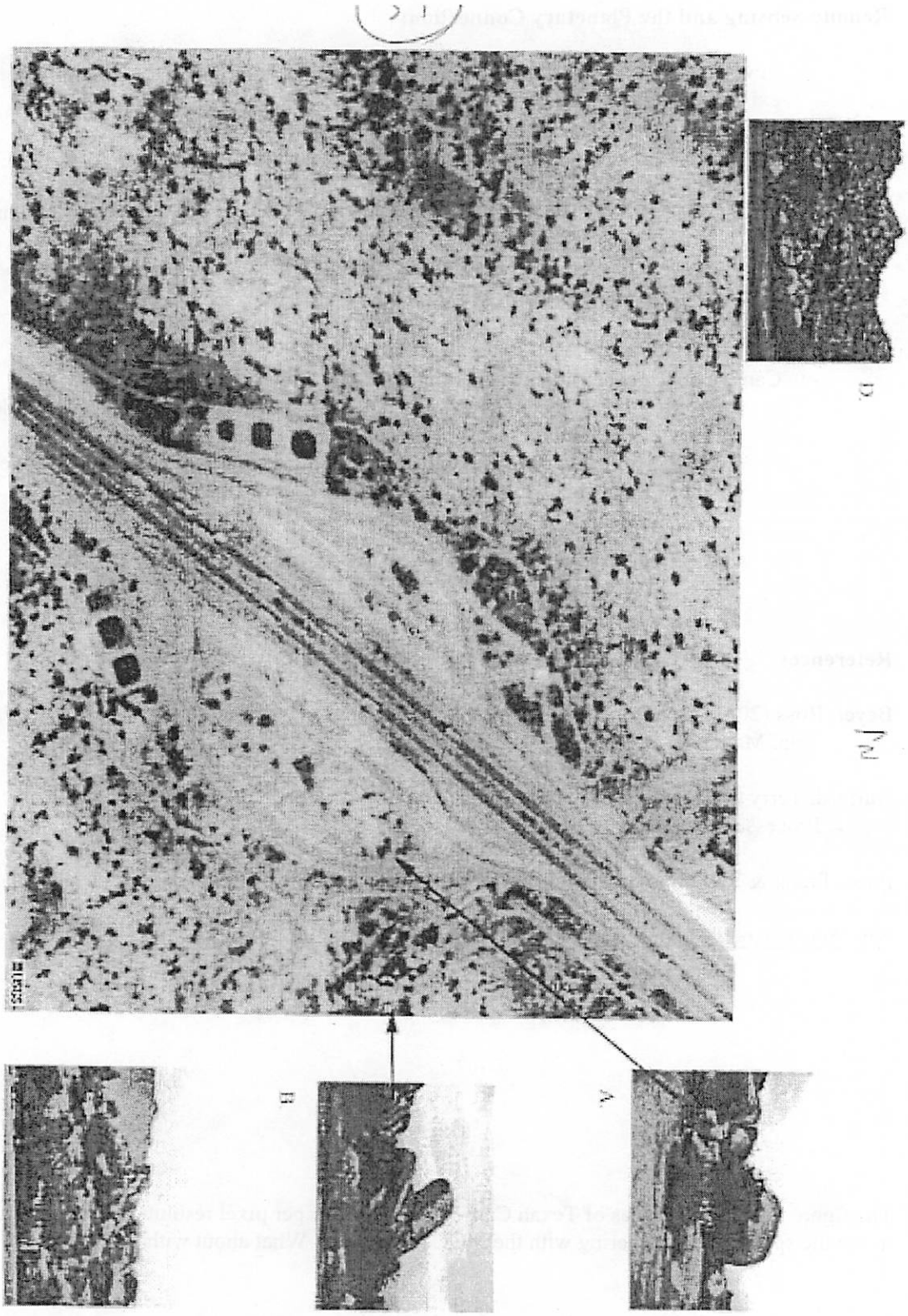

Figure 4: Stolen from Terry, this shows an overhead view of Texan Canyon. Can you see the spheroidal weathering?

Granitic Intrusions in Southeastern Arizona

Jason W. Barnes

The giant granitic boulders prevalent in Texas Canyon were formed 50 Myr ago when silica-rich magma intruded into the crust from below. This magma cooled slowly, resulting in the coarse-grained (i.e., large crystals) granite you see. In the intervening geological ages, the strata that were above this formation eroded away, leaving the boulders exposed on the surface for the first time.

Other granite now exposed on the surface in Arizona can be found in the Santa Catalina mountains, the Rincons, the Silverbells, and in selected locations among the Pinalenos and Chiricahuas. In general, the ages of granites in this area are bimodal, with episodes of volcanism occurring about 70 and 30 million years ago. This may perhaps be the result of the subduction angle of the Pacific plate shallowing, then steepening again over time.

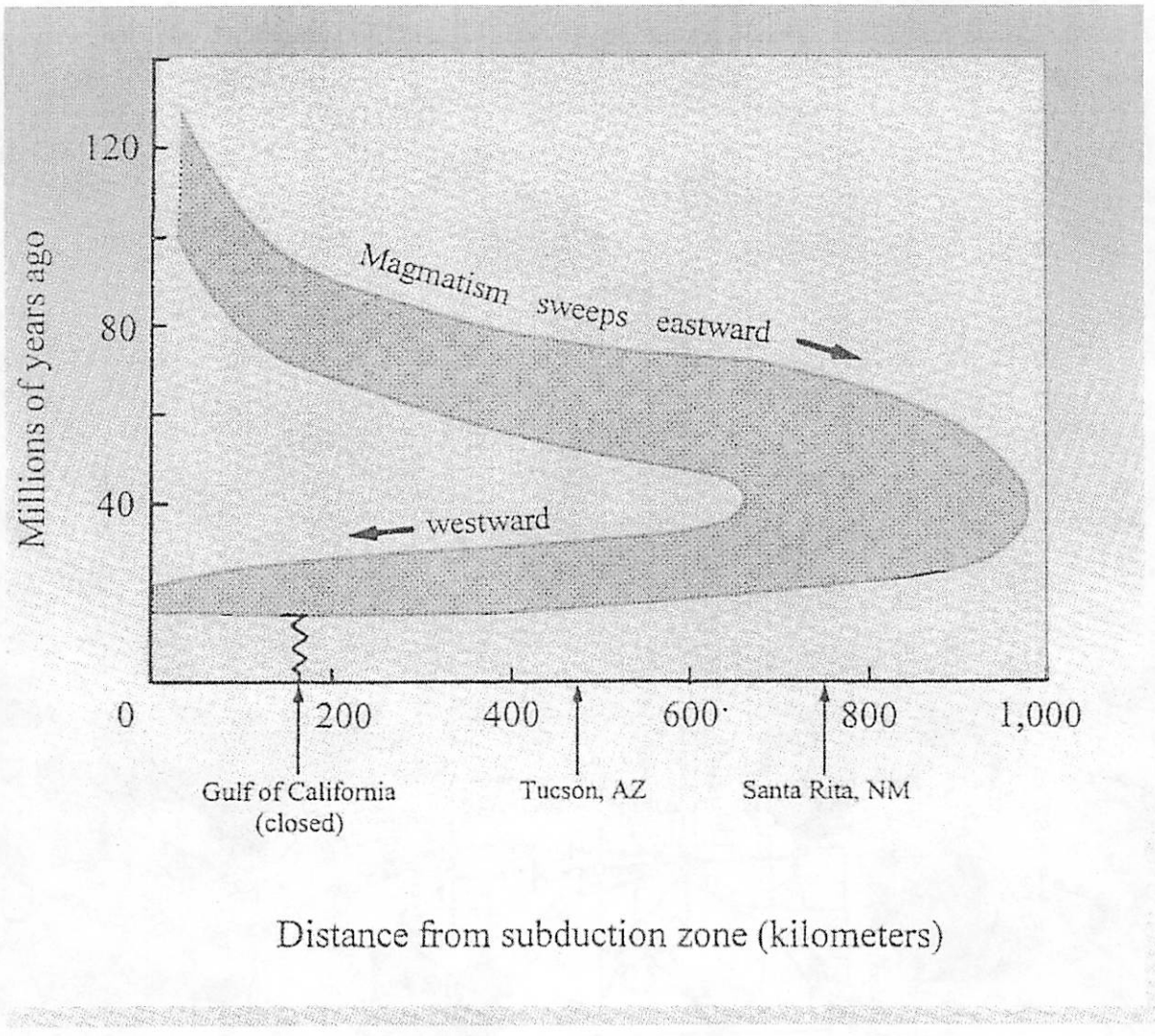

Figure 1: Ages of volcanic deposits in the SW USA.

Figure 2: From the Geologic Highway Map of Arizona. Tg is Tertiary Granite, about 30 Myr old. TKg is Tertiary/Cretaceous granite, and is like 70 Myr old.

Wilcox Playa: Age and Likelihood of Meteorite Finds

Dave O'Brien

1 Age and Size of the Playa

Wilcox Playa covers an area of approximately 130 km^2 [1,2,3]. Estimates of its age (the point at which the ancient Lake Cochise dried up) can be made from radiocarbon dating of sediments (primarily small shells and other organic carbonate deposits) in the playa and along its shoreline. Long [1] found an age of approximately 10,000 yr, while more recent studies by Waters *et al.* [2,3] find evidence for more recent lake activity and put the age between 3,000 and 4,000 yr.

2 Meteorite Fall Rate

The frequency of meteorite falls (here used to denote a meteorite landing on the surface of the Earth, but not necessarily recovered immediately) can be estimated in several ways. A number of automated camera networks have been set to record the trajectories and magnitudes of incoming fireballs, and (given some model dependent parameters) an estimate of their initial and terminal masses. Many of these fireballs are inferred to result in actual meteorite falls, although only about 4 have actually been recovered. Using data from the Canadian MORP network over a period of 11 years, Halliday *et al.* [4] estimate that the fall rate of meteorites to be about 380 (per 10^6 km^2 per yr) for meteorites larger than 10 g in mass (terminal mass).

Fall rate can also be estimated from studies of regions where a large number of meteorites are found (primarily wind-excavated desert areas). Zolensky *et al.* [5] studied 68 meteorite fragments (representing 49 individual falls) recovered in an 11 km^2 area of Roosevelt County, New Mexico. Thermoluminescence dating of the sandy surface on which they were found indicated an age of around 16,000 yr. Making some estimates of the decay rate of meteorites (due to terrestrial weathering), he estimated a fall rate of 940 (per 10^6 km^2 per yr) for meteorites larger than 10 g in mass, about a factor of 3 larger than the estimate of Halliday *et al.*

Which of these estimates is closer to the truth is up for debate. Zolensky *et al.* believe that their estimate is correct, and is larger than that of Halliday *et al.* because the meteorite flux may be variable over time and their 16,000 yr baseline provides a better estimate of the average value than the 11 yr baseline of Halliday *et al.*, which may sample an anomalously low point of the meteorite flux. In a followup paper, Halliday *et al.* [6] argue that the estimate of Zolensky *et al.* may be too high because they assume a weathering rate that is too small.

3 Likelihood of Finding a Meteorite on the Playa

The number of meteorites which have fallen on the playa can be estimated from

$$N_{playa} = N_{>M} \times Area_{playa} \times Age_{playa} \quad (1)$$

For a total playa area of 130 km^2 and using the lower estimates of age and fall rate, about 170 meteorites larger than 10 g should have fallen on the playa over its lifetime. Using the upper estimates of age and fall rate, as many as 1,200 meteorites larger than 10 g could have fallen on the playa.

These numbers may not accurately represent the actual number of meteorites on the playa today, since terrestrial weathering can destroy the oldest meteorites. Using the method of Zolensky *et al.*, who assume a terrestrial weathering half-life of 3,500 years ($\lambda = 0.000197$ yr^{-1}) (based on studies of meteorites found in arid regions), the number of meteorites on the playa when falls and weathering are in equilibrium is

$$N_{playa} = N_{>M} \times Area_{playa}/\lambda \quad (2)$$

Since the half-life for weathering is the same as the lower limit for the playa age, this equation probably does not apply in the case of a younger Wilcox Playa. For the upper limits of the age and fall rate (where the age is several times the weathering half-life and falls and weathering are more likely to be in equilibrium), the estimate decreases to about 620 meteorites larger than 10 g on the playa (about a factor of 2 less than the total number which have fallen over time.

Averaging these estimates, we can assume that there are probably several hundred meteorites larger than 10 g in mass on Wilcox Playa today (a few per square kilometer). Two meteorites (both ordinary chondrites) have already been found on the playa, one in 1979 and one in 2001, and are aptly named Wilcox Playa and Wilcox Playa 002 [7]. Happy hunting!

4 References:

[1] Long, A. (1966). Late Pleistocene and recent chronologies of playa lakes in Arizona and New Mexico. Ph. D. Thesis, University of Arizona.

[2] Waters, M. R. (1989). Late Quaternary lacustrine history and paleoclimatic significance of pluvial Lake Cochise, southeastern Arizona. *Quaternary Res.* **32**, pp. 1-11.

[3] Waters, M. R. and Woosley, A. I. (1990). The geoarchaeology and preceramic history of the Wilcox Basin, SE Arizona. *J. Field Archaeology* **17**, pp. 163-176.

[4] Halliday, I. *et al.* (1989). The flux of meteorites on the Earth's surface. *Meteoritics* **24**, pp. 173-178.

[5] Zolensky, M. E. *et al.* (1990). The accumulation rate of meteorite falls at the Earth's surface: The view from Roosevelt County, New Mexico. *Meteoritics* **25**, pp. 11-17.

[6] Halliday, I. *et al.* (1991). The frequency of meteorite falls: Comments on two conflicting approaches to the problem. *Meteoritics* **26**, pp. 243-249.

[7] http://www.lpl.arizona.edu/SIC/arizona_meteorites/az_stars_map.html

Robotic Geology in Extreme Environments: The Nomad Robot and Beyond

Fred J. Ciesla

The Nomad Explorer

Robotic vehicles are being proposed and used with increasing frequency in space exploration. As discussed by Pedersen *et al.* (1999) a serious limitation in such exploration is the constant need to constantly monitor these vehicles by controllers on Earth. This is done for the safety of the robot as well as for rapid interpretation of the data to give the robot its next set of commands.

A group of scientists and engineers have been working on developing the Nomad robot to help usher in the next generation of robotic explorers. This robot is being designed with a level of Artificial Intelligence allowing it to navigate over dangerous terrain in extreme environments, identify rocks that it comes across along its traverse, and store the interesting data to send back to Earth when the opportunity arises. It is equipped with a laser rangefinder, orientational sensors, a high resolution camera, a manipulator arm, and a visible to near-IR spectrometer.

Nomad identifies rocks using reflectance spectrometry. It has a computer onboard to determine where the absorption features are in the spectrum. From this measurement, the computer determines how "interesting" the rock is. For example, the Nomad explorer has undergone tests in the Atacama desert and in Antarctica in order to determine its ability to identify meteorites. Thus the computer compares the spectra taken of the various samples and compares them to the spectra of rocks expected to be found in the area. Preliminary tests have shown that the computer does very well (when compared to the human explorers in ANSMET) in discriminating between meteorites and terrestrial samples. The most common mistakes are that the computer will often identify quartzite as a meteorite and iron meteorites as being terrestrial rocks.

The Future

The type of technology being developed for the Nomad robot could be in high demand for future space missions. A number of ambitious missions are being discussed which will not allow for idling of the craft while it awaits orders to be uploaded from Earth. Some of these include airplane, balloon, and helicopter flights for Mars and/or Titan. Also, such capabilities on a rover may allow for fewer limitations of Martian surface exploration (or other bodies!).

Discussion

I hope that this presentation will lead to some (civilized) discussion about both science and science policy issues. Among the questions that we could discuss are:

- For meteorite identification, are there any other instruments to put on Nomad?
- If Nomad proves successful, should we continue with ANSMET?
- Should we divert resources away from studies of manned exploration of Mars and towards development of better AI and tools for programs such as Nomad?
- If completely trustworthy AI were available today, what missions in solar system exploration would you most like to see developed?

References

Pedersen, L. *et al.* 1999. Robotic rock classificiation using visible light reflectance spectroscopy: Preliminary results from the robotic Antarctice meteorite search program. *LPSC XXX.*

see also the web page for the program at:

http://www.frc.ri.cmu.edu/projects/meteorobot2000/

C L A Y D U N E S

Joe Spitale

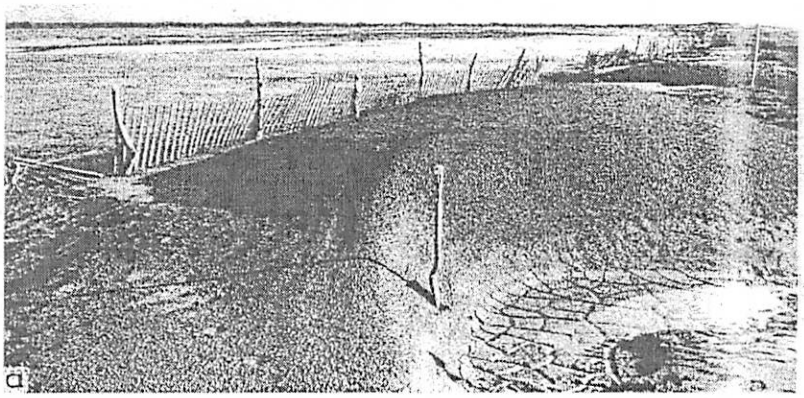

From [2]

Description
- 20% or higher clay content by weight
- as tall as 30 m, but typically 5-15 m
- occur on tidal mud flats and margins of saline playa
- do not migrate
- horns point toward instead of away from wind

Formation
(a) during dry season:
  - briney crust formed on surface
  - dessication polygons form
  - dessication polygons broken down into sand-size pellets by:
    - growth of salt crystals
    - mechanical breakdown of delaminated polygons blown blown along the ground
  - pellets blown to the shore where they accumulate on:
    - vegetation
    - trash line
    - existing dunes
(b) during wet season, humidity stabilizes the clay accumulations
(c) goto (a)

==> new layer formed every season

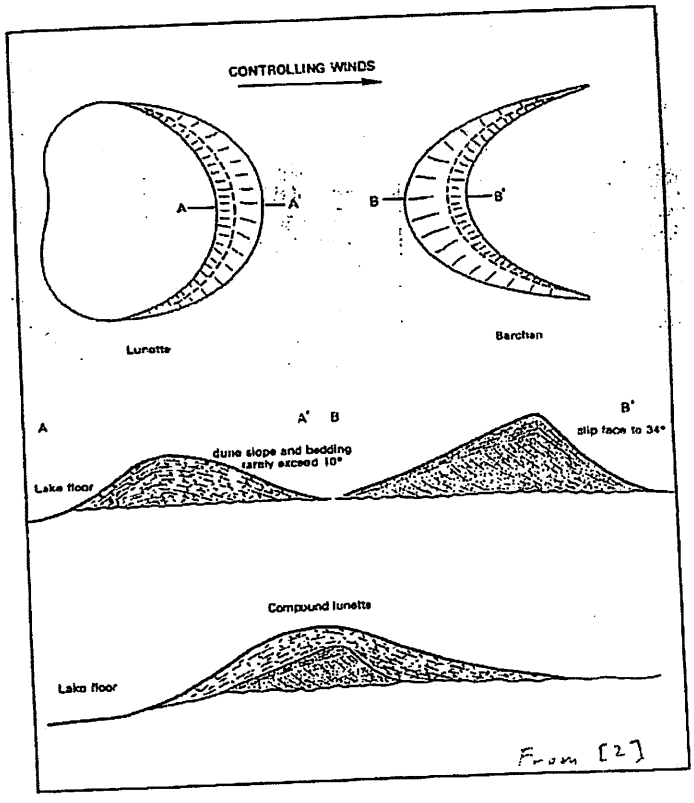
CONTROLLING WINDS
A
A'
B
B'
Lunette
Barchan
A
A' B
B'
slip face to 34°
dune slope and bedding rarely exceed 10°
Lake floor
Compound lunette
Lake floor
From [2]

Necessary conditions
- saline envoronment
  - inhibits vegetation
  - salt crystals help break down the polygons
- seasonal flooding
  - replenishes salts
- rapid drying
  - needed to dessicate surface early enough in the dry season so that there will be time for wind to act before clay is stabilized in next humid season
  - high temperatures
    - lower water table sufficiently to expose wide expanse of bare mud flats
    - dry the mud and cause salt crystals to grow
- unidirectional wind
  - provides consistent transport of material to the shore during the dry season

==> Useful Indicator of paleoenvironment
  - hot dry season with strong unidirectional wind, seasonal flooding

References:
[1] Schreiber, J.F. Jr. Geology of the Willcox Playa, Cochise County, Arizona. In: Land of Cochise; southeastern Arizona. 1978
[2] Bowler, J.M. Clay Dunes: Their Occurrence, Formation and Environmental Significance. Earth-Science Reviews. 9; 4, Pages 315-338. 1973.
[3] Armstrong, P.W., Kornicker, L. S. Marine and lagoonal deposits in clay dunes, Gulf Coast, Texas. Journal of Sedimentary Petrology. 31; 2, Pages 245-255. 1961.
[4] Coffey, G.N. Clay dunes. Journal of Geology. Pages 754-755. 1909.

Magnetometer Surveying

Pete Lanagan and Gareth Collins

Background

Magnetic Field Components

1. Main magnetic field
   a. dipole field
   b. nondipole field
   c. secular variation
      1. westward drift (0.2 degree longitude / year)
      2. decreasing moment of dipole field

2. External Magnetic Field
   a. generated by electric currents in ionosphere
   b. diurnal component
   c. solar storms may cause erratic fluctuations

3. Anamalous Magnetic Field: ferromagnetic minerals in crust - this is what we're concerned with

Surveying Considerations

1. Instrument Drift
2. Diurnal Variations
3. Secular Variations

Geologic Sources of Magnetic Anomalies

1. Magnetism of Minerals

- Paramagnetic minerals
  - Atoms with odd numbers of electrons align with polarizing field
  - Low magnetic susceptibility - can ignore for mag surveys

- Diamagnetic Minerals
  - Atomic moment align opposite to polarizing field
  - Negative magnetic susceptibility - can ignore for mag surveys

- Ferromagnetic Minerals

- Magnetic domains: electron orbital and spin motions cause strong magnetism in small sections of crystal structure
- True ferromagnetic minerals: all atomic element align in same direction
- Antiferromagnetic minerals: atomic moments align equally in one or the other of two opposite directions; no net magnetic moment
- Ferrimagnetic minerals: atomic moments align in two opposite directions, one of which is preferred; domain posseses a net magnetic moment

Magnetic Bodies

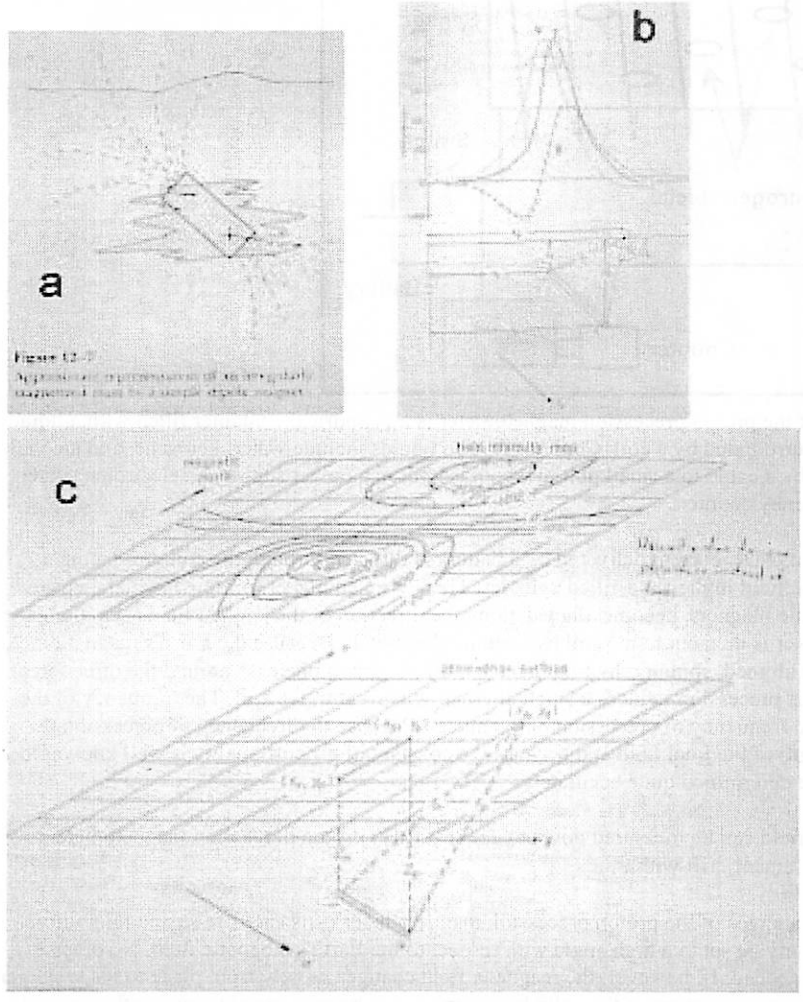

Proton Precession Magnetometer

(stolen from http://www.mines.edu/fs_home/tboyd/GP311/MODULES/MAG/NOTES/proton.html)

For land-based magnetic surveys, the most commonly used magnetometer is the proton precession magnetometer. The proton precession magnetometer only measures the total size of the Earth's magnetic field. These types of measurements are usually referred to as *total field* measurements. A schematic of the proton precession magnetometer is shown below.

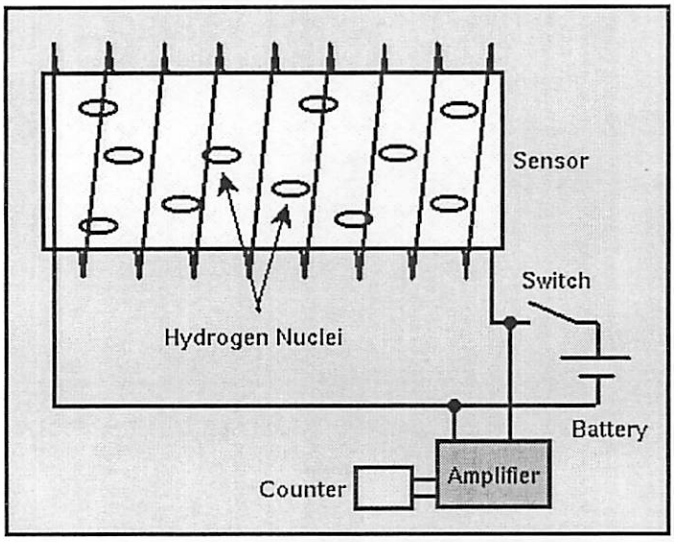

The sensor component of the proton precession magnetometer is a cylindrical container filled with a liquid rich in hydrogen atoms surrounded by a coil. Commonly used liquids include water, kerosene, and alcohol. The sensor is connected by a cable to a small unit in which is housed a power supply, an electronic switch, an amplifier, and a frequency counter.

When the switch is closed, a DC current delivered by a battery is directed through the coil, producing a relatively strong magnetic field in the fluid-filled cylinder. The hydrogen nuclei (protons), which behave like minute spinning dipole magnets, become aligned along the direction of the applied field (i.e., along the axis of the cylinder). Power is then cut to the coil by opening the switch. Because the Earth's magnetic field generates a torque on the aligned, spinning hydrogen nuclei, they begin to precess* around the direction of the Earth's total field. This precession induces a small alternating current in the coil. The frequency of the AC current is equal to the frequency of precession of the nuclei. Because the frequency of precession is proportional to the strength of the total field and because the constant of proportionality is well known, the total field strength can be determined quite accurately.

The strength of the total field can be measured down to about 0.1 nT. Proton precession magnetometers show no appreciable instrument drift with time.

One of the important advantages of the proton precession magnetometer is its ease of use and reliability. Sensor orientation need only be set to a high angle with respect to the Earth's magnetic field. No precise leveling or orientation is needed. If, however, the magnetic field changes rapidly from place to place (larger than about 600 nT/m), different portions of the cylindrical sensor will be influenced by magnetic fields of various magnitudes, and readings will be seriously degraded. Finally, because the signal generated by precession is small, this instrument can not be used near AC power sources.

Magnetic Survey of Dos Cabezas Dike

Below are the results of a magnetometer survey across Dos Cabezas Dike, a basaltic dike we'll see as we drive on Rte 186. Magnetometer readings were collected along a (very roughly) 500-m stretch of Rte 186 across the Dos Cabezas Dike. Also note the spike at a reading taken next to a signpost (labeled in the profile).

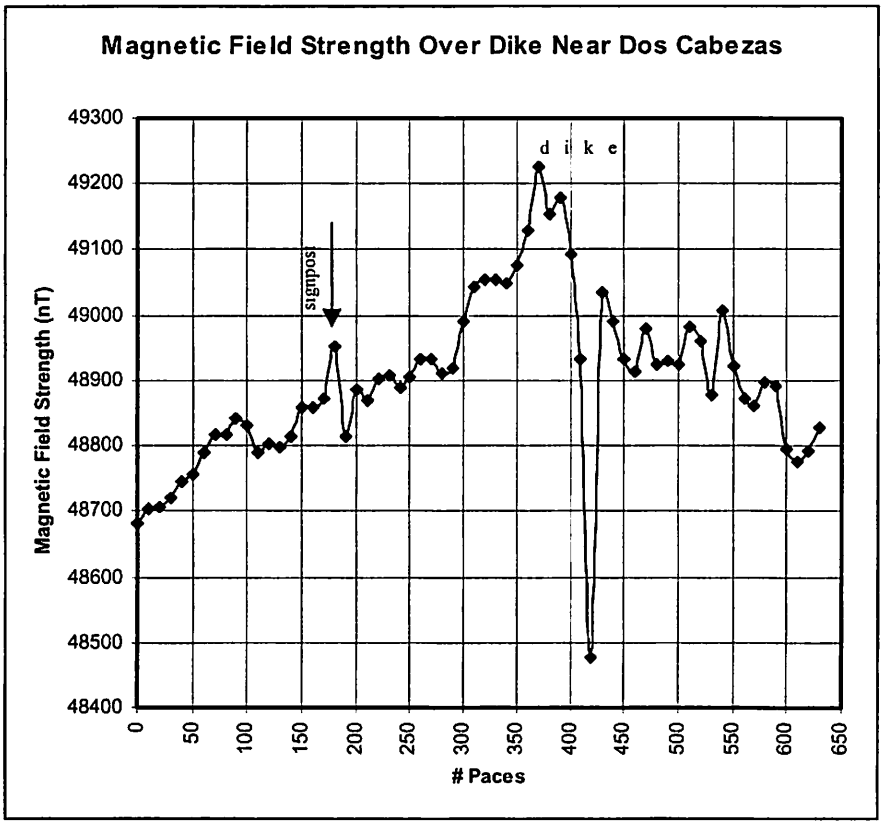

References:

- Robinson, E.S. and C. Coruh. Basic Exploration Geophysics. John Wiley & Sons. New York. 562 pp. 1988.
- Proton Precession Magnetometers: http://www.mines.edu/fs_home/tboyd/GP311/MODULES/MAG/NOTES/proton.html

Cavernous Weathering

Terry A. Hurford

Description

Cavernous weathering is the combination of mechanical and chemical weathering processes which forms round hollows or caverns. These hollows can be numerous and small covering the surface of the rock, known as honeycomb weathering. They can also form quite large caverns, big enough to sit in comfortably.

Cavernous weathering is a phenomenon that can be observed throughout the world on shorelines, in deserts and in the Antarctic. It might even be extraterrestrial. Photos from the Viking space mission in 1977 show rocks with patterns that resemble cavernous weathering features found on sandstone. Others have argued Patherfinder images also show evidence of cavernous weathering similar to the weathering seen in Dolerite on Earth [1][2].

The Cause

Cavernous weathering can develop by either or both of these two mechanisms: case hardening and core softening. By case hardening, silica and other minerals (often iron rich) precipitate into fractures along the surface of the rock which strengthens the outer portions of the rock from further mechanical or chemical weathering. A breech in this protected area will allow the less resistant interior to preferentially erode away, forming a hollow. In the case of core softening, water-assisted chemical and physical weathering disintegrates individual crystal grains from one another in the rock's interior, weakening it. Once this weak interior is exposed the softer interior materials break down and are removed.

The case hardening form of cavernous weathering occurs easily in dry environments found in deserts and the Antarctic. The repeated cycle of wetting and drying the rock will produce the protective outer shell of precipitates.

Honeycomb weathering is similar to cavernous weathering but forms innumerable

small cavities on the surface of the rock. It happens mostly to fine grain rocks such as sandstones and tuffs. Water flowing along fractures throughout the rock will deposit an erosion resistant cement between the grains. Once exposed the areas between the fractures, which lack this cement, will be removed more easily.

Extraterrestrial?

Images from Pathfinder showed rocks on the surface of Mars that may be sedimentary in nature. These rocks seem to be composed of finer rocks held together by some sort of cement [1]. Even though images of the rocks near Pathfinder show small pits on their surfaces these mostly show the location of pebbles that have been removed and not the effects of cavernous weathering. In fact cavernous weathering is not clearly evident in the Pathfinder photos. However if water once flowed on Mars cavernous weathering probably occurred somewhere on the surface. The problem may be in identifying the cavernous weathering.

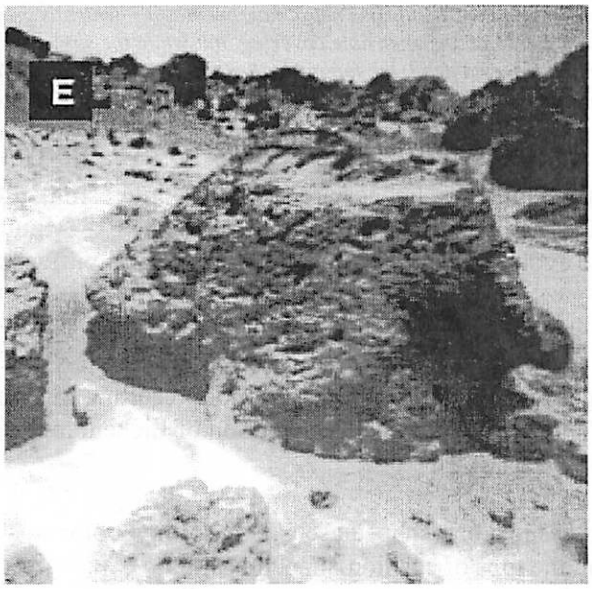

References [1] Mars Pathfinder Rover Team (1997) *Science* **278**:1765-1768 [2] Harvey, R.P. (2001) Workshop on the Martian Highlands and Mojave Desert Analogs [3] Turkington A.V. (2002) AAG abstract

Lichens and Planetary Science
LPL Fieldtrip – Spring 2003
Presented by John Keller

"Alice was *all gal* and Francis was a *fun guy*.
The two took a *liken'* to each other and built a *thallus* palace together."

So goes the classic biology classroom joke we have all suffered through regarding the supposed mutualistic symbiosis of an algae and a fungus known as a lichen. The algae or cyanobacteria provides food through photosynthesis; the fungus provides protection, water storage, and an anchor to a stable substrate. However, it turns out that Francis may not be such a fun guy after all. Researchers in lichenology have tended back towards a view of controlled parasitism (Ahmadjian 1993) originally put forth by the father of the field, Simon Schwendener in 1869:

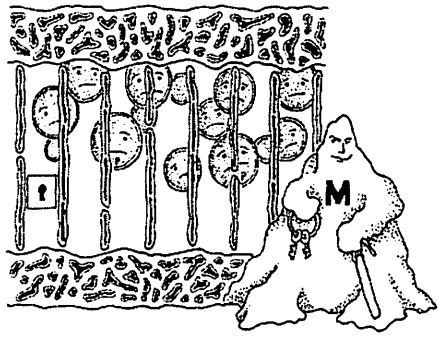

"As the result of my researches, the lichens are not simple plants, not individuals in the ordinary sense of the word; they are, rather, colonies, which consist of hundreds of thousands of individuals, of which, however, one alone plays the master, while the rest, forever imprisoned, prepare the nutriment for themselves and their master. This master is a fungus of the class Ascomycetes, parasite which is accustomed to live upon others' work. Its slaves are green algae, which it has sought out, or indeed caught hold of, and compelled into its service. It surrounds them, as a spider its prey, with a fibrous net of narrow meshes, which is gradually converted into an impenetrable covering, but while the spider sucks its prey and leaves it dead, the fungus incites the algae found in its net to more rapid activity, even to more vigorous increase . . ."

Regardless of the balance of power in the symbioses, lichens are incredibly interesting, diverse, widespread, and adaptable players in the Earth's biosphere. During the "Lichen 15-Minutes of Fame" fieldtrip stop, we will discuss the evolution, morphology, and planetary significance of this unique interspecies marriage.

Lichen Basics: (Baron 1999)

- "A lichen is an association of a fungus and a photosynthetic symbiont resulting in a stable thallus (body) of specific structure." (1982 International Association of Lichenology definition)
- Mycobiont: the fungus
    - Ascomycota: produce spores in a bag-shaped ascus, 95% of mycobionts
    - Basidiomycota: spores on the tops of cushion-shaped basidia
    - Euteromycota: imperfect fungi that only reproduce asexually
    - 20-25% of known 72,000 species of fungi are lichenized
    - Most genera contain both lichenized and non-lichenized species
- Photobiont: the algae and/or cyanobacteria
    - Algae: 90% of photobionts
        - *Trebouxia*: produces cell packets, makes up 50-75% of algae in lichens
        - *Trentepohlia*: has branched chains of cells and orange pigment
        - *Myrmecia* and *Coccomyxa*: other algae genera

- Cyanobacteria: 10% of photobionts
  - Nitrogen-fixing prokaryotes: lack cellular nucleus
  - *Nostoc*: most common genera, blue-grey to brown tinge
  - *Scytonema* and *Stigonema*: other genera
- Photobiont species can live either independently or as part of lichen

- Thallus: the body or structure that is unique to any given mycobiont/photobiont match
  - Cortex: upper and sometime lower, protection, water retention
  - Algal Layer: the food supply
  - Medulla: made of fungal hyphae, stores water
  - Rhizines: attach foliose lichens to substrata
  - Transfer between individuals occurs through specialized structures:
    - Appressoria – hyphae press against photobiont cells
    - Haustoria – hyphae penetrate into photobiont cells
    - Fungal chemicals can make algal cells leak up to 80% of its sugar
- Three primary types of lichen: crustose, foliose, fructiose

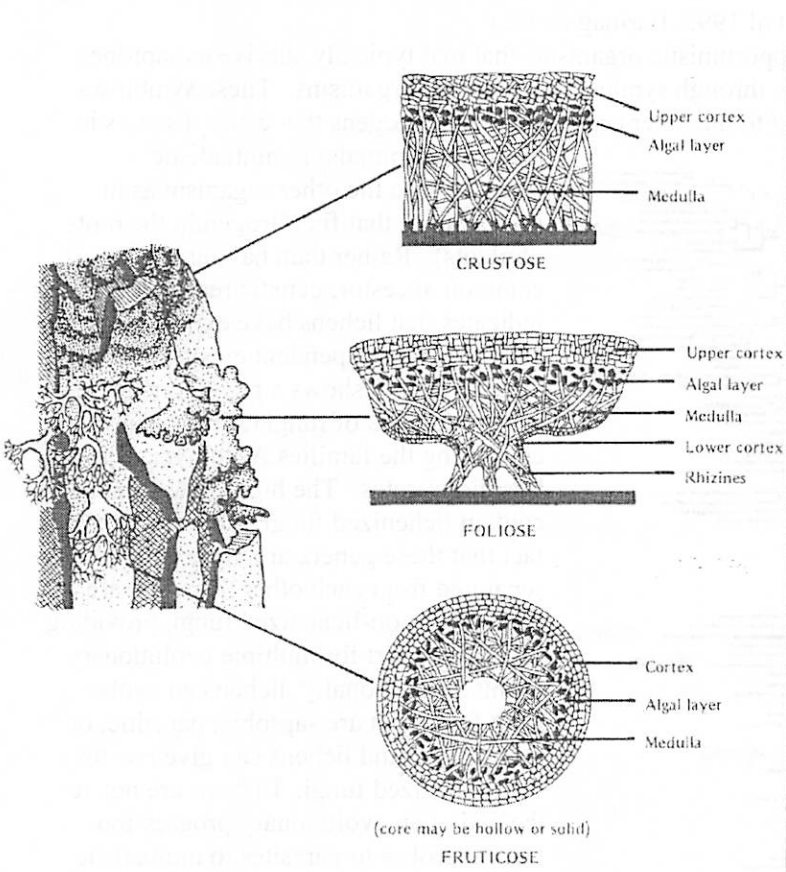

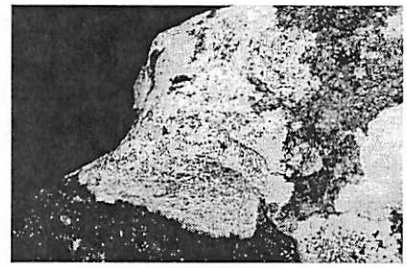

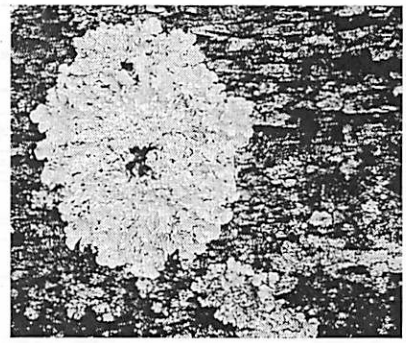

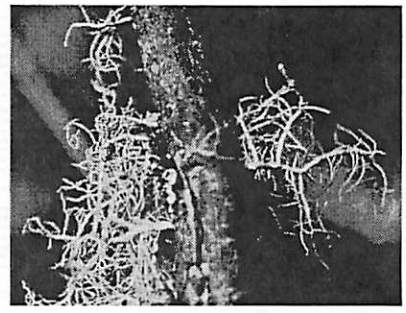

- Endoliths: community of organisms living entirely within a rock
    - Found especially in desert regions and Antractic dry valleys

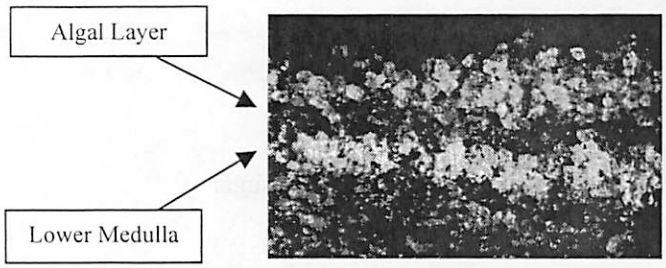

Evolution of Lichens: (Gargas et al 1995, Barinaga 1995)
Lichen is a lifestyle. Fungi are opportunistic organisms that that typically survive as saprobes (living off dead organic matter) or through symbioses with other organisms. These symbioses can vary from parasitic (damaging to the other organism as in pathogens that cause diseases in plants and animals) to mutualistic (beneficial to the other organism as in mycorrhizae that fix nitrogen in the roots of plants). Rather than having one common ancestor, genetic research indicates that lichens have evolved through a number of independent events. The diagram below shows a phylogenetic analysis a class of fungi (Amastigomycota) containing the families Ascomycetes and Basidiomycetes. The highlighted genera contain lichenized fungi. Of note is the fact that these genera are more widely separated from each other than they are from other non-lichenized fungi, providing genetic support for multiple evolutionary events. Additionally, lichen can evolve from fungi that are saprobic, parasitic, or mutualistic, and lichens can give rise to non-lichenized fungi. Lichens are not at the end of an evolutionary progression from saprobes to parasites to mutualistic symbioses. They are just one of many ways to survive.

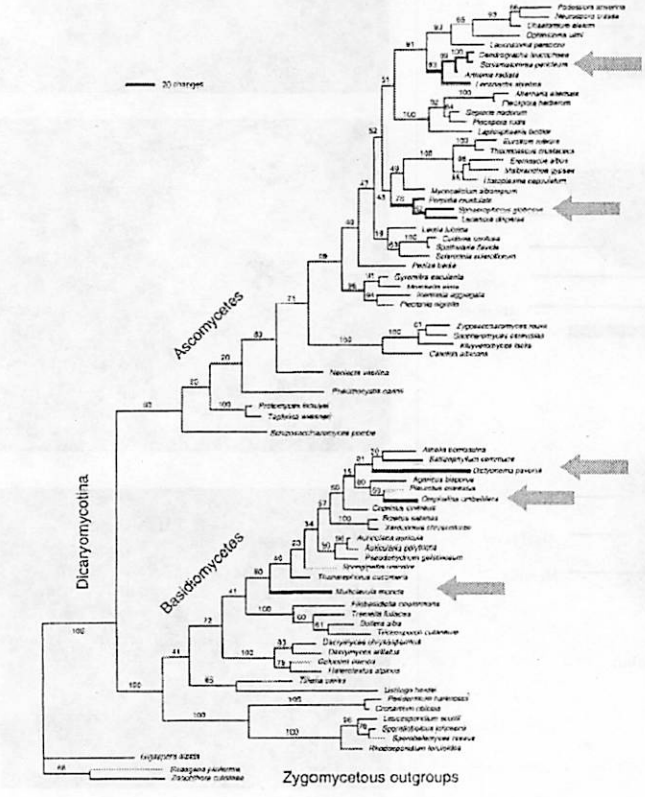

Lichen Planetary Connection #1: Substrate Weathering: (Adamo & Violante 2000)

- Biogeophysical weathering: breakup of rock through physical penetration into minerals
  - Mechanical action of lichen thalli causes physical breakup of mineral surfaces
  - Thallus swelling and shrinking with changes in water content also important
  - Amount of breakup depends on both properties of rock and nature of lichen
  - Mineral fragments can become incorporated into the thallus
- Biogeochemical weathering: breakup of rock through chemical reactions (i.e. carbonic acid)
  - Dissolution of rock minerals mainly through organic acids
  - Carbonate and ferromagnesian minerals especially corroded by lichens
- Neogenesis of minerals: secondary products formed through dissolving and chelating
  - Oxalates: Oxalic acid secreted by lichen leads to precipitation of oxalates
    - $CaC_2O_4*H_2O$ (whewellite) and $CaC_2O_4*(2+x)H_2O$ (weddellite)
    - Heavy metal ions can be removed into oxalates
  - Iron Oxides and hydroxides, siliceous relicts, alumino-silicates
  - Lichen acids: possible chelating agents released by lichen

Lichen Planetary Connection #2: Atmospheric Biomarkers: (Richardson 1992)
Unlike plants, lichens lack roots and vascular systems for transporting water. As such, they depend solely upon the atmosphere and substrate to which they are attached for nutrients and water. As such, lichen are extremely sensitive to atmospheric conditions and pollutants and serve as important and effective biomarkers for atmospheric chemistry. Below is a non-exhaustive list of atmospheric issues to which lichen are sensitive:

- Sulfur dioxide and acid rain
- Tropospheric ozone and nitrogen compounds
- Fluorides from aluminum smelting, brick firing, glass making, and volcanoes
- Aromatic hydrocarbons (including dioxins, furans, and PCBs)
- Metals
- Radioactive elements (from nuclear bomb testing, nuclear-powered satellites and reactors)

Sulfur Dioxide near Belfast	Fluoride from Mount Etna	US Snap-9A Satellite Crash
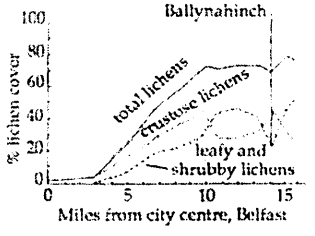	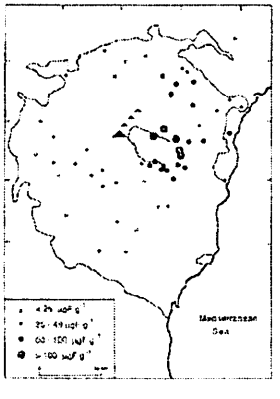	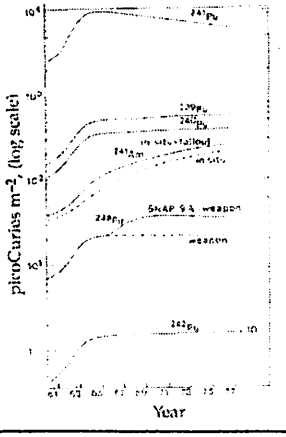
Fenton, 1960	Davies & Notcutt, 1988	Holm, 1977

Lichen Planetary Connection #3: Astrobiological Analogue: (Wynn-Williams & Edwards 1999, Wynn-Williams et al. 1999, Cockell et al. 2000)

- Antarctica presents array of environmental conditions approaching those found on Mars.
    - Scarcity of water (very little liquid water, humidities approaching 0%)
    - Low ambient temperatures
    - Enhanced UVB radiation resulting from stratospheric ozone depletion
    - Penguins
- Lichen and endoliths show biochemical adaptations to these environmental extremes
    - Cryptoendoliths live within translucent rock, providing UV protection
    - Metabolites believed to act as protectives and antibiotics
    - Pigments (parietin, atranorin, carotenoids, scytonemin) protect UV damage
    - Dark pigmentation aids in heat absorbtion
    - Compatible solutes (glycine betaine, polyols) provide cellular antifreeze
    - Water replacement molecules (sugar trehalose) reduce desiccation
- Laser-based Fourier-transform Raman spectroscopy (FTRS)
    - Remote, non-intrusive analytical technique
    - Suitable for detecting biochemicals in both living and fossil samples
    - Provides possible analysis technique for identifying signs of life on Mars

References:

Adamo, P., & Violante, P. 2000. "Weathering of rocks and neogenesis of minerals associated with lichen activity." *Applied Clay Science* 16: 229-256.

Ahmadjian, V. 1993. *The Lichen Symbiosis.* New York: John Wiley & Sons.

Barinaga, M. 1995. "Origins of lichen fungi explored." *Science* 268: 1437.

Baron, G. 1999. *Understanding Lichens.* England: Richmond Publishing Co.

Bungartz, F., Rosentreter, R., & Nash, T. 2002. *Field Guide to Common Epiphytic Macrolichens in Arizona.* Phoenix: ASU Lichen Herbarium.

Cockell, C., Catling, D., Davis, W., Snook, K., Kepner, R., Lee, P., & McKay, C. "The ultraviolet environment of Mars: Biological implications past, present, and future." *Icarus* 146: 343-359.

Gargas, A., DePriest, P., Grube, M., & Tehler, A. 1995. "Multiple origins of lichen symbioses in fungi suggested by SSU rDNA phylogeny." *Science* 268: 1492-1495.

Ovstedal, D., & Smith, L. 2001. *Lichens of Antarctica and South George.* Cambridge: Cambridge University Press.

Richardson, D. 1992. *Pollution Monitoring with Lichens.* England: Richmond Publishing Co.

Weber, W. 1963. "Lichens of the Chiricahua Mountains, Arizona." *University of Colorado Studies Series in Biology* 10: 1-27.

Wynn-Williams, D., & Edwards, H. 1999. "Antarctica ecosystems as models for extraterrestrial surface habitats." *Planetary and Space Science* 48: 1065-1075.

Wynn-Williams, D., Edwards, H., & Garcia-Pichel, F. 1999. "Functional biomolecules of Antarctic stromatolitic and endolithic cyanobacterial communities." *European Journal of Phycology* 34: 381-39.

Ignimbrite Deposits, Ash Flows and Cooling Units

Ross Beyer

ignimbrite Welded or unwelded, pumiceous, ash-rich deposit of pyroclastic density current(s). This term was formerly used for strongly welded deposits only.

pyroclasitc density current A particulate flow moving along the ground. This term includes both pyroclastic flows and pyroclastic surges but has no connotation of particle concentration or flow steadiness.

The amount of volatiles in a magma determine what will happen when that magma erupts and how explosive the eruption is. In the case of low volatile content, the magma will most likely burp out of the ground and produce viscous lava flows like those seen in Hawaii. In the case of high volatile content, the magma will be fragmented and spewed from the vent at high velocities. This kind of eruption produces volcanic ash and tephra. There is a special case where the erupted particles do not travel ballistically away from the vent, because they are too dense. Instead they are lofted up, but then come rushing back down and travel away from the vent along the ground in a pyroclastic density current. The material that this density current leaves behind is known as an ignimbrite.

The above process may seem simple and straightforward, but rarely happens. When it does it is cloaked in a cloud of ash, so it is difficult to observe and measure. Ignimbrite deposits have a characteristic structure and a complicated depositional pattern which made them difficult to interpret to early volcaniologists studying them.

Standard Ignimbrite Flow Unit

An ignimbrite deposit is not one homogeneous mass of rock. Near-horizontal boundaries separate it into several depositional flow units. Each of these flow units is the product of a single pyroclastic flow and can be anywhere from a few centimeters thick to tens of meters thick. The *standard ignimbrite flow unit* consists of three layers (Figure 1), which are representative of different regions within the pyroclastic density current [3]:

Layer 1 Deposit laid down at the flow front during strong interaction with ambient air and ground surface

Layer 2 Deposit of the main body and tail, i.e., the major portion of the flow

Layer 3 Deposit from the overriding dilute ash cloud

All three layers are rarely present, often layer 1, layer 3, or both are missing.

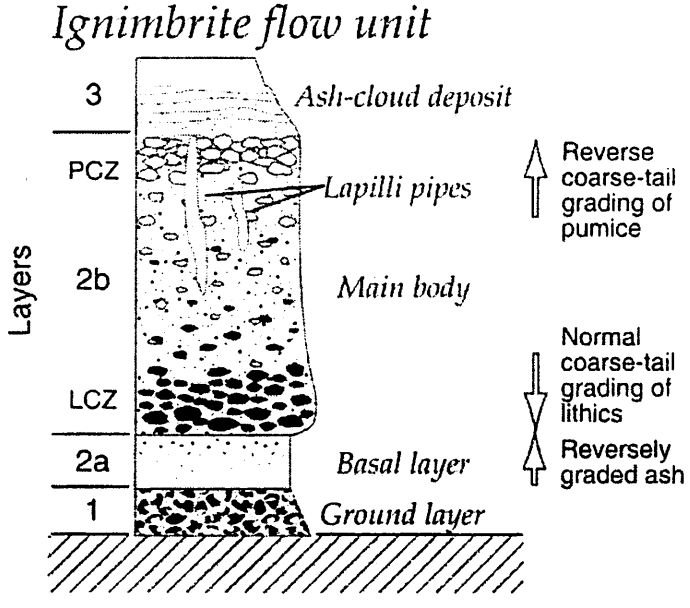

Figure 1: Idealized flow unit of ponded ignimbrite. Layer 2 can show a variety of grading structures from no grading to extremely enriched lithic and pumice concentration zones (LCZ and PCZ). Different layer 1 and layer 3 facies are discussed in the text. White particles are pumice, black particles are lithics, and dots are ash [3].

Pyroclastic Density Currents

There are several ways that pyroclastic flows can be initiated, and they are illustrated in Figure 2. Ignimbrites are typically formed from pyroclastic density currents as a result of the vertical eruption and column collapse mechanism.

The structure of a *standard ignimbrite flow unit* is rather complex, and confused early volcanologists, because they could not understand how a single eruption could produce the differences in clast size and grading observed. The answer lies in the complicated physics of a collapsing pyroclastic column (Figure 3), and the fluidized nature of the pyroclastic density current.

Deposition

An outflowing pyroclastic density current has a significant amount of energy and is capable of overtopping topographic barriers. The pyroclastic density current will preferentially fill up topographic lows, but will leave a thin veneer on ridges that it passed over (Figure 4). This characteristic also plagued early researchers until the collapsing column mechanism was understood.

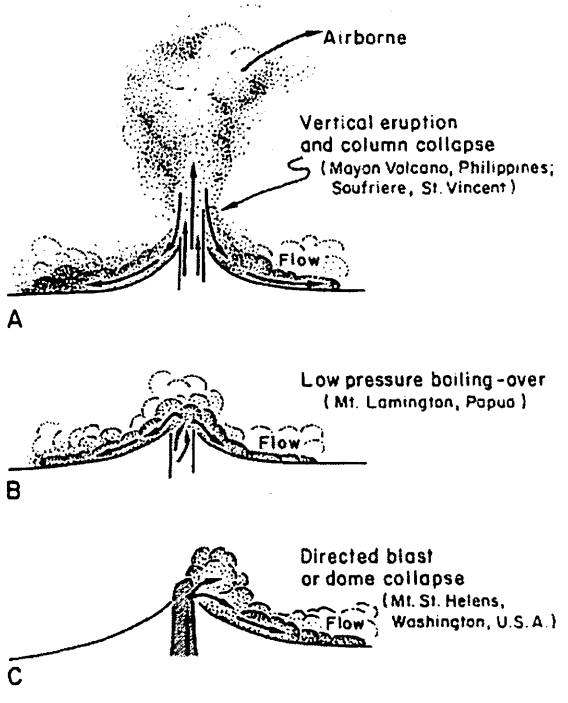

Figure 2: Some ways that pyroclastic flows can originate. [1]

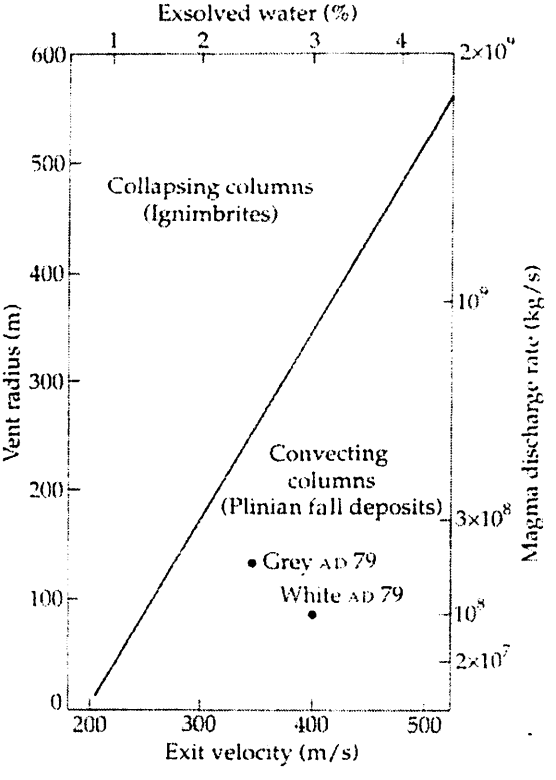

Figure 3: Stability fields for convecting and collapsing columns, in terms of vent radius and magmatic volatile content. Magma discharge rate (right side) is largely a function of vent radius (left side) while exit velocity (bottom) is largely a function of volatile content (top). [2]

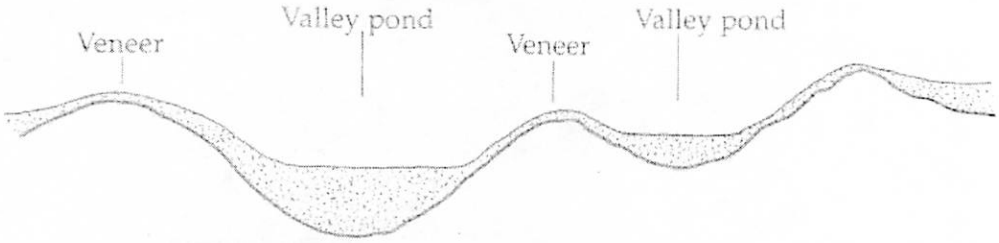

Figure 4: Valley pond ignimbrites and ignimbrite veneers. Valley ponds may be tens of meters thick; veneers 0.5-3 meters thick. Veneers are products of only the most energetic pyroclastic flows, which overrun topography, rather than being confined by it. They are preserved only as thin skins over ridges. [2]

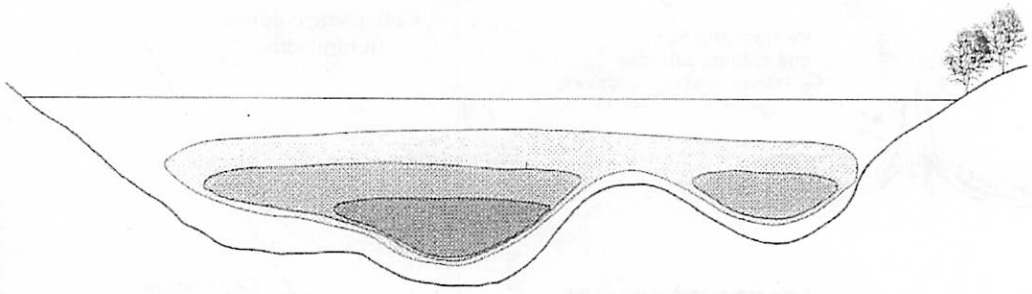

Figure 5: Variations in degree of welding in an ignimbrite, seen in cross-section. Density of shading indicates degree of welding. Material in contact with ground and at top of deposit is unwelded. Dense, glassy welding is usually found only in the thickest part of deposit. [2]

Welding

Once the pyroclastic density current has settled, the ash and pumice particles that have been deposited are still quite hot. As they cool, these initially airborne particles become welded together to form the ignimbrite rock mass. As such, thicker areas of deposit will undergo a higher degree of welding as seen in Figure 5.

References

[1] R. V. Fisher and H.-U. Schmincke. *Pyroclastic Rocks.* Springer-Verlag, 1984.

[2] Peter Francis. *Volcanoes, A Planetary Perspective.* Clarendon Press, 1993.

[3] A. Freundt, C. J. N. Wilson, and S. N. Carey. *Encyclopedia of Volcanoes*, chapter Ignimbrites and Block-and-Ash Flow Deposits. Academic Press, 2000.

Geologic History of the Chiricahuas: Emphasis on Ignimbrite Deposits

Abby Sheffer

The Chiricahuas are part of a large volcanic system in southern Arizona, New Mexico, and northern Mexico. One magma chamber was present just south of the Chiricahua National Monument, where it intruded into older volcanics and sedimentary rocks 27 million years ago. An proposed eruption sequence is shown in the figure below.

Rhyolite: Volcanic equivalent of a granite, consisting mostly of alkali feldspar and quartz (high Si, light colored).

Dacite: Volcanic equivalent of a granodiorite, consisting of plagioclase feldspar and quartz with hornblende (less Si, somewhat darker).

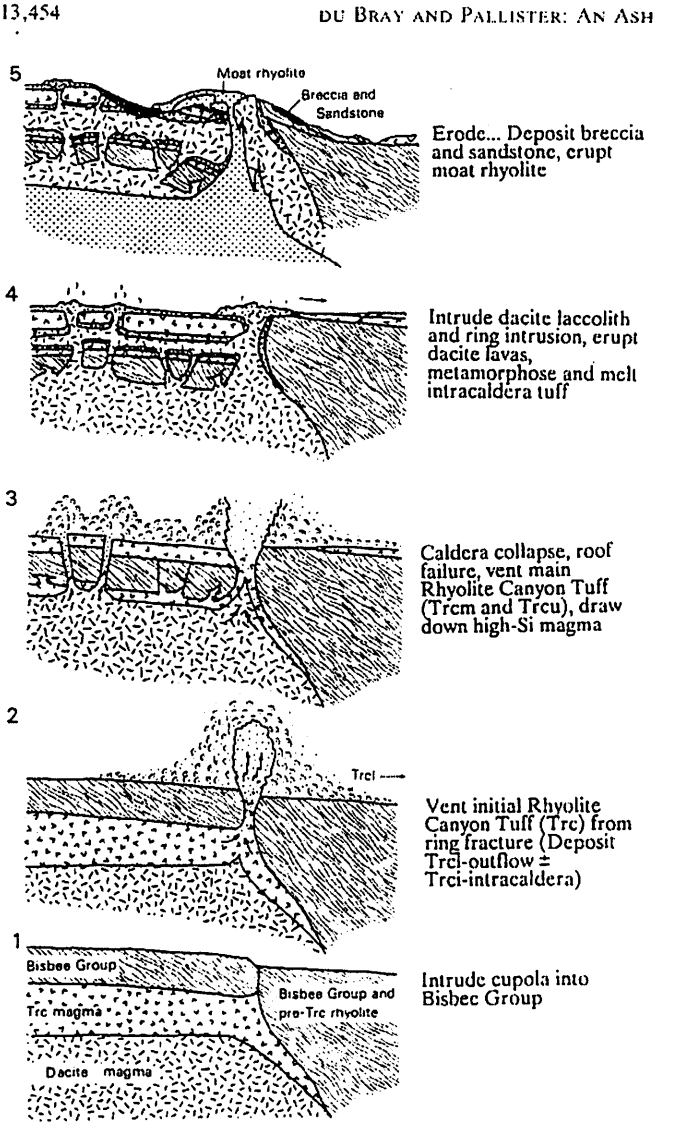

Fig. 18. Proposed structural model for stages in the evolution of the Turkey Creek caldera. Unit identifiers as in Figure 2.

Du Bray and Pallister, 1991

The eruption left a large caldera, 5000 feet deep and 12 miles across, primarily filled with the Rhyolite canyon tuff. Just about the only dacite we'll see is on the top of Sugarloaf Mtn. The thickness of the rhyolite tuff varies from a few hundred feet to 3000 feet. The total eruption volume is about 1000 times that of Mt. St. Helens.

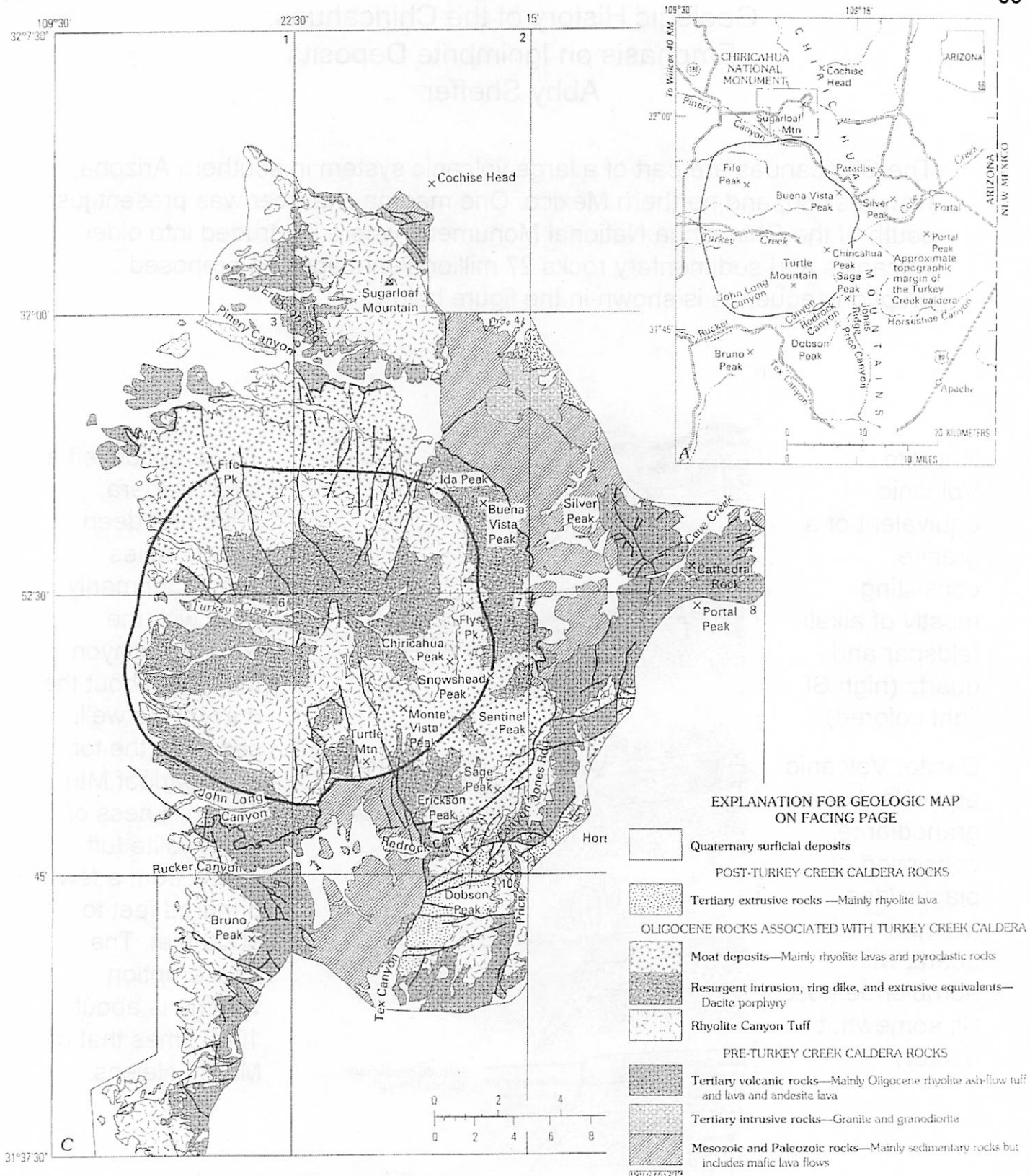

EXPLANATION FOR GEOLOGIC MAP ON FACING PAGE

Quaternary surficial deposits

POST-TURKEY CREEK CALDERA ROCKS

Tertiary extrusive rocks —Mainly rhyolite lava

OLIGOCENE ROCKS ASSOCIATED WITH TURKEY CREEK CALDERA

Moat deposits—Mainly rhyolite lavas and pyroclastic rocks

Resurgent intrusion, ring dike, and extrusive equivalents—Dacite porphyry

Rhyolite Canyon Tuff

PRE-TURKEY CREEK CALDERA ROCKS

Tertiary volcanic rocks—Mainly Oligocene rhyolite ash-flow tuff and lava and andesite lava

Tertiary intrusive rocks—Granite and granodiorite

Mesozoic and Paleozoic rocks—Mainly sedimentary rocks but includes mafic lava flows

Precambrian rocks—Granite

Contact

Topographic margin of Turkey Creek caldera

Structural margin of Turkey Creek caldera

Fault

Figure 1 (above and facing page). Location of the Turkey Creek caldera and important geographic and geologic features in the Chiricahua Mountains area, Cochise County, Arizona. *A*, Area location, roads, and important geographic features. *B*, U.S. Geological Survey quadrangle names in the area and existing geological maps (cited in parentheses). *C*, Generalized geology.

Du Bray and Pallister, 1995

What we'll see in the monument north of the caldera is one of the thickest and most complete sections of the Rhyolite Canyon Tuff. Things to notice in the tuff itself include the compressed pumice fragments called fiamme (flame). These appear as flattened and elongated white inclusions in the background ash. The ash itself is composed of microscopic pieces of volcanic glass and crystal fragments (mostly quartz and sanidine, a high T K-feldspar). Some of the most unusual features are fossil fumaroles, preserved vertical steam vents. We may also see surge beds, caused by the first, smaller ash flows out of the vent. These are transient, unsteady flows that occur as pulses or a series of pulses with a rapid kinetic energy decay.

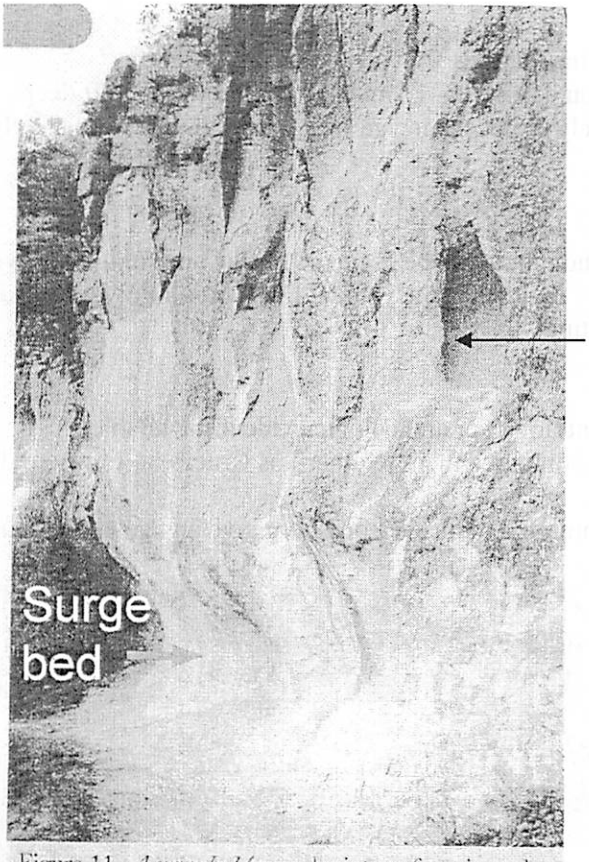

Figure 11. *A surge bed (arrow) mixture of pumice and fine ash that was ejected forcefully from a volcano. The surge bed grades upward into tuff, a mixture of ash, rock and crystal fragments, and pumice, from which the hot gases have escaped. The surge bed is softer than the tuff and is more easily eroded.*

From Bezy, 2001

Paleolake Animas
or
How I Wrote My Handout in 20 minutes
by
®

Glossary
Paleolake – a lake that once was but now isn't.
Paleoclimate – take a guess.
Playa – a big flat area where a lake once was.

Lake statistics
1) Three stages of shoreline features
2) At high stage (elevation 4195 ft.) – 17 mi long, 8 mile wide, 50 ft deep; 150 sq mi
3) Shoreline soils are likely Holocene in age while the high-stand was likely Pleistocene

Regional Features
1) Paleolake Animas is thought to be the drainage for the ancestral Gila river.
2) Current Animas Valley features include Giant Desiccation Polygons and Alkali deposits in a playa setting.

Shoreline dating
1) No radiometric, paleontologic, or archeologic evidence available.
2) Studied lake soils and compared them to other Las Cruces lakes where dates are known.
3) The discovery of mammoth remains in Lordsburg give an age upper bound of Pleistocene

All figures and info are from:
Fleischauer, H. L., Jr., and W. J. Stone. (1982) "Quaternary geology of Lake Animas, Hidalgo County, New Mexico." **New Mexico Bureau of Mines & Mineral Resources Circular**, 174,

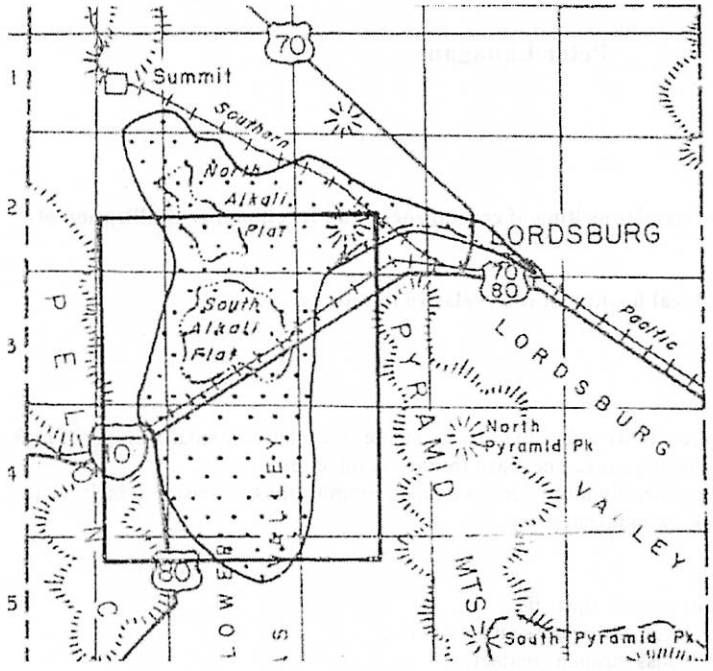

Upper Left: Map of AnimasValley area.

Bottom of page: Chronologies of similar western lakes.

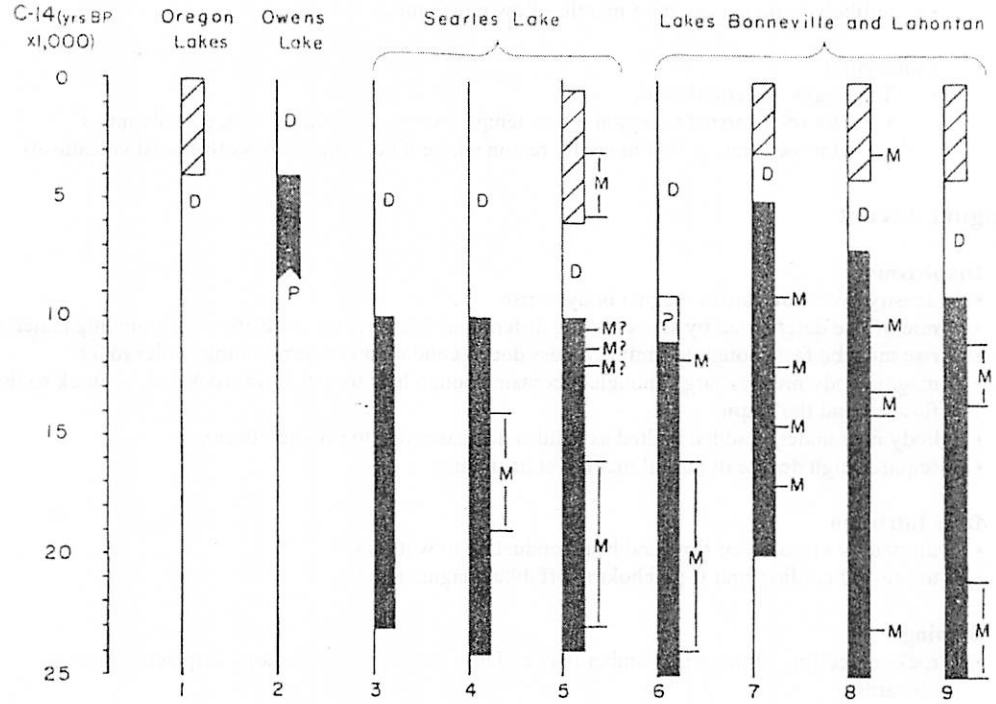

FIGURE 12—Synopsis of chronologies of some Quaternary lakes in the western United States. Solid bars span the duration of the late Wisconsinan lacustral interval. Cross-hatched bars span the duration of the middle and late Holocene lacustral intervals. M represents maxima or culminations of lake expansions; D represents dry periods or periods of extremely low lake level. Sources by columns are: 1) Van Winkle, 1914, 2) Gale, 1915, 3) Flint and Gale, 1958, 4) Stuiver, 1964, 5) Smith, 1979, 6) Broecker and Orr, 1958, 7) Broecker and Kaufman, 1965, 8) Morrison and Frye, 1965, 9) Benson, 1978. Columns 5-9 are summarized from time-space diagrams in the respective papers.

Mechanics of Silicic Volcanism

Peter Lanagan

Origin of Silicic Magmas

- **Magma produced as result of partial melting of crustal rocks and fractional crystallization of silicic melts**
- **Magma production requires local heating of rock relative to solidus**
- **Heat sources**
  - Radioactive heating
    - requires heat from radioactivity to be able to accumulate in a relatively small volume of rock
    - heat production must locally exceed heat lost through conduction
    - thermal conductivities generally lower for more felsic compositions, so easier to melt felsic rocks than mafic rocks via radioactivity
  - Viscous dissipative heating
    - heating from friction in viscous shear flow
    - heating is the product of the shear stress and strain rate
    - VDH countered by heat loss through conduction
    - unlikely to be important in mantle - flow rates limited by
  - Convection
    - Two ways this could work
      - Hot rock carried to region where temps. exceed the solidus, rock partialy melts
      - Hot rock transported to cooler region where it heats those rocks (bimodal volcanism)

Magma Ascent

- **Diapirism**
  - density inversion causes magma body to rise
  - rate of rise determined by size of body, differential density, and viscosity of surrounding material
  - rise must be fast enough to limit heat loss due to conduction to surrounding cooler rocks
  - magma body must be large enough to contain enough heat to soften wallrock and roofrock so they flow around the diapir
  - body may undergo added melted as solidus decreases due to pressure decrease
  - requires high degree of partial melting at beginning
- **Dike Intrusion**
  - limited by viscosity of flow and heat conduction to wallrock
  - to prevent cooling rind from choking off dike, magma must
- **Stoping**
  - rocks on ceiling of magma chamber may collapse and collect on bottom, displacing magma upwards
  - not really viable since volume of fallen rocks greater than unfallen rocks due to introduction of void spaces
  - volume increase of rock will likely choke off flow

Extrusion vs. Intrusion

- **As magma temperature decreases, crystallinity increases**
- **As crystallinity increases, viscosity increases**
- **If viscosity too high, magma will cease to flow**

- **Observational Limits**
  - mafic lavas have no more than 55% phenocrysts, suggesting magmas that have crystallized beyond this point are to viscous to erupt
  - critical crystallinity seems to decrease for more silicic magmas (~20%)

- **Thermal Probability**
  - Thermal probability (P_T): The probability of observing a magma at a particular temperature
  - If a magma body cools quickly through a temperature range, the chances of seeing the magma at that temperature is small
  - If a magma body spends a while in a narrow temperature range, the probability of seeing the magma at that temperature is high
  - Crystallizing phenocrysts will release latent heat which will tend to keep the magma at that temperature
  - P_T = thermal probability = dX/dT'
  - X = volume fraction of crystals
  - T' = (liquidus temperature - solidus temperature) / temperature
  - (T' = 0 when T = solidus temp.; T' = 1 when T = liquidus temp.)

- **Rheological Probability**
  - Rheological probability (P_R): The probability that a lava will be observed with a particular visosity
  - $P_R \sim 1$ at liquidus; $P_R \sim 0$ at critical crystallinity

- **Eruption Probability**
  - Eruption probability (P_E): The probability that an magma will erupt
  - $P_E = P_T P_R$
  - Since the critical crystallinity for granitic melts is much lower than that for mafic melts, P_E will be small, and the granitic melt will most likely form a pluton

Reference

Marsh, B.D. Mechanics and Energetics of Magma Formation and Ascension, in *Explosive Volcanism: Inception, Evolution, and Hazards*. 1984.

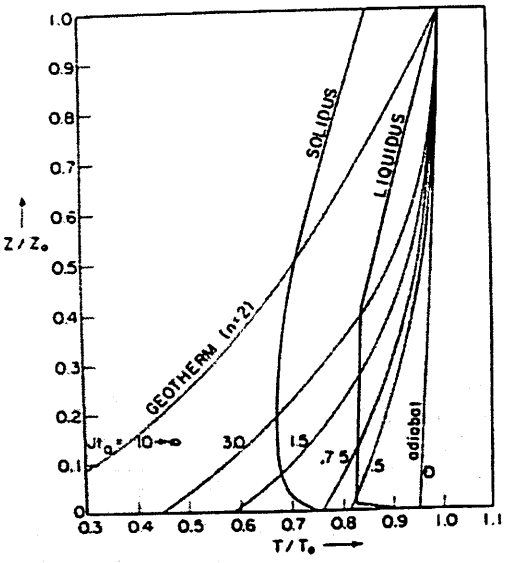

FIGURE 5.2 Cooling curves describing the average temperature (horizontal axis) in a magma ascending (depth, vertical axis) at a constant velocity by diapirism, stoping, or as a dike. The shape of the family of curves comes from the geotherm shown. As the ascent time decreases, the cooling curve approaches the adiabat. A representative solidus and liquidus for a magma containing about 1 wt. % water also is shown, and the magma is initially free of crystals (after Marsh and Kantha, 1978).

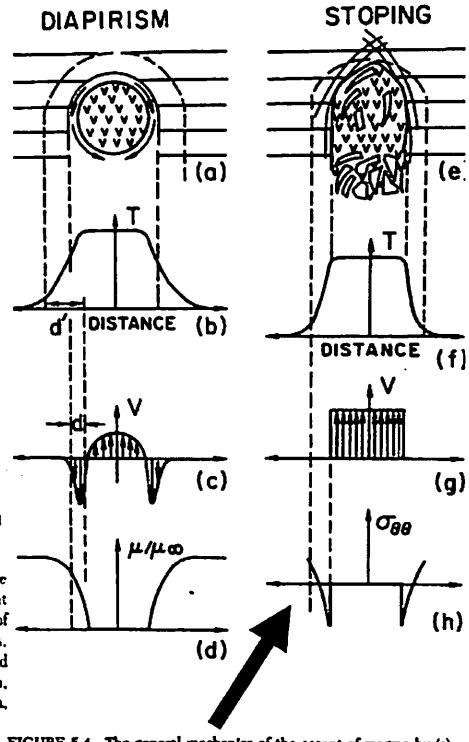

FIGURE 5.4 The general mechanics of the ascent of magma by (a) diapirism and (e) stoping, and their respective temperature fields (b, f), velocity fields (c, g), viscosity field (d), and thermal stress field (h) (from Marsh, 1982).

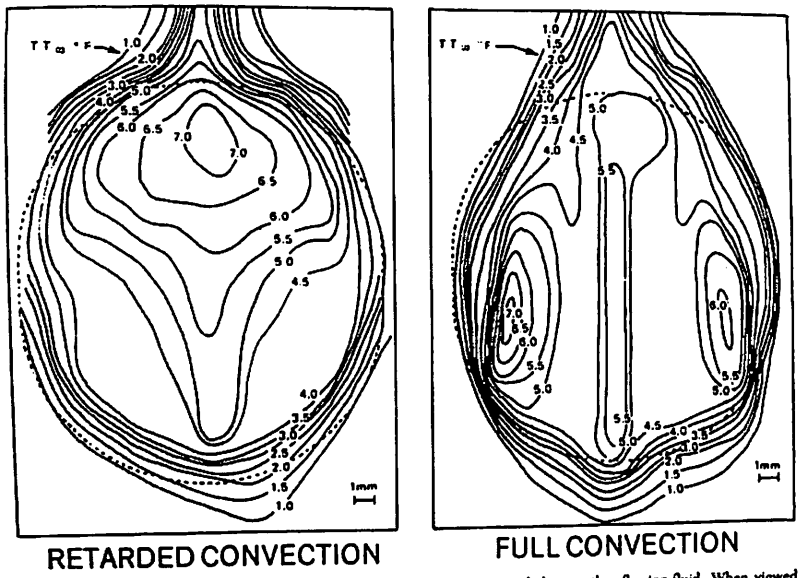

FIGURE 5.3 The distribution of temperature in a hot drop of fluid suspended in another flowing fluid. When viewed upside down, these temperatures should be analogous to those in an ascending diapir of magma. In one case the drop is not convecting (left), and in the other (right) it is convecting (after Head and Hellums, 1966).

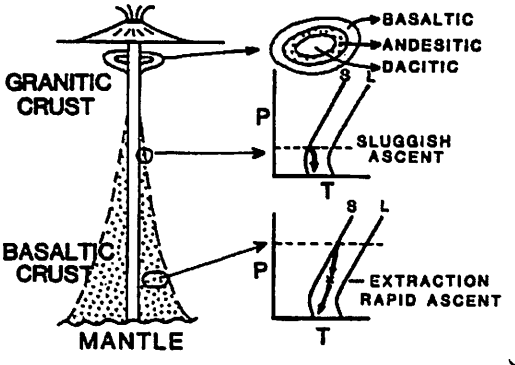

FIGURE 5.8 Magma production and extraction near a hot magmatic pathway leading to the formation of zoned plutons. The first magma to the surface is basaltic from a mantle source. Melting in the basaltic lower crust gives rise to a diapir ascending a considerable distance that allows extraction of an andesitic magma that continues to ascend and intrude the original basalt. Later partial melting in the upper granitic crust produces a sluggish (small-density contrast) diapir that may not ascend far enough to allow melt extraction, yet this body may intrude the others, forming a zoned pluton.

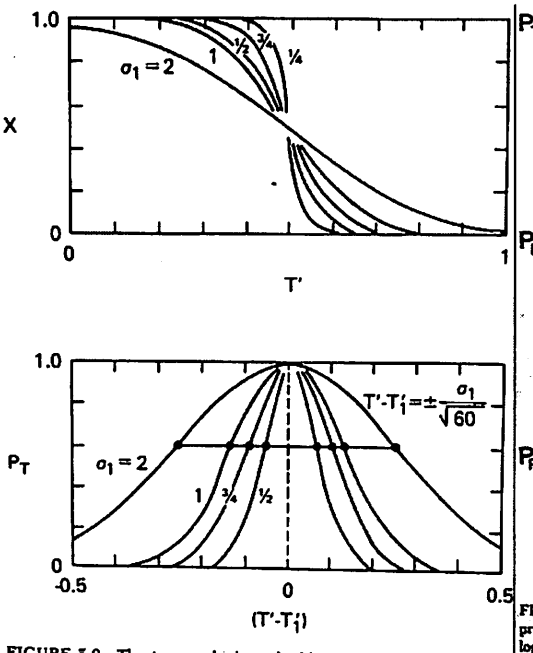

FIGURE 5.9 The top graph shows buildup of crystallinity (X) with decreasing temperature (T') that can be described analytically by the error function with an appropriate value of σ_1. For small σ_1, most crystallization occurs over a narrow temperature range. The probability of finding the magma at any temperature between solidus ($T' = 0$) and liquidus ($T' = 1$) is given by the slope of the curve at that temperature. These *thermal probabilities* (P_T) are given in the bottom graph. The most probable temperature at which to find the magma is when crystals are appearing most rapidly. The standard deviation about this most probable state also is shown.

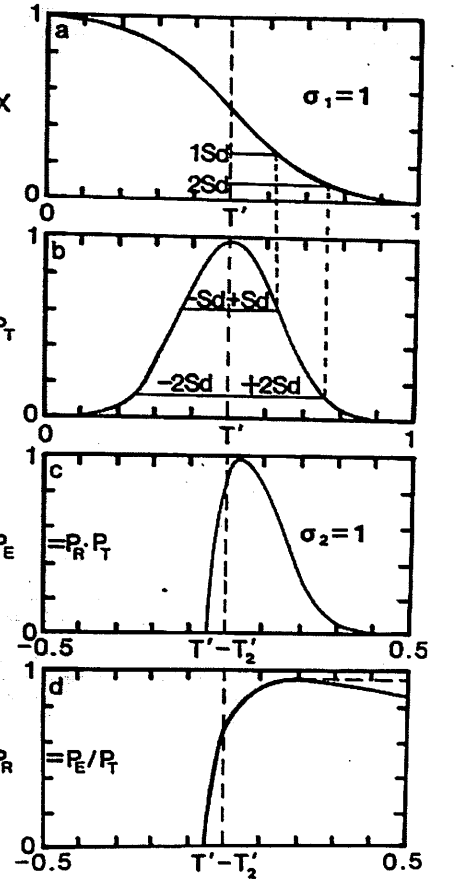

FIGURE 5.10 Relationship between the crystallinity (X), the thermal probability (P_T), the eruption probability ($P_E = P_R P_T$), and the rheological probability (P_R). (The crystallization for the ± 1 and the ± 2 standard deviations from the most probable P_T also are shown.) The rheological probability describes the viscous state of the magma with respect to its ability to be erupted. Near its liquidus there is no rheological constraint on eruption, but near a crystallinity of 0.55 (for a basaltic magma) the crystals approach closest packing, causing a drastic increase in viscosity and a precipitous decrease in P_R. The overall ability to be erupted (i.e., eruptions probability, P_E) is given by $P_R P_T$, and it should be measured by the observed histogram of lava crystallinity. If a magma cools to $X > 0.55$ it goes on to become a pluton. For granitic magmas the critical P_R is at lower degrees of crystallinity ($X \approx 0.20$), and the probability is great that the body will form a pluton.

Joint formation in welded tuffs

by Brandon Preblich

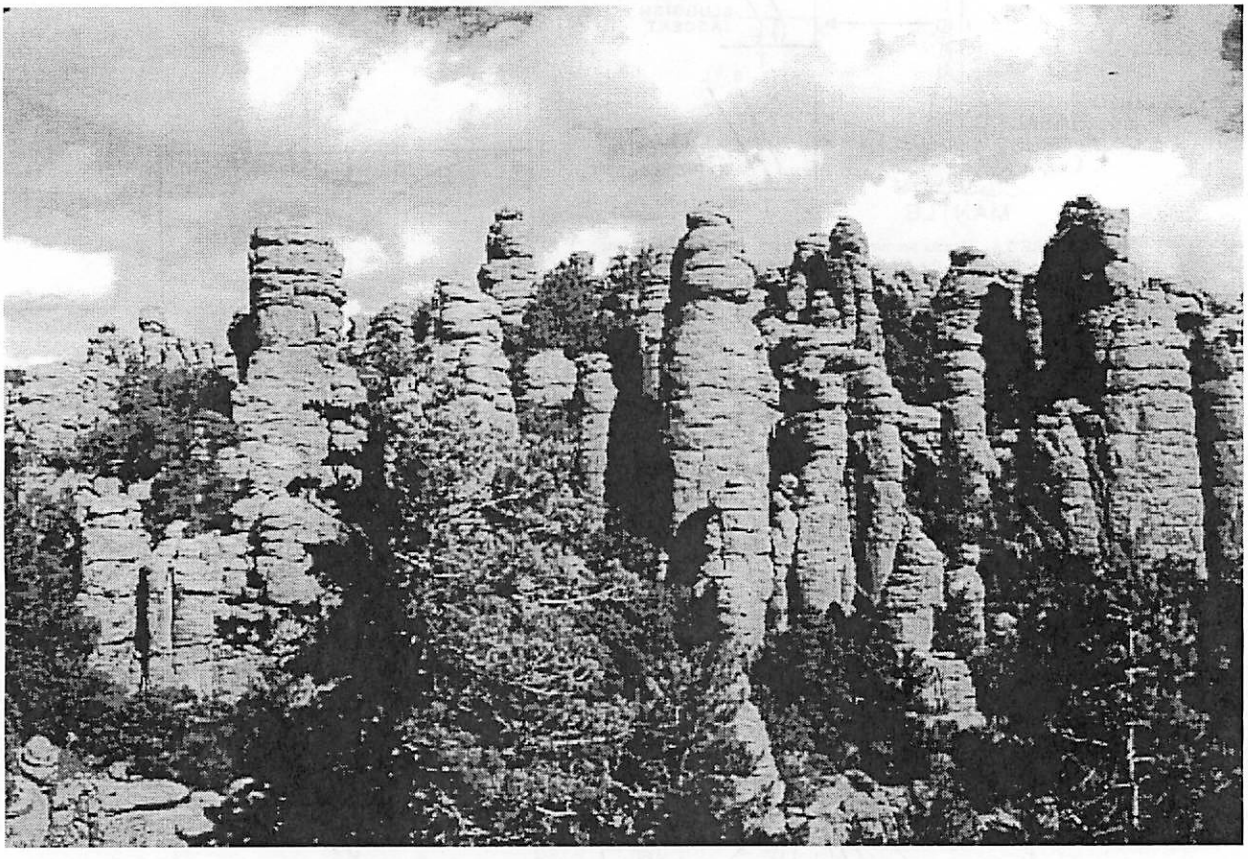

FIGURE 1 – *Joint formation in welded tuffs create rock spires in the Chiricahuas*

- **Joints**: Fractures in rock along which no appreciable movement has occured
- **Welded tuff**: Volcanic ash hardened by the welding together of its glass shards under the combined action of the heat retained by particles, the weight of overlying material, and hot gases

- In short, what is happening here is that the welded tuff undergoes jointing and subsequent erosion, until the welded tuff is shaped into the spires we see (Fig 1)

How were the spires created?

FIGURE 4 – *Polygonal columns in lava flows, similar to those in ash flows, except ash flows have 4 sided polygons*

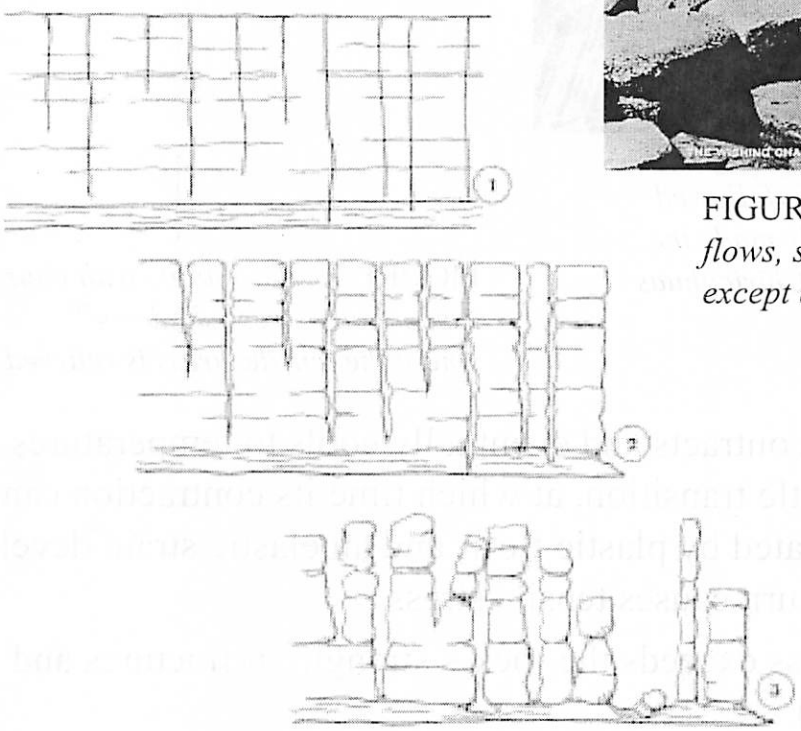

FIGURE 3 – *Spires form from erosion along joints*

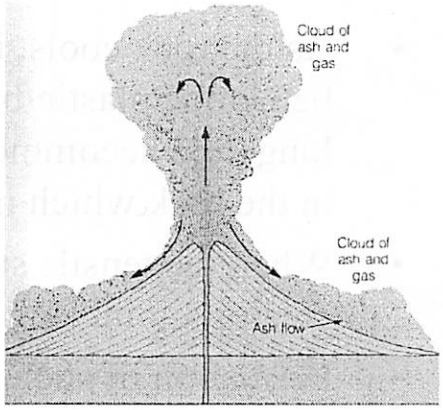

FIGURE 2 – *Diagram of an ash flow*

- Hot volcanic ash flows which come to rest are fused into rock called volcanic tuff (Fig 2)
- As the ash unit cools, it contracts and joints begin to form (Fig 3)
- The joints are perpendicular to the cooling surface and parallel to cooling fronts that move through the ash (thus the joints are vertical)
- The joint spacing is indicative of how long it took the ash to cool (cool quickly = small spacing; cool slowly = large spacing), and can range from a few cm to more than 3 m in diameter, and up to 30 m in length

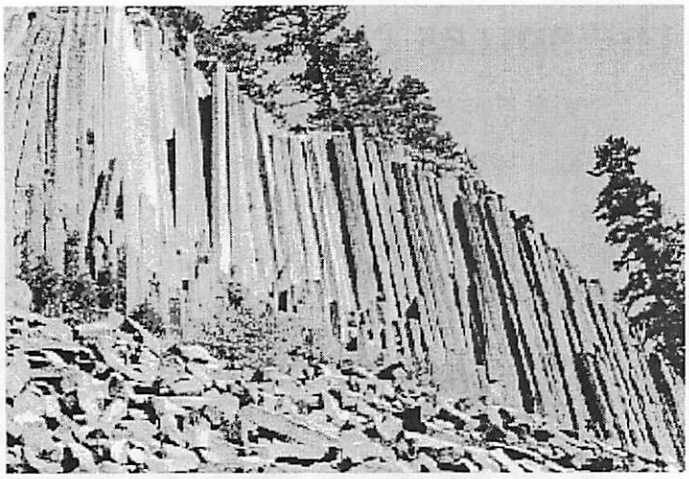

FIGURE 5 – *Columnar jointing, which is the same process (followed by erosion) that eventually made the rock spires we see in the Chiricahuas*

FIGURE 6 – *Tensile stresses open joints that are perpendicular to the direction of pulling*

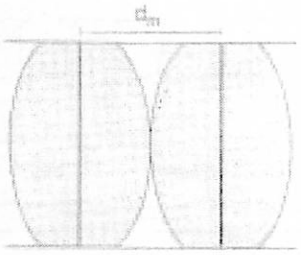

FIGURE 7 – *Two joints with their associated "stress shadows", where the tensile stress is relieved*

- As the rock cools, it contracts and eventually cools to temperatures below the plastic/brittle transition, at which time its contraction can no longer be accommodated by plastic flow, and an elastic strain develops in the rock which in turn causes tensile stress
- When the tensile stress exceeds the rock's strength, it fractures and creates a joint (Fig 6)
- Formation of such a joint relieves the tensile stress for a characteristic distance (Fig 7)
- The columns grow in bands (Fig 1)
- Since the flow cools from the outside in, the bands form from the top down and the bottom up, but since the bottom is warmer, they meet below the middle of the flow
- Cross joints (horizontal ones cutting across the vertical joints) aid erosion of these columns in making the spires
- Weathering and erosion widen these joints, and erode along zones of weakness
- Spires, "totem poles" and balanced rocks will form due to further erosion

Planetary Connection: Mars

- Somewhere in the numerous lava flows on Mars one would expect to see columnar jointing
- In their 2003 LPSC abstract, Moses, Lazlo, Alfred, and Windy suppose that if volcanic eruptions on Mars trigger water outflows, this water may follow the same paths as the lava and consequently flow over some hot lava flows
- This would cool the lava flow very quickly: the water would sink into the flow and take away heat through boiling and evaporation of the water, thus quickly cooling the lava and creating joints in these lava flows
- Their idea is that if they can observe jointing on Mars, or at least observing the blocks falling from the frozen lava, they can model the amount of water it took, and thus provide a lower limit on the amount of liquid water available on Mars at the time of eruption of the lava

References

-Chronic, H. (1995) Roadside Geology of Arizona. *Mountain Press Publishing Company.*

-Davis, G.H. & S.J. Reynolds (1996) Structural Geology of Rocks and Regions. *John Wiley & Sons, Inc.*

-Long, P.E. & B.J. Wood (1986) Structures, textures, and cooling histories of Columbia River basalt flows. *Geological Society of America Bulletin.* v. 97, pp. 1144-1155.

-Milazzo, M.P., L.P. Keszthelyi, A.S. McEwen, W. Jaeger (2003) The formation of columnar joints on Earth and Mars, LPSC XXXIV.

-Pollard, D.D., A. Aydin (1988) Progress in understanding jointing over the past century. *Geological Society of America Bulletin.* v. 100, pp. 1181-1204.

-van der Pluijm, B.A., S. Marshak (1997) Earth Structure, *WCB/McGraw-Hill*

-Williams, H. & A.R. McBirney (1979) Freeman, *Cooper and Company.*

Jonathan Fortney, in association with the LPL Spring Field Trip '03, presents:

Inverted Pendulum Paleoseismometers
or
This Pretty Cool Way to Constrain Ground Motion Over Fairly Long Timescales by Looking at Precariously Balanced Rocks

Precariously balanced rocks are quite useful in placing constraints on the ground motion (acceleration) during the lifetime of the balanced rock. If it can be estimated what ground acceleration would have toppled a rock some time since its formation, and since the rock is still there, you can obtain a rough upper limit on ground acceleration. Since historical records of earthquake ground motions do not go very far back in time, this method is an interesting and valuable way of trying to get a grasp of the relationship between earthquake strength and frequency.

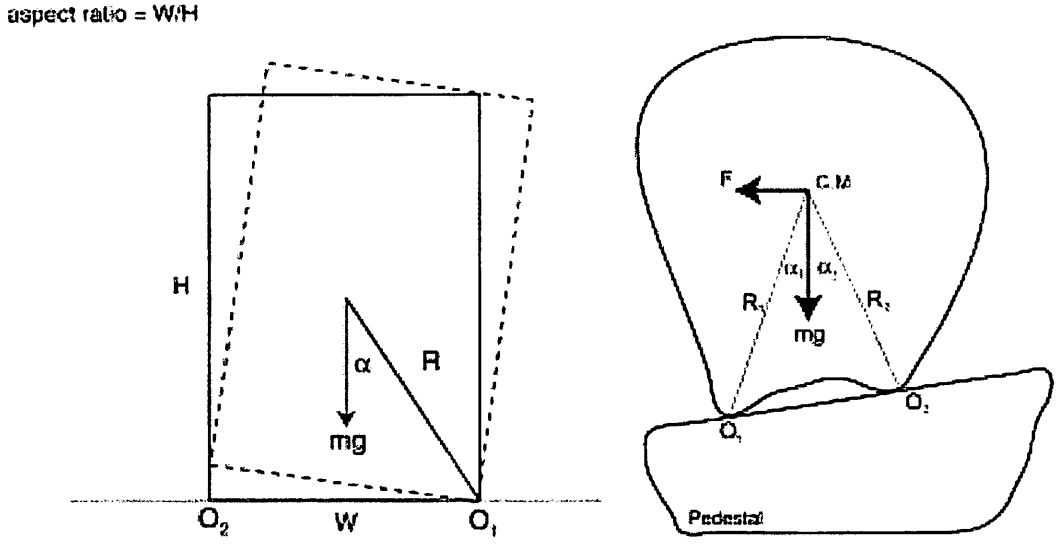

Rock parameters, such as the location of the center of mass, angles between touch points, and distances to different points, are measured (or estimated) in the field, or after-the-fact from photographs.

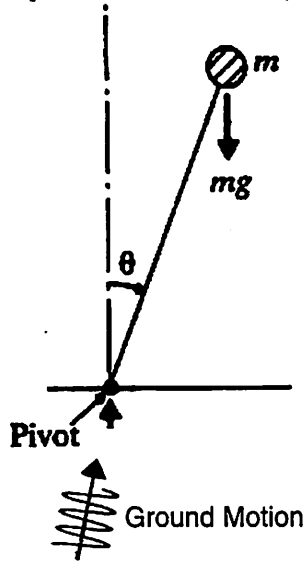

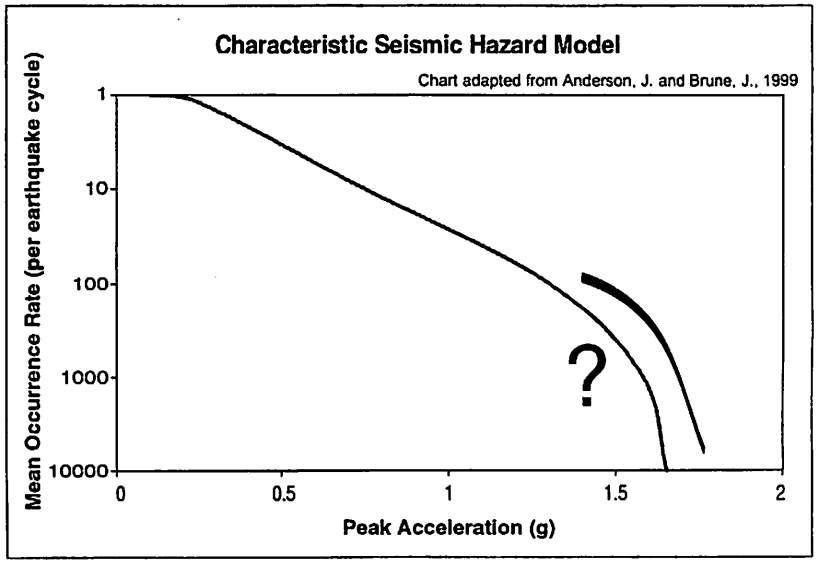

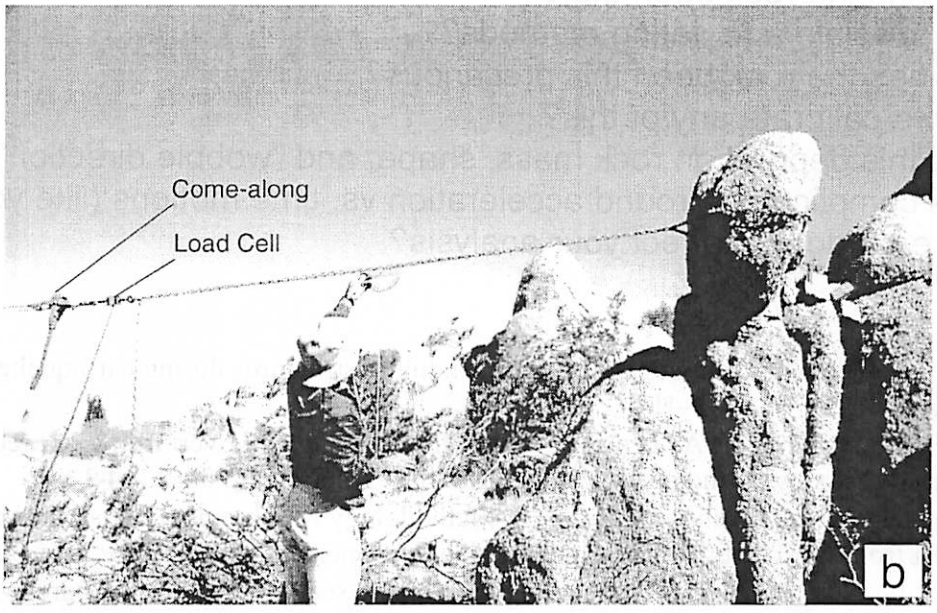

Figure 3. The pulling technique to measure the quasi-static toppling force. The force is increased to a maximum value at which point the rock begins to rotate as the applied horizontal force decreases in magnitude.

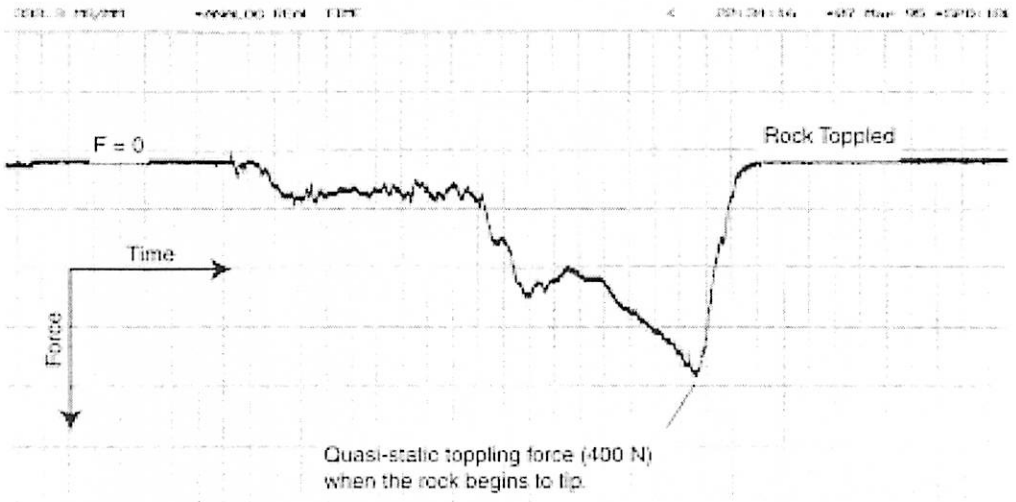

Figure 4. Strip chart record of a field experiment to determine the quasi-static toppling force of a precarious rock.

Issues to worry about:
How long has the rock been there?
What are possible age dating methods?
How long has the rock been this precarious?
How can we calibrate any of this?
How does this depend on rock mass, shape, and "wobble direction?"
How does complicated ground acceleration vs. time motions (like you'd get in an actual earthquake) affect your analysis?

FYI:

- Housner, GW. The behavior of inverted pendulum structures during earthquakes. Bull. Seism. Soc. Am., 1963, 53, 403-417.
- Shi, B, Anooshehpoor, A, Zeng, Y, Brune, JN. Rocking and overturning of precariously balanced rocks by earthquakes. Bull. Seism. Soc. Am., 1996, 86, 1364-1371.
- Anooshehpoor, A, Brune, JN, Zeng, Y. Methodology for obtaining constraints on ground motion from field tests of precariously balanced rocks, *Bull. Seism. Soc. Am.* 2002.
- Brune, J., 1999, Precarious rocks along the Mojave section of the San Andreas Fault, California: constraints on ground motion from great earthquakes, *Seismological Research Letter*s, 70:1, pp.29-33
- Bell, J., Brune, J., Liu, T., Zreda, M. and Yount, J., 1998, Dating precariously balanced rocks in seismically active parts of California and Nevada, *Geology*, 26:6, pp.495-498
- Anderson, J. and Brune, J., 1999, Probabilistic seismic hazard analysis without the Ergodic Assumption, *Seismological Research Letter*s, 70:1, pp.19-28

The Great Sonoran Earthquake of 1887

Presented by Carl Hergenrother

Spring of 2003
LPL Field Trip

- This earthquake is known by numerous names: the Sonora, the Bavaspe, the San Bernardino Valley, the Pitaycachi, and I'm sure there are others.
- Date of occurrence: 03 May 1887
- Time of occurrence: around 3 pm
- Location: 30.8_ N, 109.1_, nearest to the city of Bavispe in the northern part of the state of Sonora, roughly 100 km south of Douglas, Arizona (Fig. 1).

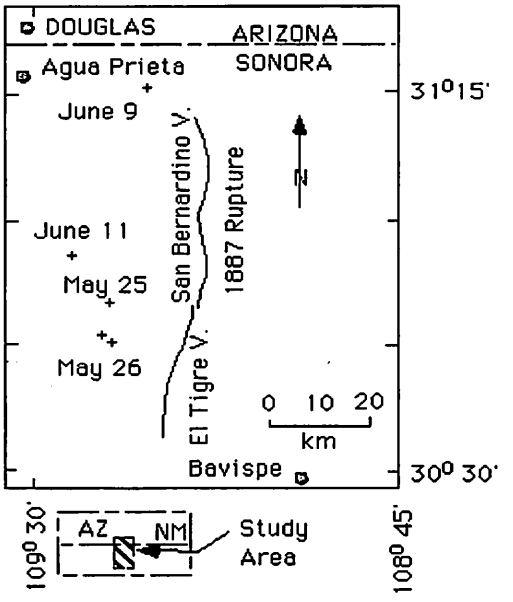

Fig. 1 - Location of Pitaycachi fault region. Solid line indicates surface rupture due to the 1887 earthquake. Dated crosses show location of swarm of recent "aftershocks" in 1989. From Wallace and Pearthree article in Arizona Geology, vol. 19, no. 3, Fall 1989, pp. 6-7.

- Magnitude: M = 7.2 to 7.4
- The quake was felt over an area of roughly ~2000000 sq. km, a region loosely bound by the cities of Yuma, Arizona; Santa Fe, New Mexico; El Paso, Texas; and Mexico City, Mexico (Fig. 2).

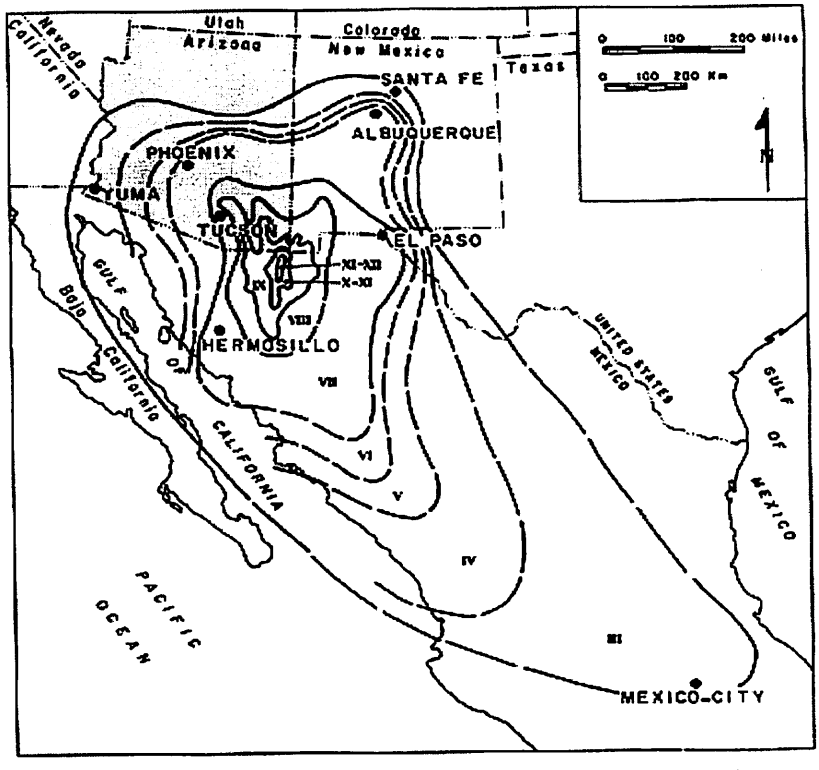

Fig. 2 - Area experiencing effects of the 1887 earthquake. The intensity value is denoted by the roman numeral. Tucson experienced an intensity of VII, the Chiricahua Mountains an intensity of IX, while the peak near the epicenter was a XI-XII. From Wallace and Pearthree (1989).

- Ruptured a long stretch (~80 km) of the Pitaycachi fault from just west of Bavispe, Sonora due north to to within ~20 km of the Arizona border (Fig. 1).
- There was much damage in the city of Bavispe, many roofs collapsed, the church was destroyed and over 42 people died.
- The quake produced many avalanches and landslides in the mountains throughout Sonora and southern Arizona.

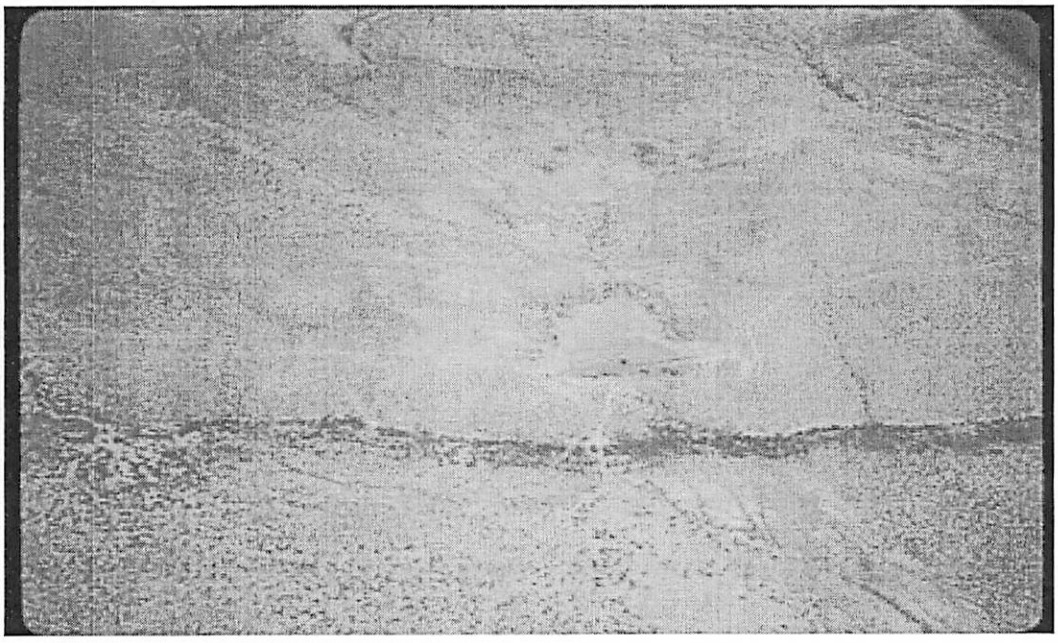

Fig. 3 - Aerial view of the surface rupture due to the 1887 earthquake in Sonora. Notice the enhanced vegetation growing along the rupture.

- In the Huachuca Mountains, "great boulders began crahsing down the mountain gulches, breaking trees and carrying havoc down to the valley below" (DuBios, S. M. Arizona Earthquakes, 1776-1980. University of Arizona, Tucson, AZ, 1982).
- Prominent aftershocks felt in southern Arizona on the following May 30, Nov. 11, and July 25, 1888.
- Aftershocks from the 1887 quake may still be occurring, a swarm of small (up to M = 4) quakes occurred in the spring and summer of 1989 (see Fig. 1).
- The Pitaycachi fault ruptures infrequently, roughly ever 100,000 years. Lengthy recurrence intervals typically have long protracted periods of aftershocks.
- The May 1887 earthquake was the largest historical earthquake in the southern Basin and Range province.

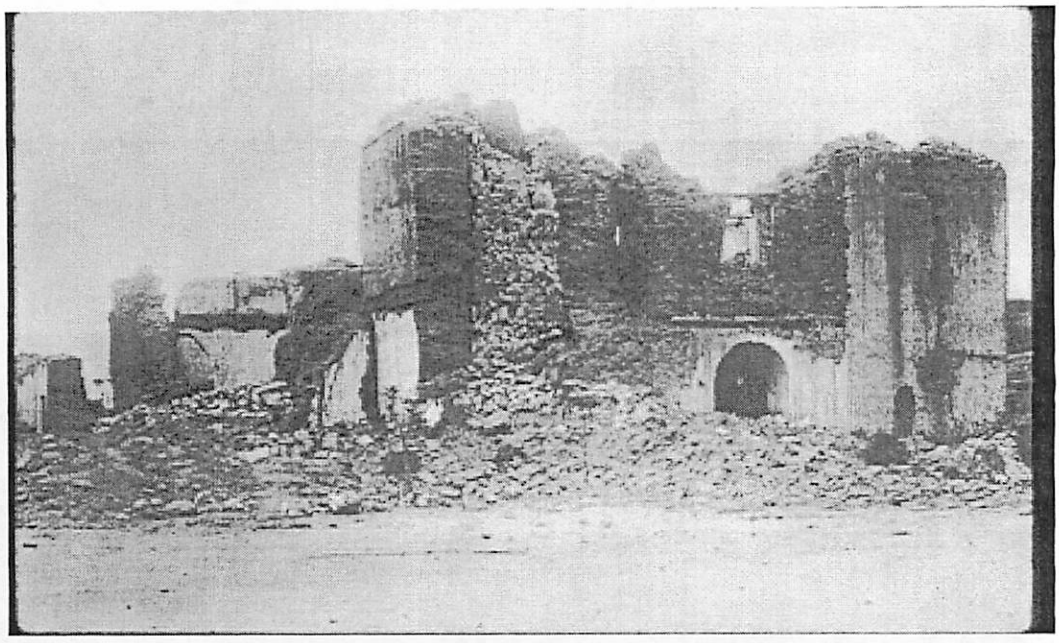

Fig. 4 - A building in Bavispe, Sonora, Mexico, destroyed during the 03 May 1887 earthquake.

Uplift of The Colorado Plateau and the Mogollon Rim

Overview of the Colorado Plateau:

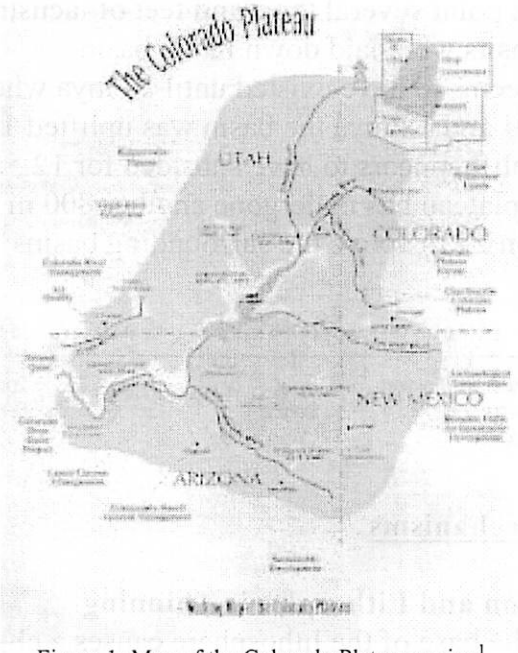

Figure 1: Map of the Colorado Plateau region[1]

The Colorado Plateau is a major tectonic and physiographic province in the southwestern United States. The plateau encompasses approximately 360,000 km^2, covering large portions of Arizona, Utah, New Mexico, and Colorado. Elevations on the Plateau range from 3,000 to 14,000 ft, with an average elevation of 5,200 ft (~1600 m)[2]. While the plateau has been relatively stable during Phanerozoic time (recent geologic time), it underwent up to 2 km of uplift throughout the Cenozoic[2].

Geophysics of the Plateau:

Seismic data suggests that the crust of the Colorado Plateau is 45 km thick, substantially thicker then the crust of the adjacent Basin and Range province south of the Plateau. Despite being uplifted 2 km, it is believed that the crust has been in approximate isostatic equilibrium both before and after the uplift occurred. Heat flow within the plateau is not significantly different from expected continental crust (55-65 mWm^{-2}), however evidence suggests a relatively high upper mantle temperature[3].

Geologic History of the Colorado Plateau

During the late Cretaceous period (144 mya), the region that was to become the Colorado plateau was close to sea level as evidenced by extensive deposits of Mancos shale. Around 80 mya the Laramide orogeny transformed the shelf region into a low basin surrounded by newly forming mountains. At this point several thousand feet of lacustrine (lake) and fluvial (river) deposits were laid down in the basin.

This basin seems to have existed until 24 mya when a period of uplift began. Between 24 and 18 mya the basin was uplifted 1.1 km above its previous floor. Uplift appears to have subsided for 12.5 mya. In the past 5.5 mya however, the plateau has undergone another 800 m of uplift, reaching its current elevation 2 km above the surrounding basins[3].

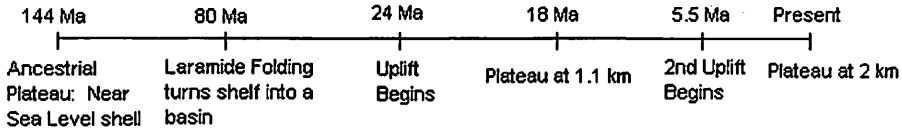

Possible Uplift Mechanisms

Thermal Expansion and Lithospheric Thinning

Heating of the base of the lithosphere causes a change in the thermal gradient thus effectively causing the lithosphere to thin. Decreasing lithospheric thickness generates buoyant uplift. (Requires 70-130 km of thinning)[3].

Specific Mechanisms:

-Heating by mantle plumes, heating due to subduction of ridge.

Crustal Thickening

Increasing the crustal thickness leads directly to isostatic uplift due to density changes. (Requires 13-22 km of thickening)[3].

Specific Mechanisms:

-Underplating of low angle subduction.

Mantle Phase Changes

Anhydrous or hydrous phase change basically converts mantle to crustal material and crustal thickening occurs[3].

Specific Machanisms:

-Expansion accompanying partial melting

The Mogollon Rim

Overview

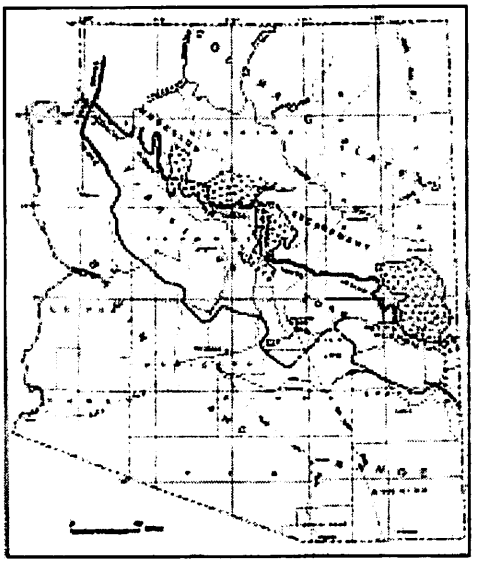

Figure 2: The Mogollon Rim including transition zone[4]

The Mogollon Rim is a 500 km long more or less continuous escarpment that trends northwest / southeast across Arizona and into western New Mexico. The geomorphic features associated with the Rim are highly variable depending on locality, ranging from 2,000 ft cliff faces in the central region to more subdued stratigraphic offsets near in the White Mountains area. The Rim is a direct consequence of the Colorado Plateau uplift, and is traditionally thought to mark the boundary between the Colorado Plateau to the north and the Basin and Range province to the south[4].

Basic Stratigraphy* [5,6]

Chinle Formation – Generally composed of Triassic aged shales
Moenkopi Formation – More Tiassic shales
Kaibab Formation – Generally composed of Permian limestones
Coconino Sandstone – Permian sandstone of eolian origin
Supai Formation – Pennsylvanian and Permian redbeds of shales, sandstones and conglomerate.

---

* This is a very generalized stratigraphy. Thus formations may or may not be present at a given locality.

A Transition Zone?

In reality, the Mogollon Rim does not represent a sharp boundary between the two physiographic regions. Instead, a complicated transition zone exists along the boundary. This transition zone is 80 km wide on average and is characterized by extensive exposures of bedrock separated by alluvial basins[7].

-Mike Bland

References:

[1] http://www.geo.arizona.edu/geos256/azgeology/cpif.html

[2] Foos, A. Geology of the Colorado Plateau. http://www.aqd.nps.gov/grd/edu/foos/plateau.pdf

[3] Morgan, P. and Swanberg, C. On the Cenozoic uplift and tectonic stability of the Colorado Plateau. *Journal of Geodynamics*, **3**, pp. 39-63, 1985.

[4] Peirce, W. The Mogollon escarpment. *Field Notes from the State of Arizona Bureau of Geology and Mineral Technology*, v. 14, 2, pp. 8-11, 1984.

[5] Blakey, R. Stratigraphy and geologic history of Pennsylvanian and Permian rocks, Mogollon Rim region, central Arizona and vicinity. *Geological Society of America Bulletin*, v. 102, pp. 1189-1217, 1990.

[6] The Mogollon Rim. *New Mexico Geological Society Field Conference #13*, 1964.

[7] Peirce, W. Arizona's backbone: the transition zone. *Field Notes from the State of Arizona Bureau of Geology and Mineral Technolog*, v. 15, 3, pp. 1-6, 1985.

Planetary Analogs for the Colorado Plateau
by Gwendolyn D. Bart
April 25, 2003, 4:35 pm

Venus, from Phillips and Hanson:

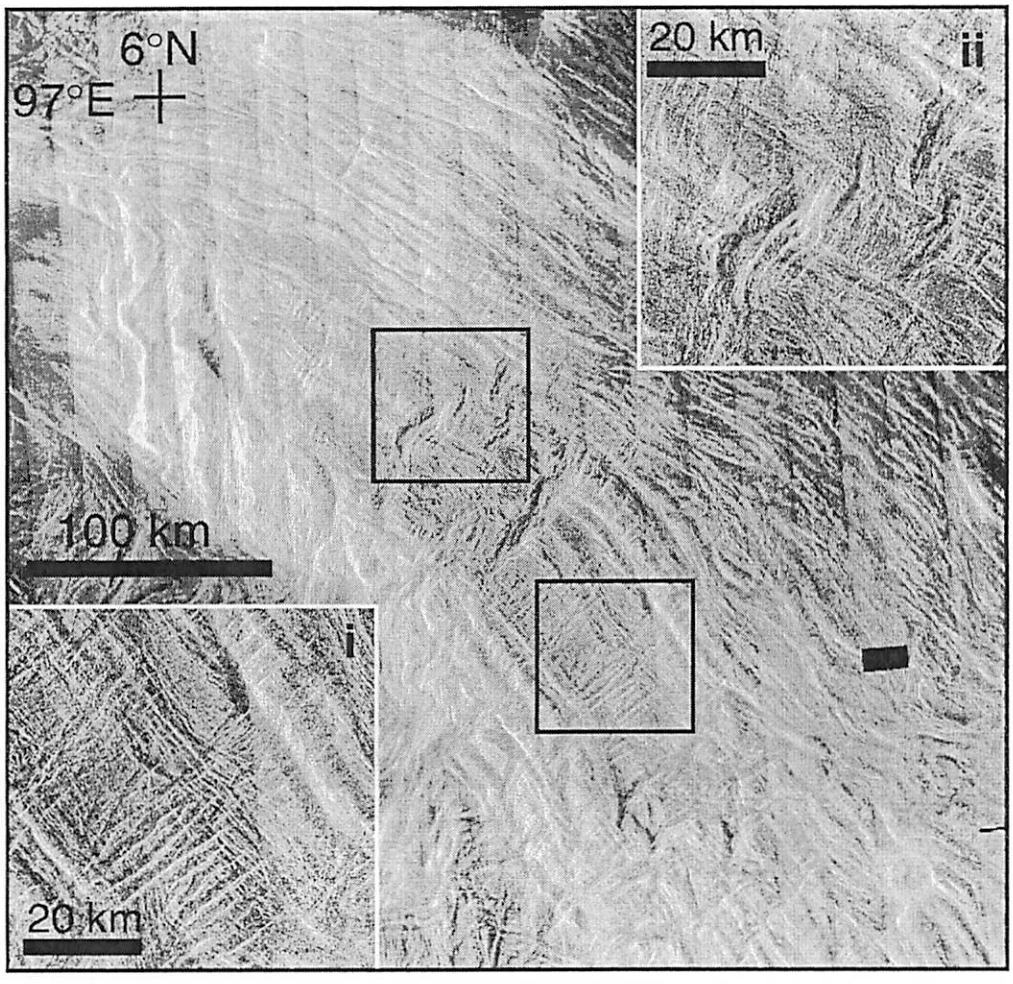

Fig. 1. Crests of NW-trending folds are cut by NE-trending lens-shaped graben. Ribbons parallel graben although they differ in structural style and geometry (insets). Ribbons (**i**) are marked by bright and dark paired lineaments >50 to 100 km long; these lineaments define alternating, flat-topped ridges and narrow, steep-sided, flat-bottomed troughs. In contrast, graben (**ii**) host numerous accommodation structures, they have aspect ratios of 3 to 4 rather than >50, their walls are sloped inward ~60°, and they are lens-shaped with the widest part of the graben superimposed on fold crests.

Mars:

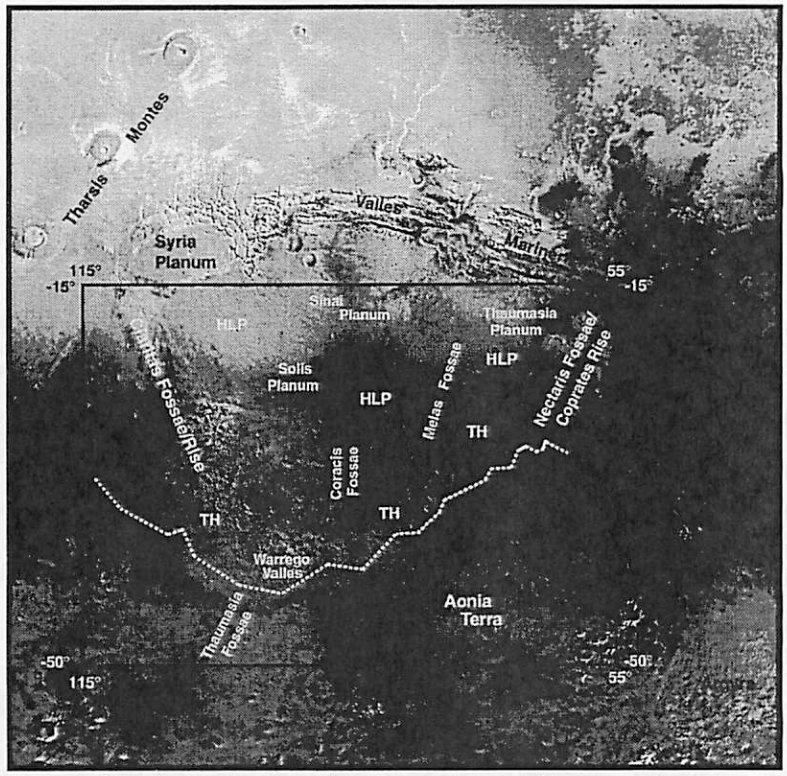

Fig. 1. Index map showing the Thausamia region (boxed area) of Mars. This region is dominated by the Thaumasia plateau (southern edge of plateau is dashed), which includes the high lava plains (HLP) of Syria, Sinai, Solis, and Thaumasia Plana and the partly surrounding Thaumasia Highland (TH) that is fractured by Thaumasia, Claritas, Coracis, and Nectaris Fossae and marked by mountain ranges (Coprates Rise, for example, is a mountain range that forms the eastern margin of the plateau).

Arizona Silicic Volcanism and the Mogollon - Datil Volcanic Field - Ages and Extent

Matt Pasek

Multiple volcanic events have occurred throughout the geologic history of Arizona. Mountains have been born, continents have collided and been ripped apart, and plumes from the mantle have burst through the crust. Most of the volcanic and igneous rocks have been covered by recent alluvium deposits.

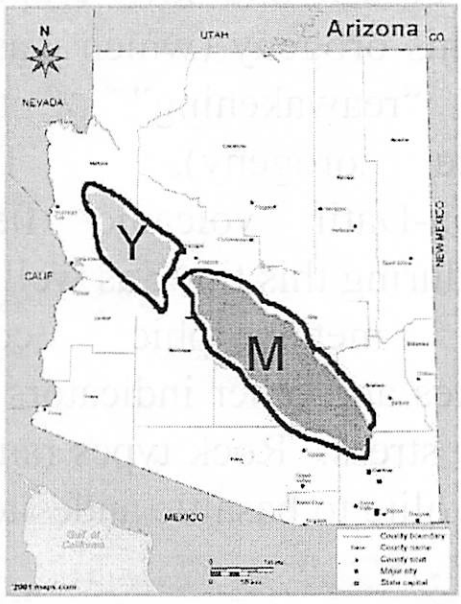

Matatzal and Yavapai Orogeny and related rocks (1400 - 1800 Ma): Two distinct provinces separated by the Moore Gulch Fault. Both units were formed during orogenic events, albeit at separate times. Rock types include granites and rhyolites. Rocks in SE AZ were also formed during this time, and are generally equivalent to the Matatzal volcanics.

Triassic and Jurassic (144 - 245 Ma) silicic volcanic rocks crop out sporadically through SE AZ. Most are undifferentiated and often occur with sedimentary units.

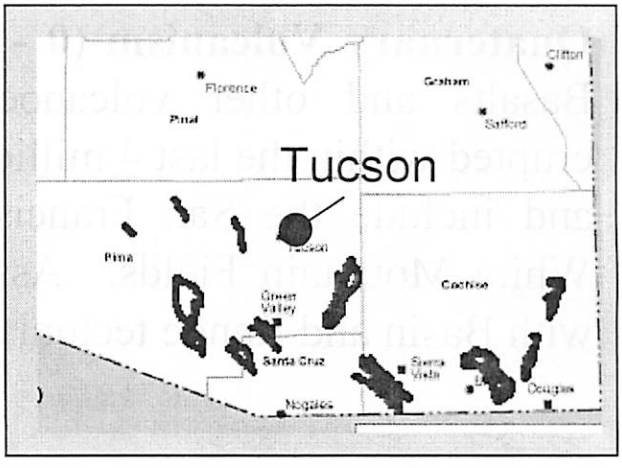

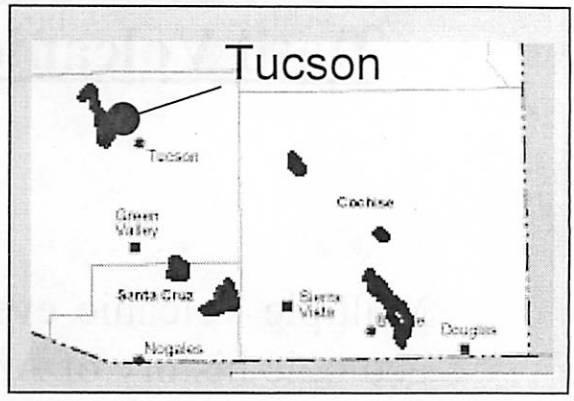

Larimide Orogeny (50 - 75 Ma). The subduction of the Pacific plate caused lots of volcanism in Arizona, especially to the SE. Many plutons were emplaced (like Kitt Peak) as well as vast granitoid batholiths. Much evidence of the Laramide orogeny has been over- printed by the subsequent Basin and Range faulting. Many AZ copper porphyry deposits were formed during this orogeny.

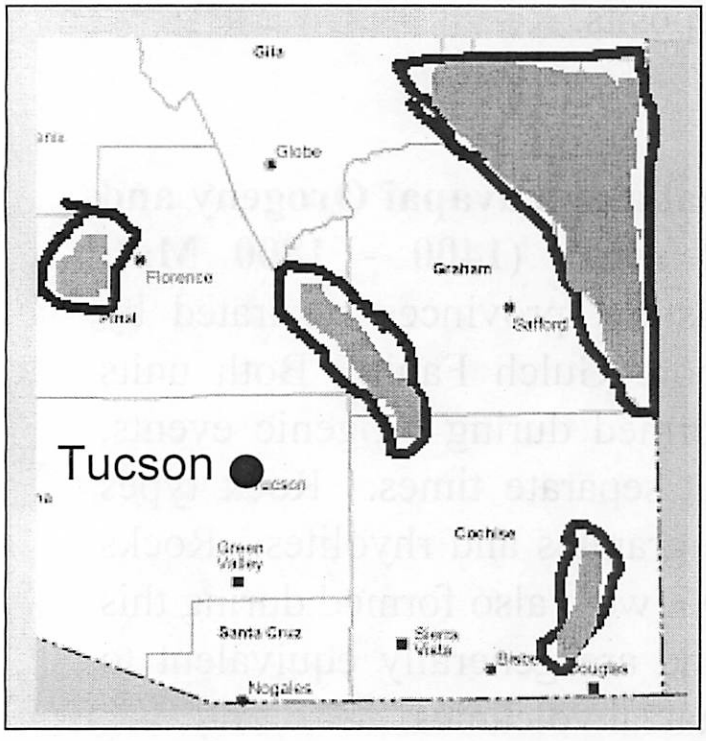

Mid-Tertiary Orogeny volcanic sequence (15 - 38 Ma). A large volume of ash and lava erupted during this orogeny (which was a sort of "reawakening" of the Laramide orogeny). The Mogollon-Datil volcanic field formed during this time, as well as several metamorphic core complexes and other indicators of geologic stress. Rock types range from rhyolite to basaltic andesite.

Quaternary Volcanism (0 - 4 Ma). Basalts and other volcanoes have erupted within the last 4 million years and include the San Francisco and White Mountain Fields. Associated with Basin and Range tectonism.

The Mogollon-Datil Volcanic Field

The Mogollon-Datil Volcanic field covers an area approximately 20000 km2, from central-western New Mexico to Eastern Arizona, with an average thickness of 2-3 km. It was active between 15 and 38 million years ago, which corresponds to the standard period of active Basin and Range volcanism.

Recent research (Davis and Hawkesworth, 1995) indicates that there were three episodes of volcanism in the Mogollon-Datil region, and that the geochemical characteristics of these episodes give us insights into the properties of the crust and mantle at the time.

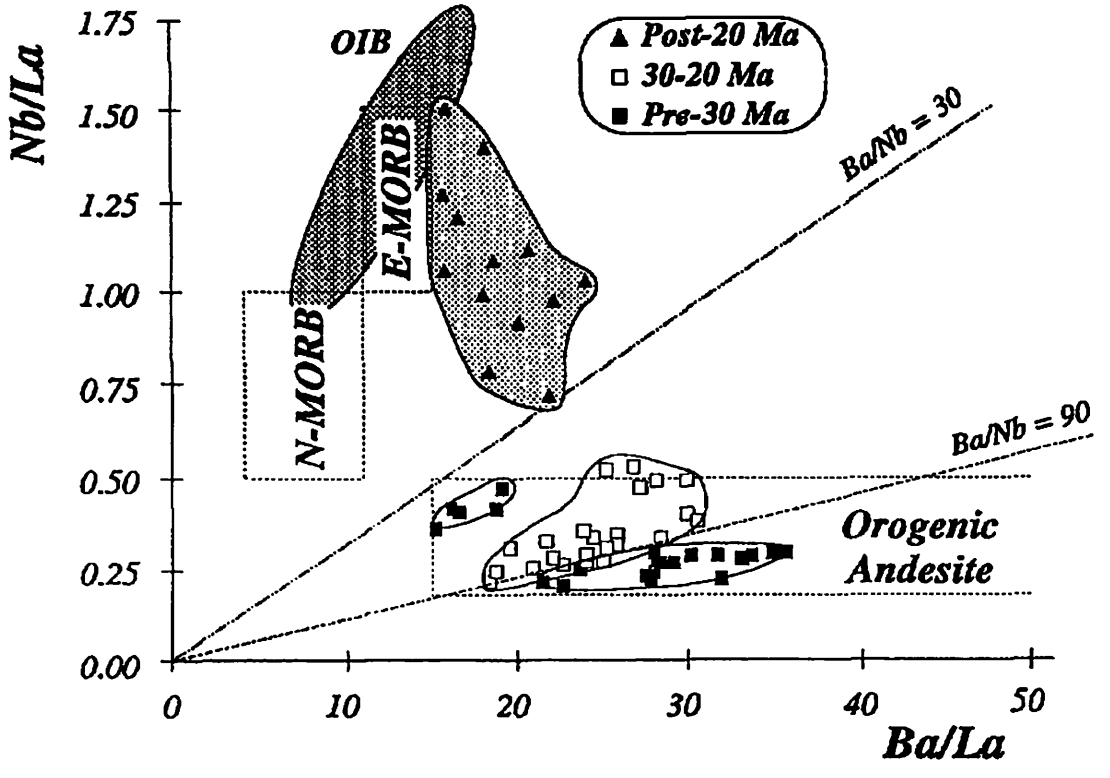

The three magma classifications are:

Pre-30 Ma: The rocks are broadly calc-alkaline, and have geochemical signatures that indicate they originated in the upper mantle.

20-30 Ma: These rocks were extruded during periods of maximum extension, and are probably the precursor to the Post-20 Ma rocks based on isotopic and trace element constituents.

Post-20 Ma: Derived from the asthenosphere based on geochemical characteristics, and seem chemically similar to ocean-island basalts.

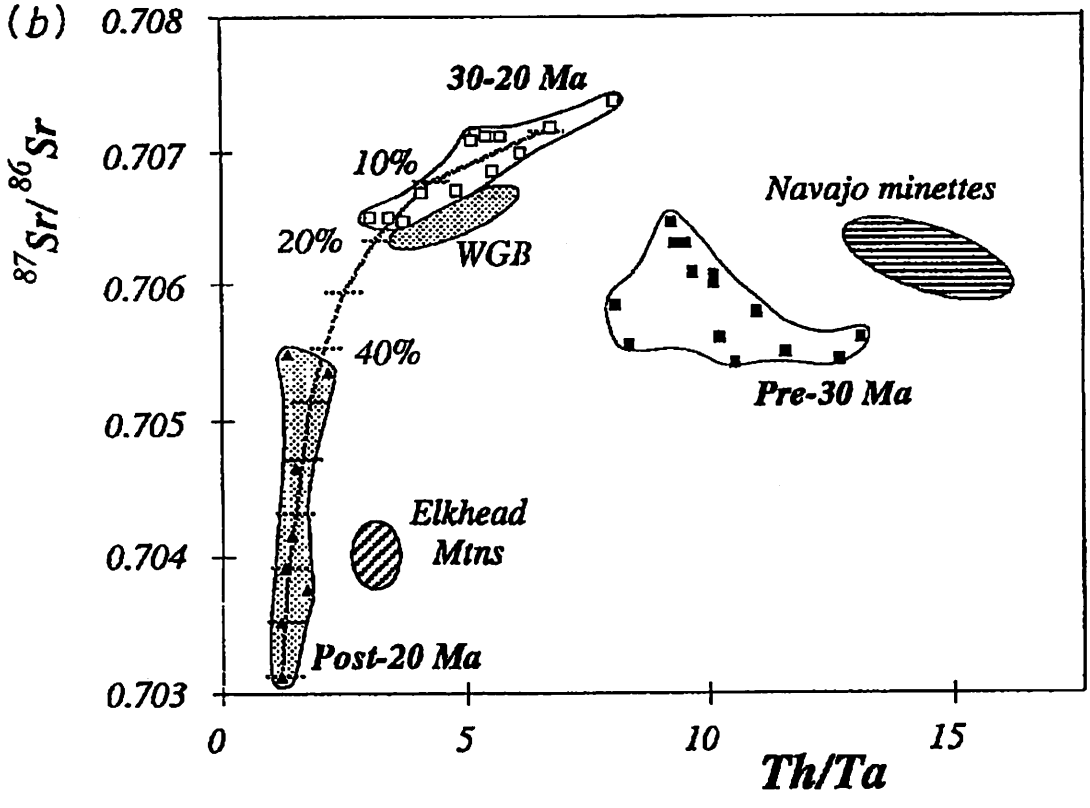

References:

Davis, J.M., and Hawkesworth, C.J., 1995, Geochemical and tectonic transitions in the evolution of the Mogollon-Datil Volcanic Field, New Mexico, USA, *Chemical Geology*, v. 119, p. 31-53.

Jenney, J.P., and Reynolds, S.J., 1989, Geologic Evolution of Arizona: Tucson, Arizona Geological Society Digest 17, p. 165-186.

Nations, D., and Stump, E., 1996, *Geology of Arizona*, Kendall/Hunt Publishing Company, Dubuque Iowa, 260 pp.

Porphyry copper deposits and the Clifton-Morenci mine

Hand out and presentation by Celinda Kelsey

Our entire society rests upon – and is dependent upon – our water, our land, our forests, and our minerals. How we use these resources influences our health, security, economy and well being. John F. Kennedy Feb. 23, 1961

porphyry copper – a kind of hydrothermal copper deposit associated with intrusive igneous rocks with porphyritic texture.

Porphyry coppers are unusually large for hydrothermal systems, influencing cubic kilometers of material around them. The primary ore mineral is chalcopyrite ($CuFeS_2$), but other copper sulfides, sulfates, oxides and even native copper will be found. There are also porphyry molybdenum and tin deposits.

The intrusions that porphyry deposits are associated with are typically arc magmatism controlled by the subduction of tectonic plates. (Mitchell & Carlile)

The Clifton-Morenci mines lie where Tertiary granite porphyry intrusions penetrated sediments, particularly limestones during the Laramide Orogeny (RGA).

FIGURE 8.25. Porphyry copper deposits in the Americas define a remarkable metallogenic province that parallels the western continental boundary. Another belt of porphyry copper deposits is being exposed and developed in the Pacific Islands. (From Skinner, 1986.)

Fig. 1 (from RE)

Planetary comparison:
Ordinary chondrites contain 85-94 ppm of copper, while enstatite chondrites contain 120-215 ppm of copper (PSC). Some OC's have metallic copper grains. The only published interpretation of metallic copper is that it is produced by shock (Rubin). Shock events (impacts on asteroids) cause injection of iron metal and sulfide melt along fractures (PM).

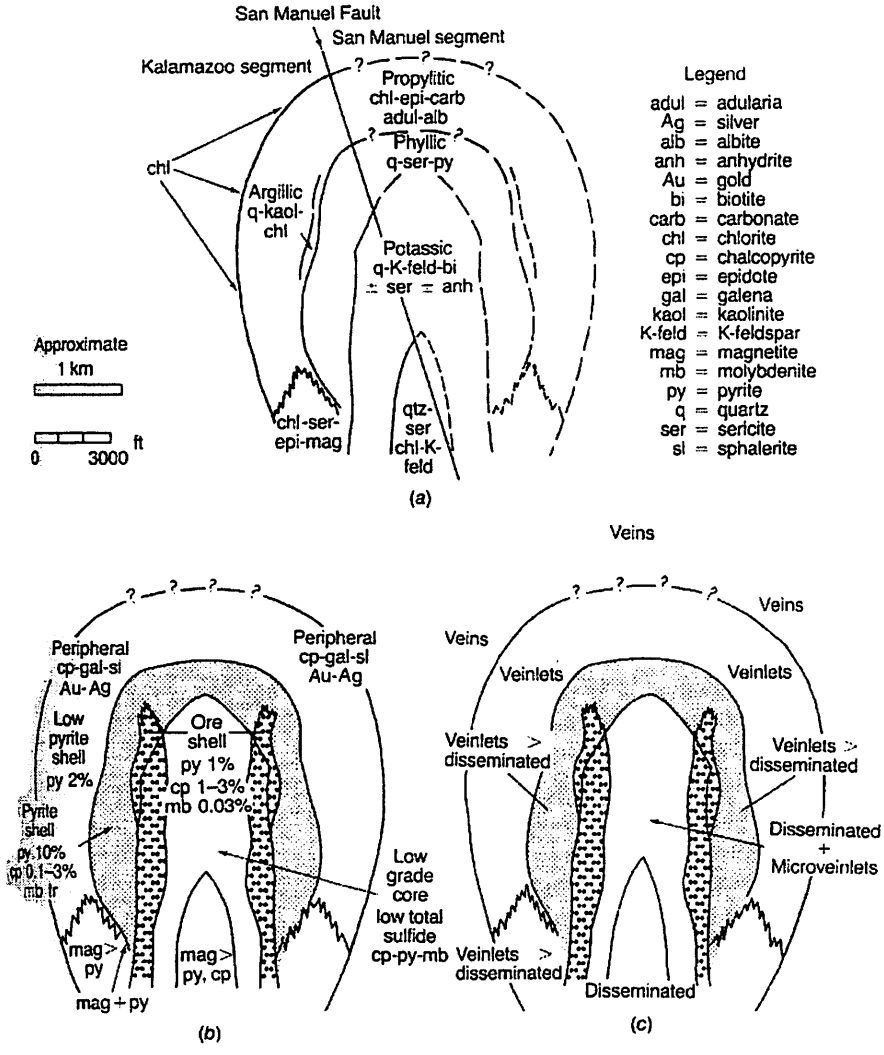

Figure 11-4. Schematic of concentric alteration-mineralization zones at San Manuel–Kalamazoo. (*a*) Alteration zones. Broken lines on the Kalamazoo side indicate uncertain continuity or location, and on the San Manuel side extrapolation from Kalamazoo. (*b*) Mineralization zones. (*c*) Occurrence of sulfides.

Fig. 2 (from OD)

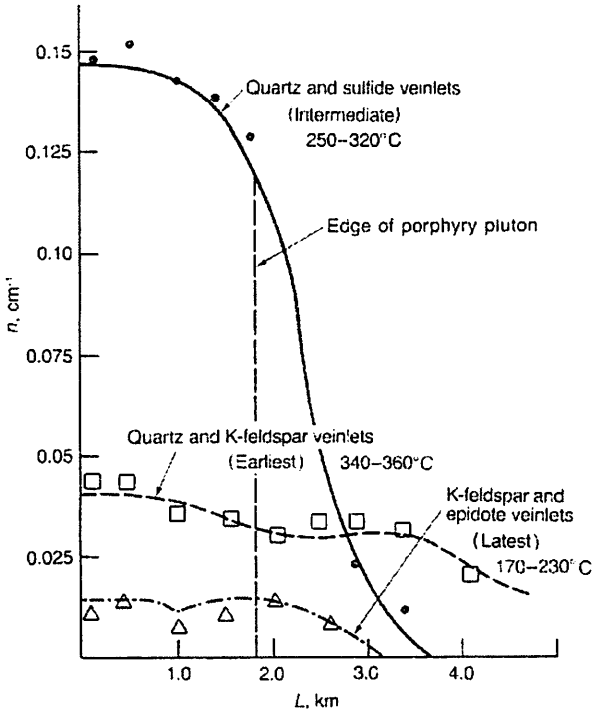

Figure 11-7. Diagram relating fracture-veinlet abundance n (centimeters of length of each type per square centimeter) to distance L from the center of the Sierrita porphyry system by earliest to latest veinlet type. The temperatures determined from fluid inclusion filling temperatures for each assemblage are high, then falling. (*After* Haynes and Titley, 1980.)

413

Fig. 3 (from OD)

Reference:

Mitchell A. H. G. and Carlile J.C. (1994) Mineralization, antiforms and crustal extension in andesitic arcs. *Geol. Mag.* **131** (2) pp. 231-242.

OD = Guilbert J.M and Park C.F. (1986) *The Geology of Ore Deposits.*

PM = Brearley A. J. and Jones R. H. (1998) Chondritic Meteorites in *Planetary Materials, Reviews in Mineralogy* **36**

PSC = Lodders, K. and Fegley B. (1998) *Planetary Scientist's Companion.*

RE = Craig J.R., Vaughan D. J. and Skinner B.J. (1996) *Resources of the Earth.*

RGA = Chronic, Halka (1983) *Roadside Geology of Arizona.*

Rubin, A.E. (1990) Metallic copper in ordinary chondrites. *Meteoritics*

Tectonics of the Safford Region

By: John Weirich

Basin and Range:

Safford is located in a region known as the Southern Basin and Range. This system was created because subduction along the West Coast created relative motion between the Pacific and North American Plates that could not be fully compensated by the San Andreas strike-slip fault. Thus a "void" was created and stresses on the crust caused the American West to expand and fill in the gap. An example of this process is found in Figure 1. At time 0 the upper crust begins to extend, this extension creates stresses which break the upper crust creating further faulting, shown at 8 Ma. During this time, erosional processes fill in the lower topographic portions, creating sedimentary layers which will eventually form the basin. As further extension occurs, the pressure release caused by the extension will create a rebound of the lower crust which will form a core-complex range.

Safford Region:

Seismic studies by Kruger (1991) suggest the Basin and Range extension does not fully explain the Safford region (Fig 3), though it does have a very similar history. Prior to the Basin and Range extension, mid-tertiary extension had already established the northwest-trending structural framework. By the time the Basin and Range extension began, the Pinaleno Mountain core complex had already begun to form. The Basin and Range extension had the result of widening the initial basin east of the Pinaleno Mountains core complex. As the complex continued to rise, the basin continued to widen and fill. This sequence of events can be seen in Fig 2, and the initial (pre-detachment) and final states of the region can be seen in Fig 4.

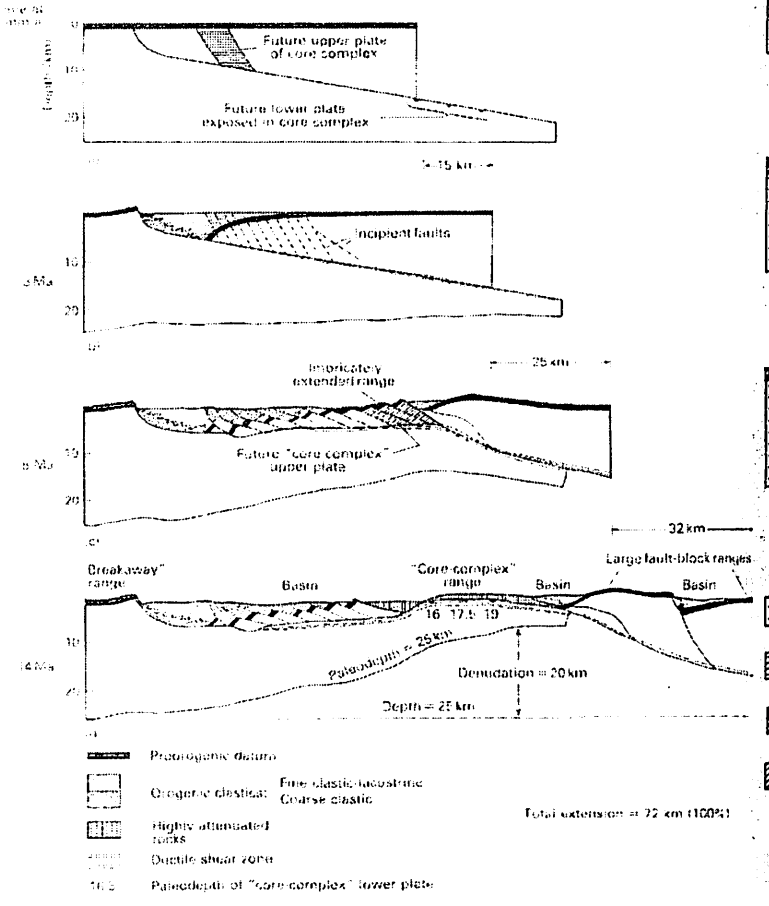

Fig. 11.39. Model of core extensional simple shear system in the upper and middle continental crust (redrawn from Wernicke, [illegible], with permission from the National Research Council of Canada).

Fig 1. Model Basin and Range formation

(Kearey et al., 1990)

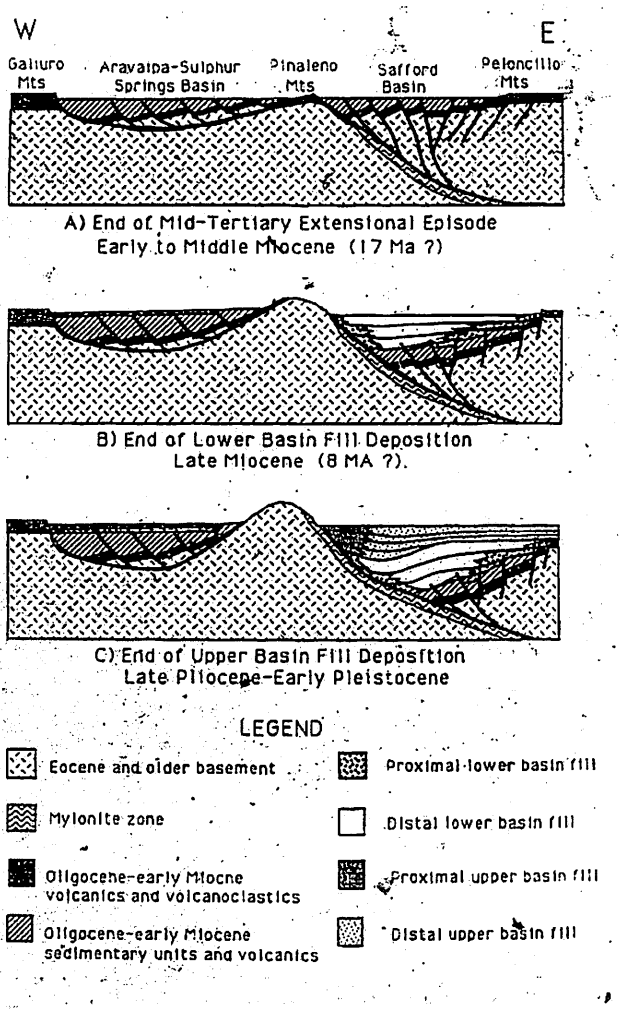

Fig 2. Proposed formation of the Safford Basin

(Kruger, 1991)

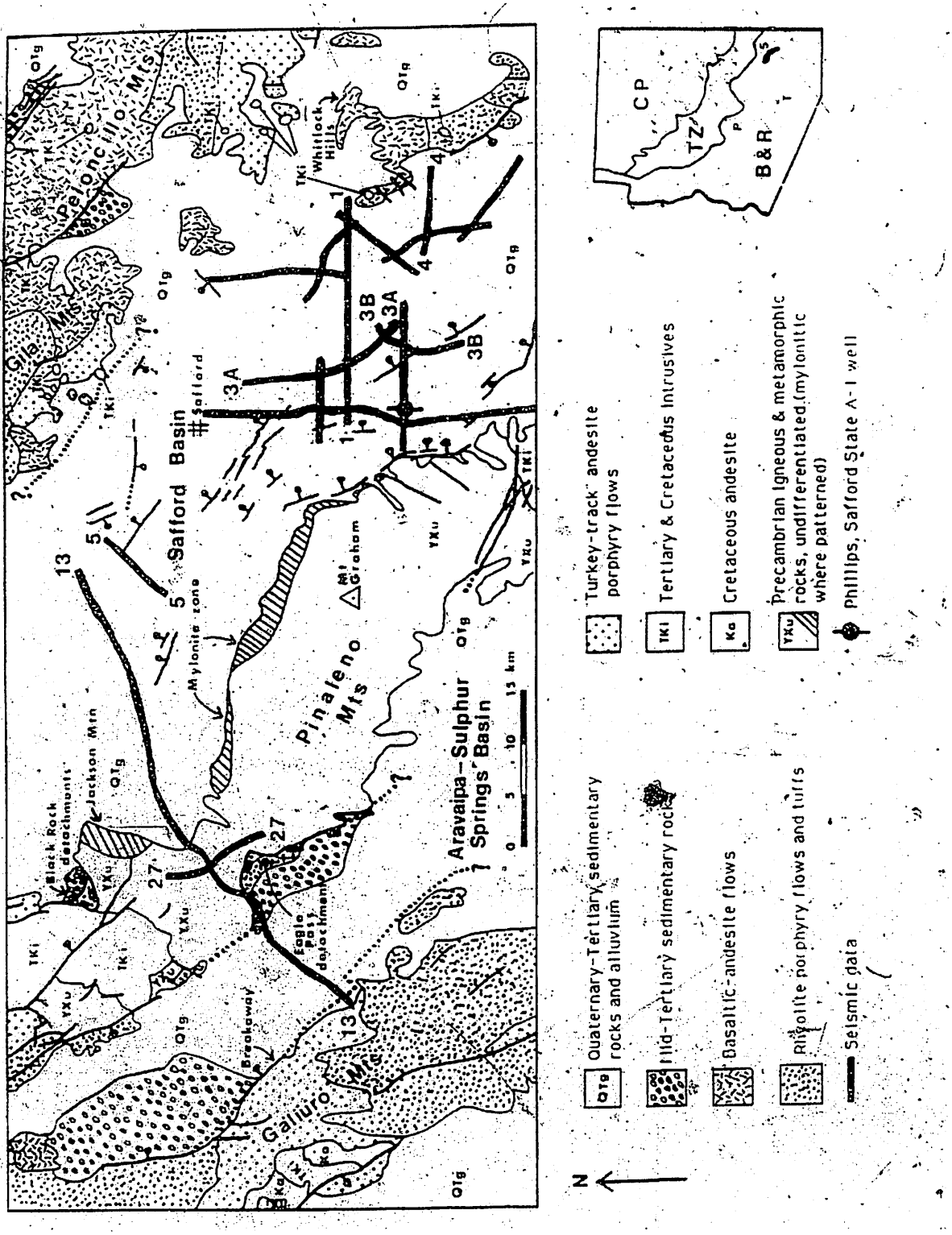

Fig 3. Safford regional context (Kruger, 1991)

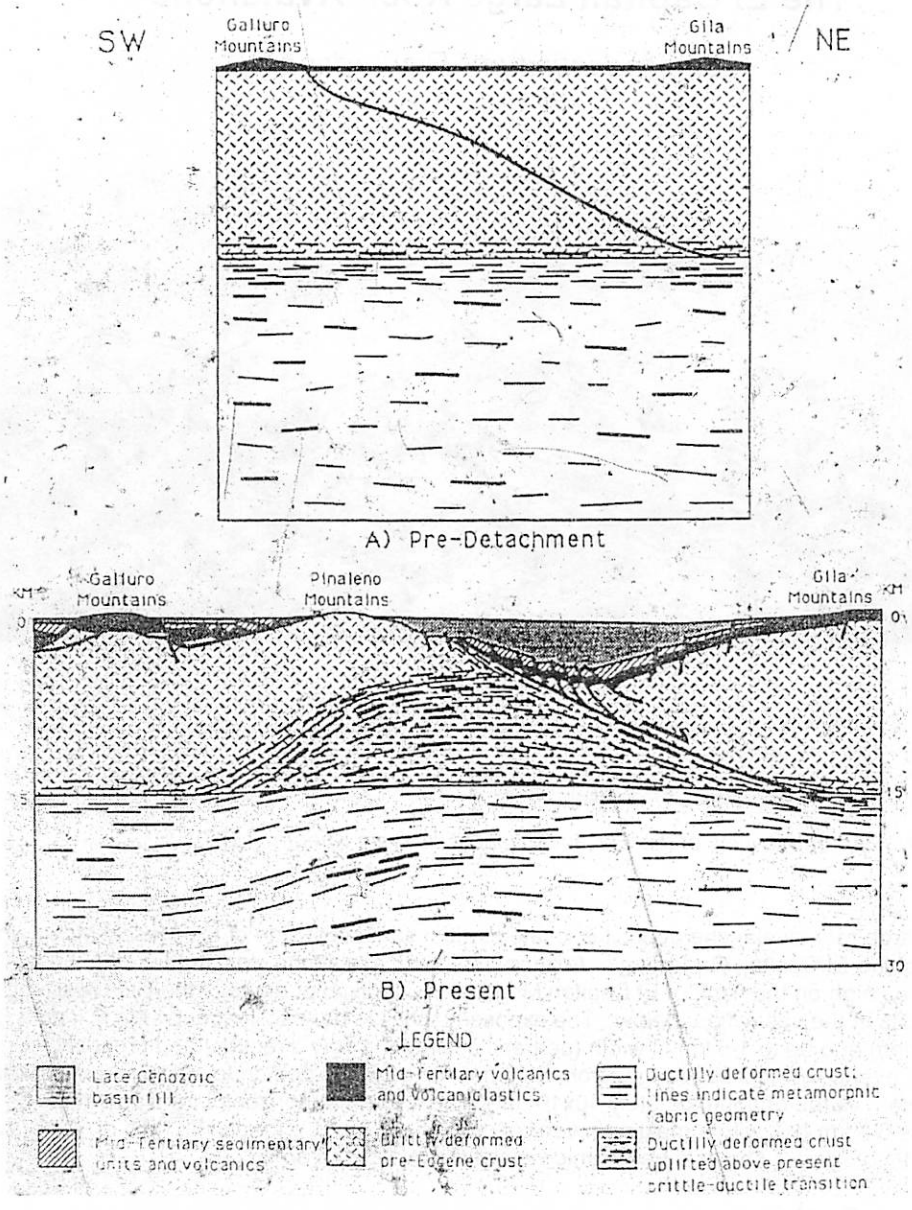

Fig 4. a) Pre-Detachment and b) Present structure of the Safford Region.

The El Capitan Large Rock-Avalanche

Jim "ad infinitum" Richardson

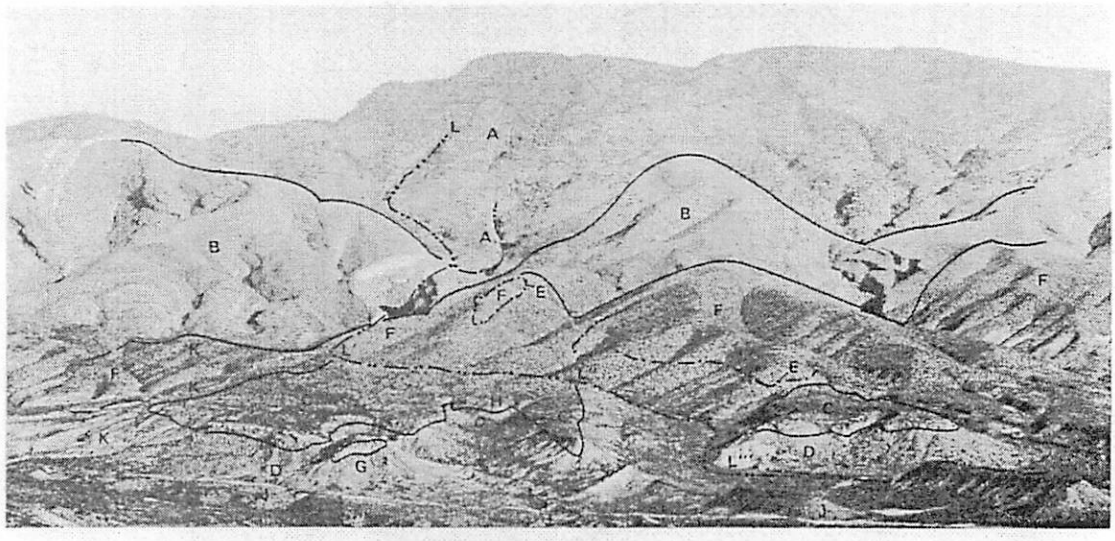

FIGURE 16.—Panorama of El Capitan landslide from Tam O'Shanter Peak (pl. 1), about 6.5 km southwest of south end of slide. Source area high on El Capitan Mountain is underlain by Troy Quartzite (A) and has been stripped of its cover of Paleozoic formations (B) (see fig. 27) by landslide and subsequent erosion. Southern part of landslide (C) rests on lakebeds (D); upper part (E) is interbedded with conglomerate (F); G is hill around which figures 18, 21, 23–26 were taken; H is location of figure 22; I is location of figures 19 and 20; J is State Highway 77; K is jeep road. Main gulch (*L–L'''*) is concealed by canyon rim where it dissects landslide from northwest to southeast (*L'–L''*).

Figure 1: *Panoramic view of the El Capitan landslide (from Krieger, 1977).*

Introduction

The El Capitan large rock-avalanche deposit is located on the southwest side of the Mescal Mountains in the eastern portion of the El Capitan Quadrangle, Arizona. The rock avalanche was shed during the late Tertiary from a source area high on the flank of El Capitan Mountain, with distal portions of the slide reaching the playa-lake deposits in the valley floor below. The exposed landslide deposit is about 4 km in length (parallel to the flow direction) and up to 1.5 km in width (perpendicular to the flow direction) and probably represents a single avalanche event. It thickness ranges from 5-10 m in its proximal portion to 10-35 m in its distal portion, with a total volume of approximately 40×10^6 m^3. The maximum horizontal transport distance of the rock avalanche is 6.8 km (H), with a maximum vertical drop of 1.3 km (L), for an H/L ratio of 0.19 (average travel slope of 11°). *Figure 1* shows a panoramic view of the avalanche area.

El Capitan Area Geology

The core of the Mescal Mountains is the Diabase and Apache Group, overlain by a Precambrian Troy Quartzsite which is extensively exposed in the upper portions of the range. Overlying these are a series of dipping limestone formations (dips of up to 20° to the southwest) consisting of a couple of thin Cambrian deposits (Bolsa and Abrigo formations), and thicker Paleozoic limestone deposits (Devonian Martin and Mississippian Escabrosa formations). At lower elevations, several layers of Tertiary aged deposits overly these bedrocks, consisting of alluviums on the lower flanks of the mountains and playa-lakebed deposits in the basin itself. See *Figure 2* for a simplified geological map of the area.

Avalanche Deposit Dating and Placement

The landslide is estimated to have occurred sometime between the late Miocene and late Pliocene periods (about 2-10 million years ago), during a time when the region was arid to semi-arid. The slide block originated in an amphitheater shaped source area high on the southwest flank of El Capitan Mountain, and consisted primarily of the highly dipping Martin and Escabrosa limestone formations. Relic stratigraphy is

preserved in most of the landslide lobe, with breccias derived from these two limestone types. The thickness of these breccia units are highly variable, but are significantly less than the formations from which they were derived.

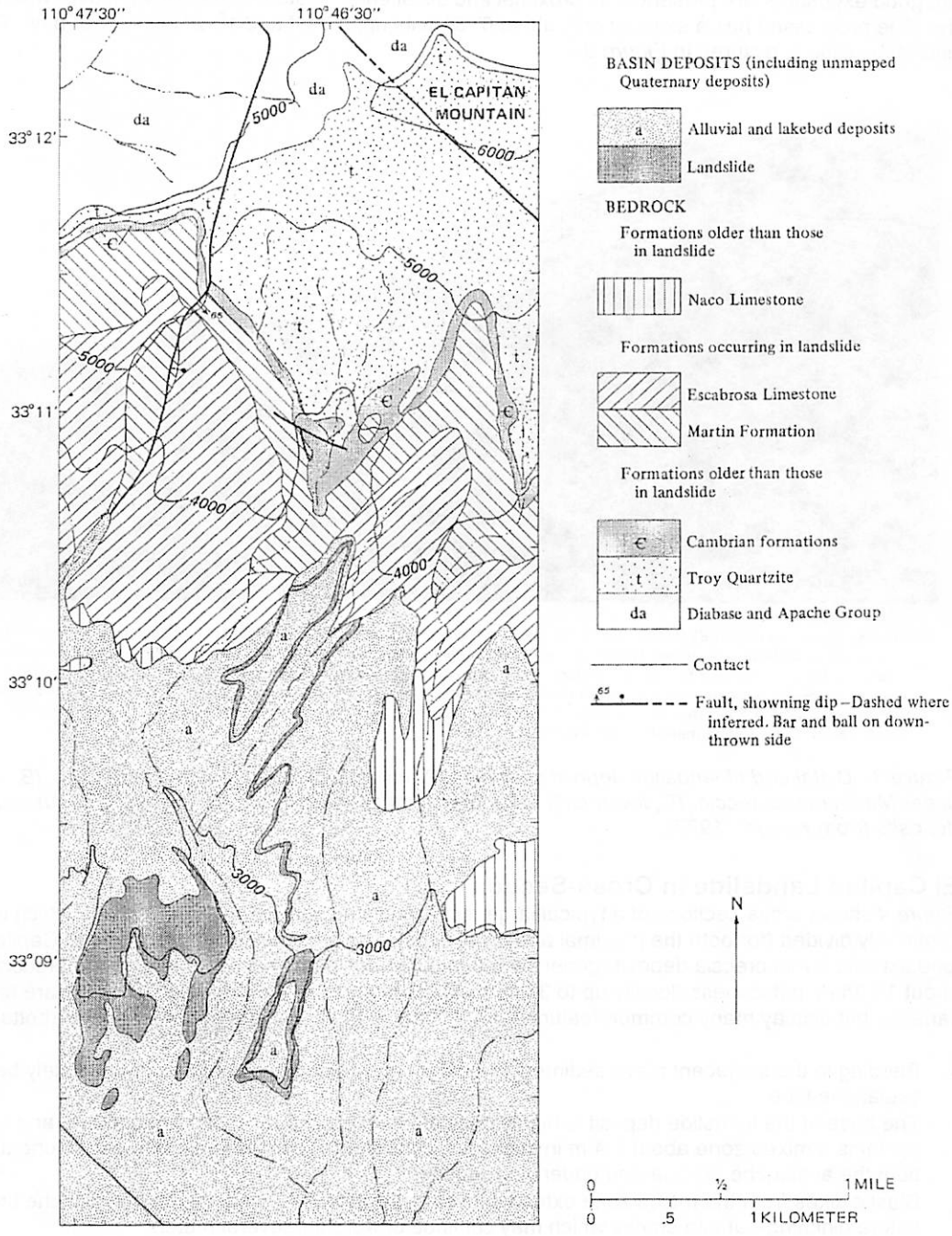

FIGURE 27.—El Capitan landslide and its source area on El Capitan Mountain. Reduced from geologic map of El Capitan Mountain quadrangle (Cornwall and Krieger, 1977).

Figure 2: *Simplified geological map of the El Capitan landslide area (from Krieger, 1977).*

The avalanche deposit straddles several lithofacies in the underlying Tertiary aged sediments: its proximal portion is interbedded with rounded limestone-cobble conglomerates derived from the Mescal Mountains to the north while its distal portion overlies calcareous mudstones and fine-grained sandstones deposited in a playa-lake setting. Much of the medial portions of the avalanche lobe have since been removed by erosion, but good exposures are present in its proximal and distal ends. Note that the alluvium over which most of the slide progressed has a slope of only about 6°-8° in its upper half and 1° -2° in its lower half. The distal end of the slide is pictured in *Figure 3*.

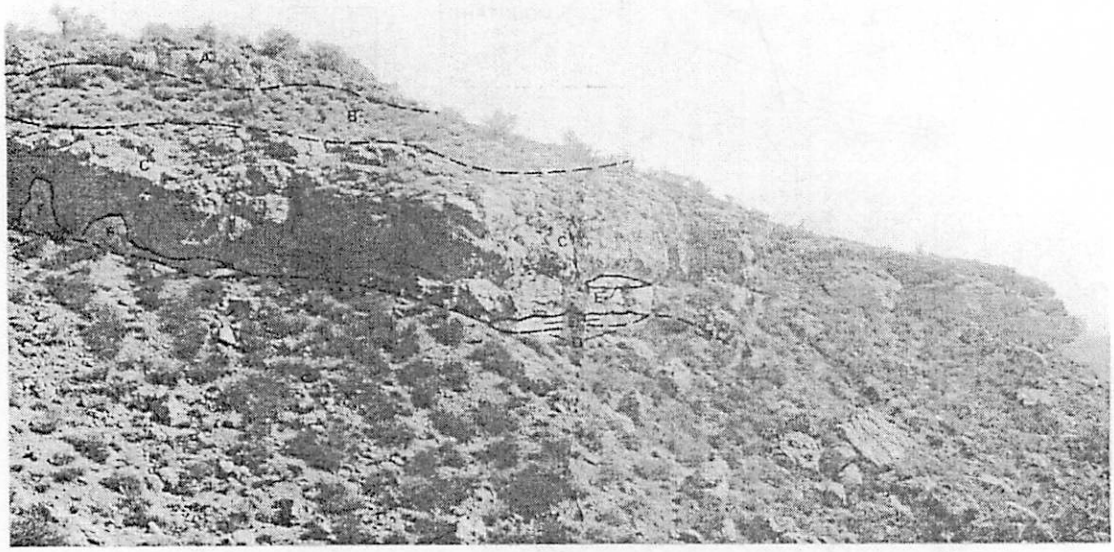

FIGURE 18.—Southern part of El Capitan landslide, showing typical exposures of formations composing landslide. Escabrosa megabreccia (A) at top is underlain by upper Martin megabreccia (B, slope) and lower Martin megabreccia (C, lower cliff). Southernmost tip (right) is keel shaped (see fig. 23). In center, contact with lakebeds (D) is nearly horizontal. Light areas (E) in and near base of breccia are gougelike zones (see fig. 21). To the left contact dips steeply east (light areas are sandstone dikes, F) and beyond picture contact rises so that Escabrosa breccia rests on lakebeds. West side of southernmost isolated mass, east of center of west edge of sec. 26, T. 3 S., R. 15 E. Approximate distance across picture is 100 m.

Figure 3: *Distal end of landslide deposit showing: (A, upper cliff) Escabrosa megabreccia, (B, upper slope) upper Martin megabreccia, (C, lower cliff) lower Martin megabreccia, and (D, lower slope) substrate lakebed deposits (from Krieger, 1977).*

El Capitan Landslide in Cross-Section

Figure 4 shows cross-sections of a typical large rock-avalanche, indicating the zones into which these are commonly divided (for both the proximal and distal ends). The proximal two-thirds of the El Capitan landslide lobe exhibits a thin breccia deposit (generally 5-8 m thick), while the distal one-third of the breccia deposit is about 10-15 m in thickness (locally up to 35 m thick). Exposures of the dissected landslide are rather variable, but display many common features. An outcrop at the distal end generally shows (bottom to top):

- Bedding in the subjacent playa sediment is locally highly folded and contorted immediately below the avalanche lobe,
- The base of the landslide deposit is highly undulatory, exhibiting relief of 10 m or more, and locally contains a mixed zone about 1-4 m in thickness, consisting of conglomeritic silty sandstone derived from both the avalanche breccia and underlying sediment,
- Clastic dikes from the mixed zone extend subvertically up to 3-4 m into the rock-avalanche breccia sheet before pinching-out into cracks which may continue upward for several meters,
- Above the mixed zone, a basal interval up to 6 m thick is dominated by matrix-rich breccia derived from the Martin formation and, more rarely, Escabrosa limestone,
- Subhorizontal comminuted slip surfaces are common in the disturbed zone, with layers of gouge up to 10 cm thick,

- The matrix-rich interval grades upward into a zone dominated by jigsaw and crackle breccia facies in which relic beds are traceable for many meters. This upper matrix-pore zone contains debris derived from the Escabrosa limestone and, secondarily, the Martin formation. In places it is capped by a concentration of large, relatively coherent avalanche blocks. See *Figure 5* for a close view.

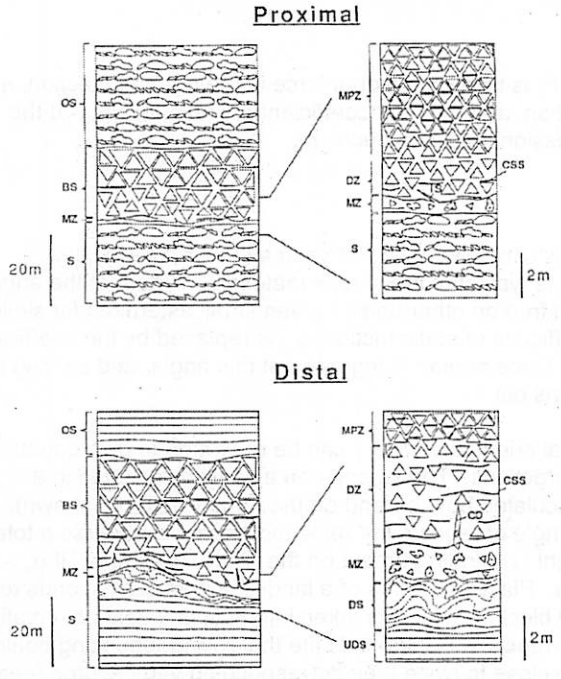

Figure 15. Characteristic features within proximal and distal portions of large rock-avalanche deposits investigated, showing: substrate (S); undisturbed substrate (UDS); disturbed substrate (DS); mixed zone of entrained substrate and comminuted breccia (MZ); disturbed zone (DZ) of the breccia sheet (BS) that displays comminuted slip surfaces (CSS), and is intruded by clastic dikes (CD) and intrusive stringers (IS; load structures and poorly-developed clastic dikes) derived from the mixed zone; matrix-poor zone (MPZ) of the breccia sheet; and overlying sediments (OS). In places, a discontinuous megabreccia cap occurs along the top of the breccia sheet.

Figure 4: *typical landslide cross-sections (from Yarnold, 1989).*

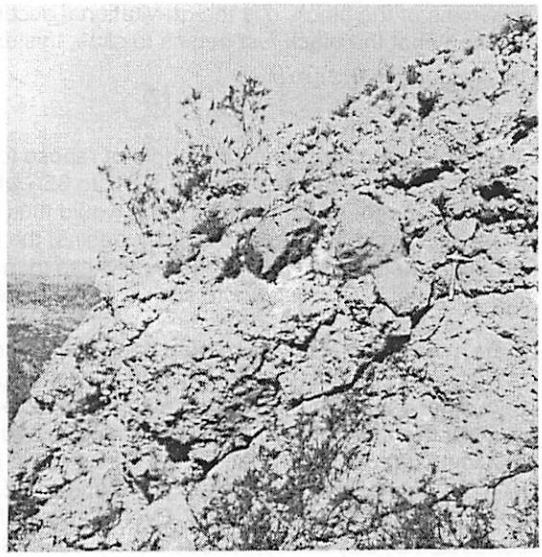

FIGURE 19.—Escabrosa megabreccia, southern part, just west of line between secs. 26 and 27, T. 3 S., R. 15E. Note wide variation in size of clasts.

Figure 5: *close-up view of Escabrosa megabreccia (from Krieger, 1977)*

Landslide Mechanics in Brief

Following this look at the landslide's geology, a ***brief*** discussion of landslide mechanics follows in order to give a basic picture of how these events occur (and the controversy surrounding their explanation). While a thorough discussion of landslide mechanics should properly include such things as the Coulomb failure of the slide block itself or pore pressure effects due to interstitial fluids, a simple understanding can be gained by first considering the simple Newtonian mechanics "block on a wedge" problem pictured in *Figure 6*, and then developing this picture a little further for a layer of rock material.

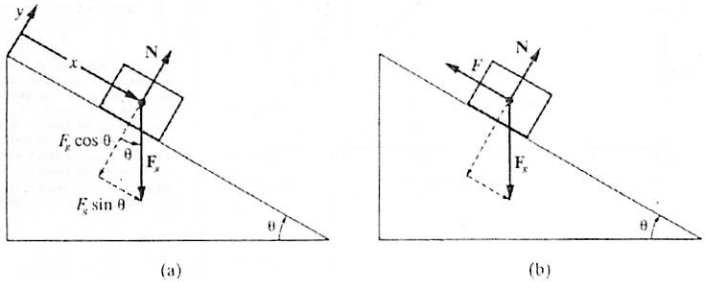

Figure 6: *Ye Olde Blocke on a Wedge force balance diagram (from Marion and Thornton, 1995)*

The force balance in the *x*-direction on a block of rock resting on a larger wedge having an upper surface at angle θ with the horizontal is given by:

$$F = F_s - \mu_s F_n$$

$$F_s = mg\sin\theta \qquad (1)$$

$$F_n = mg\cos\theta$$

where F_s is the shear force in the downhill direction, F_n is the gravitational force in the normal direction, m is the mass of the block, g is the gravitational acceleration, and μ_s is the coefficient of static friction. At the moment that the block *just* begins to slide, this expression quickly reduces to:

$$\mu_s mg\cos\theta = mg\sin\theta$$

$$\mu_s = \tan\theta_r \qquad (2)$$

in which θ_r roughly defines the angle of repose for this simple model. For values of μ_s = 0.6-0.7, this corresponds to angles of repose of 31° to 35°, which is typical of many rock materials. Note that the angle of repose is independent of gravity and would thus hold true on other bodies (even small asteroids) for similar materials. Once motion of the block begins, the coefficient of static friction, μ_s, is replaced by the coefficient of kinetic friction, μ_k, which is generally less than μ_s. Once motion is triggered at this angle, and as long as $\mu_s > \mu_k$, the block will continue to slide until the slope runs out.

If the axes in *Figure 6* are rotated back to their normal orientation, *Eq. 1* can be re-written to give equations of motion in both the vertical (*y*) and horizontal (*x*) directions. The wedge can also be terminated in a horizontal plane, and the path-length of the block calculated both on and off the ramp (math not shown). In general it is found that, beginning on a ramp at the angle of repose, the released block will traverse a total horizontal (*x*) distance of about twice its starting height (*y*), ending up out on the plane. Example: if μ_s = 0.6, μ_k = 0.4, y_o = a, and x_o = 0, then y_f = 0 and x_f = 2.27a. Placed in terms of a landslide, this corresponds to H/L ratios in the range of 0.6 to 0.4. Even if rolling of the block (boulder) is taken into account, field observations conducted by Jay Melosh at Strawberry Cone (San Francisco Peaks) indicate that rolling, bouncing boulders still tend to wind up at horizontal distances which are close to twice their corresponding vertical drop (near angle-of-repose travel slopes).

While this gravity and friction driven model seems to work relatively well for individual boulders and small volume landslides, it *does not* work very well for large, and especially, very large landslides. The El Capitan rock-avalanche has an H/L ratio of 0.19, and is fairly typical for landslides of its size. Recall that the Mount St. Helens rock-avalanche (one of the largest on record) has an H/L ratio of 0.09. H/L ratios can be shown to be a function of landslide size, and this is illustrated in *Figure 7* (for both terrestrial and martian landslides). Obviously, some alternative explanation is order, and the geological literature is certainly not lacking in them!

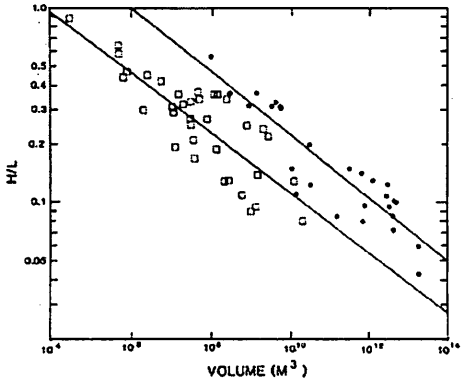

Figure 1. Plot of *H/L* (height of drop/length of runout) vs. landslide volume. Circles are data points from Valles Marineris (from Table 1); squares are terrestrial data points for dry-rock avalanches of nonvolcanic origin (Scheidegger, 1973; Hsü, 1975). Lines are linear least-squares fits to each data set.

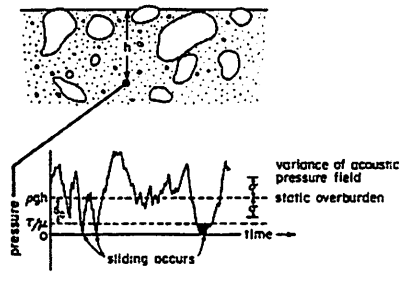

Fig. 1. Schematic diagram of the pressure variations as a function of time (lower graph) at depth h in a mass of rock debris (upper sketch). Shown on the pressure graph is the static overburden ρgh about which the pressure fluctuates randomly with variance σ. Sliding occurs when the pressure falls to within τ/μ of zero (τ is the applied shear stress and μ is the coefficient of friction). Here s_z is the pressure deviation from the mean when sliding occurs. Although the pressure in a mass of rock debris can never actually be less than zero, the linear elastic model described in the paper occasionally allows this to occur. This defect is removed in the nonlinear model described in the appendix.

***Figure 7:** H/L vs. Volume for various terrestrial and martian landslides (from McEwen, 1989)*

***Figure 8:** Illustration of sliding excursions during acoustic fluidization (from Melosh, 1979).*

Developing the simple friction model further, *Eq. 1* can be expanded to involve a layer of rock of thickness *h* resting on the surface of the wedge. This will give:

$$F = \iota - \mu P$$

$$\iota = \rho g h \tan\theta \qquad (3)$$

$$P = \rho g h$$

where ι is the shear stress at the bottom of the layer and *P* is the normal component of the overburden pressure. Again looking at the point where sliding just begins:

$$\frac{\iota}{\mu} \geq P \qquad (4)$$

This implies two ways in which the sliding of the rocky layer (slide block) can be extended once an event is triggered and an initially high slope runs out (with a corresponding reduction in the shear stress): (1) lower the coefficient of friction, or (2) reduce the overburden pressure (lowering the viscosity of the layer is included in this second form).

Proposed slide mechanisms which reduce the coefficient of friction (i.e. *lubricate* the slide):

- Movement over a molten basal layer, melted by friction and high pressure (Erismann, 1979)
- Segregation of water into a saturated basal layer (Johnson 1978)
- Vaporization of water to partially fluidize the mass or lubricate the base (Habib, 1975, Goguel, 1978)
- Frictionless support on a layer of trapped and compressed air (Shreve, 1966, 1968)

Proposed slide mechanisms which reduce the overburden pressure or fluidize the slide particles:

- Fluidization by air (Kent, 1966)
- Grain flow with friction reduced by the presence of dust (Hsu, 1975).
- Inertial grain flow or mechanical fluidization (Davis, 1982).
- Effective fluidization by seismic energy (Melosh, 1979, 1987).

Many of these mechanisms are not supported by landslide deposit observations in the field (for example, the lack of melt sheets associated with landslides), or do not take into account the presence of long-runout landslides on such diverse (and airless) planetary bodies as our Moon, Mars, and Phobos. One of the more misunderstood, but more promising explanations is the effective fluidization of the slide zone due to high-frequency seismic energy produced by the slide itself (called "acoustic fluidization"). In order to illustrate the basic premise of this mechanism, we add a final component to *Eq. 4:*

$$\frac{\iota}{\mu} \geq P - s \qquad (5)$$

where *s* is the amplitude of the seismic waves, which cause excursions above and below the overburden pressure at the point at depth *h*. Occasionally, these excursions are large enough to cause the condition in *Eq. 5* to be met (relieving the overburden pressure, *P*) and sliding of the rock layer can momentary occur. This is illustrated in *Figure 8*.

At high seismic frequencies (about 2-20 kHz) these sliding excursions can occur frequently enough to cause an effective lowering of the viscosity of the rock layer at depth *h*, hence the term "acoustic fluidization." As long as the seismic energy density in this layer (at depth) can be maintained, the sliding process can continue. Note that in this mechanism, the stratigraphy of the layer can be preserved as it moves, with surface/slide interactions creating the observed mixed and disturbed regions. Finally, it should be mentioned that acoustic fluidization is applicable not only to landslides, but also to the process of large crater collapse and motion along earthquake faults.

References

Krieger, M.H. (1977). Large landslides, composed of megabreccia, interbedded in Miocene basin deposits, southeastern Arizona. *Geological Survey Professional Paper 1008*, USGS.

Marion, J.B. & Thornton, S.T. (1995). *Classical Dynamics of Particles and Systems*. Orlando: Harcourt Brace and Co.

McEwen, A.S. (1989). Mobility of large rock avalanches: Evidence from Valles Marineris, Mars. *Geology*, **17**, 1111-1114.

Melosh, H.J. (1979). Acoustic fluidization: A new geological process?: *Journal of Geophysical Research*, **84**, 7513-7520.

Yarnold, J.C. & Lombard, J.P. (1989). A facies model for large rock-avalanche deposits formed in dry climates, *in* Colburn, I.P., Abbott, P.L., and Minch, J. (eds.), *Conglomerates in basin analysis: A symposium dedicated to A.O. Woodford*, Pacific Section of the Society of Economic Paleontologists and Mineralogists, **62**, 9-31.

San Pedro Valley Cenozoic Fossils

1. Introduction

Vertebrate fossils were discovered and unearthed in San Pedro Valley in the winter of 1920 and 1921 by Kirk Bryan and G.E.P Smith of the U.S. Geologic Survey.[1,3] Follow-up excavation was performed by James W. Gidley and published in a second report in 1926.[2] This handout's figures are taken from the Gidley reports, which contain fossils from two sites at the other end of the San Pedro Valley southeast of Tucson. Other sites have been found since the original find reported in Gidley (1922). The current site is listed as the "diatomite beds," which I describe below.

2. Locations

Fossils originating from several periods in geologic history have been unearthed in the San Pedro Valley. The original locations discovered by Kirk Bryan include a small area of badlands about 3 miles east of the Curtis ranch and a site about 2 miles south of Benson. The bulk of the material excavated by Gidley came from the first site, but fewer species are represented in the fossils of the first group than the second group. The fossils of the first location are Irvington Land Mammal Age; from the Benson site, the ages are Early Blancan. More recently, several other sites have been found featuring fossils from different geologic eras than the fauna collected by Gidley. Harrison (1972) analyzed the fauna of the St. David Formation, which are intermediate in age between the fauna of the Gidley site, the era known as Late Blancan. Harrison (1972) reported 23 mammalian taxa included in the Wolf Ranch local fauna; she makes no attempt to study the non-mammalian fossils of the St. David Formation site.

3. Fauna Forms

I show in Figure 1 the fossil vertebrate groups represented in the original Gidley (1922) sample. This sample included 23 mammal species, 8 species of birds, and 3 reptile species. Reconstructions of the reptiles found in the sample were reported in Gidley (1926) and are shown in Figure 3.

Harrison analyzed the mammalian fauna of the St. David Formation site and identified 23 species of mammals at the site.

More recent analyses of the fauna (Lammers 1970) suggest that the Benson faunas are of the late Pliocene and early Pleistocene. The Curtis ranch fauna are believed to be middle Pleistocene.

4. Diatomite Beds

This location is characterized by diatomized beds. Diatomite consists of the skeletal remains of single-cell aquatic plants known as diatoms. Figure 4 shows a few. A good description of them is given in the Mineral Information Institude website:

"A diatom is an organism that is a member of the phylum of algae called Bacillariophyta. There are about 60,000 species of these algae presently known. Experts estimate that there are more likely 600,000 to 6,000,000 species in total. Diatoms are single-celled (unicellular) organisms that live as individuals or in groups called colonies. They exist in all the waters of the Earth, both salt and fresh. They form shells made out of silica (the mineral name of this silica is opal, which they extract from the water. As can be seen in these pictures, their microscopic shells are very intricate and beautiful and have rightly been called 'the jewels of the sea.' Diatoms are very abundant and provide food for many aquatic animals. When diatoms die, their silica shells accumulate on the floor of the water in which they lived. Thick layers of these diatom shells have been fossilized (preserved) in the rock record. Such layers, or beds, of diatoms are called diatomaceous earth, or diatomite. Diatomaceous earth is white to cream color. It is very porous which makes it useful in a number of filtering applications."[6]

5. References

[1] James W. Gidley (1922), "Preliminary Report on Fossil Vertebrates of the San Pedro Valley, Arizona," *U.S. Geological Survey, Professional Paper* 131-E, USGS/Dept. Interior, Washington, D.C. p. 119-31.

[2] James W. Gidley (1926), "Fossil Proboscidea and Edentata of the San Pedro Valley, Arizona", *U.S. Geological Survey, Professional Paper* 140, USGS/Dept. Interior, Washington, D.C. p. 83-94.

[3] Jessica Anne Harrison (1972), "The Mammals of the Wolf Ranch Local Fauna St. David Formation, Cochise County, Arizona", Master's Thesis, *Department of Geosciences, Graduate College, The University of Arizona.*

[4] Robert Stephen Gray (1965), "Late Cenozoic Sediments in the San Pedro Valley Near St. David, Arizona," Ph. D. Dissertation, *Department of Geology, Graduate College, The University of Arizona.*

[5] George Eber Lammers (1970), "The Late Cenozoic Benson & Curtis Ranch Faunas from the San Pedro Valley, Cochise County, Arizona," Ph. D. Dissertation, *Department of Biology, Graduate College, The University of Arizona.*

[6] Mineral Information Institute, http://www.mii.org/Minerals/photodiatom.html

Figure 1: San Pedro Valley Major Vertebrate Fossil Groups Reported by Gidley (1922)[1]

Preliminary list of fossil vertebrates from the San Pedro Valley, Ariz.

	Number of species.	
	Benson.	Curtis.
MAMMALIA.		
Proboscidia:		
Elephantidae:		
Cf. *Dibelodon*, probably n. sp.		2
Cf. *Gomphotherium*, probably n. sp.	1	
Perisso lactyla:		
Equidae:		
Equus, undet.		2
Pliohippus, undet.	1	
Hipparion, undet.	1	
Artiodactyla:		
Camelidae:		
Lama, n. sp.		1
Cf. *Procamelus*, undet.	1	1
Cf. *Pliauchenia*, undet.	1	1
Tayassuidae:		
Platygonus cf. *P. vetus*, or n. sp.	1	
Cervidae:		
Odocoileus, n. sp.		1
Merycodus near *M. necatus*	1	1
Cf. *Merycodus*, n. sp.		1
Carnivora:		
Canids, 3 n. sp.	1	2
Felid?, n. sp.		1
Mustilid, sp.	1	1
Rodentia:		
Sciuridae:		
Citellus cochisei, n. sp.		1
Citellus bensoni, n. sp.	1	
Geomyidae:		
Geomys parvidens, n. sp.		1
Geomys minor, n. sp.	1	
Cratogeomys bensoni, n. sp.	1	
Heteromyidae:		
Dipodomys minor, n. sp.	1	
Muridae:		
Subfamily Cricetinae:		
Peromyscus brachygnathus, n. sp.	1	
Peromyscus minimus, n. sp.	1	
Peromyscus sp.	1	
Eligmodontia arizonae, n. sp.	1	
Onychomys pedroensis, n. sp.		1
Onychomys bensoni, n. sp.	1	
Sigmodon curtisi, n. sp.		1
Sigmodon minor, n. sp.		1
Sigmodon medius, n. sp.	1	
Subfamily Neotominae:		
Neotoma fossilis, n. sp.	1	
Subfamily Microtcinae:		
Neofiber sp.		1
Lagomorpha:		
Leporidae:		
Lepus, 3 sp., possibly new	2	1
Sylvilagus or *Brachylagus* sp.	1	
Edentata:		
Glyptodontidae:		
Glyptotherium, n. sp.		1
Total Mammalia	23	22
REPTILIA.		
Testudines:		
Testudinidae:		
Testudo, 2 sp. undet.	1	1
Kinosternidae:		
Kinosternon, new sp.	1	1
Batrachia:		
Salientia:		
Ranidae:		
Rana or *Bufo*, not yet determined	1	
Total Reptilia	3	2
AVES.		
Galliformes:		
Odontophoridae:		
Undetermined		1
Colinus sp. undet.	1	
Family undet.	1	
Anseriformes:		
Anatidae:		
Dendrocygna, n. sp.	1	
Branta, n. sp.	1	
Charadriiformes:		
Scolopacidae:		
Micropalama, n. sp.	1	
Family undet., medium-sized form	1	
Columbiformes:		
Family undet. A pigeon somewhat smaller than the domestic dove		1
Passeriformes:		
Fringillidae:		
Small sp., undet.	1	
Other passerines represented by scanty material	1	1
Total Aves	8	3

Figure 2a: Fossils Excavated in 1922 by J.W. Gidley.1

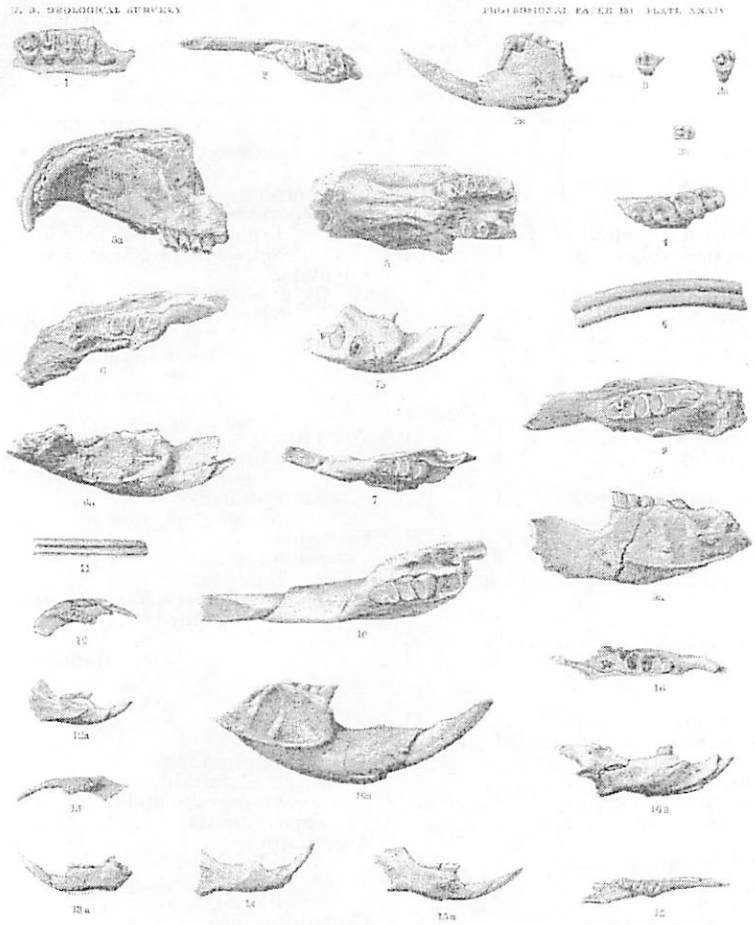

FOSSIL VERTEBRATES OF SAN PEDRO VALLEY, ARIZ.

PLATE XXXIV.

[All figures about twice natural size.]

130

Figure 2b: 2nd Plate from Gidley (1922).[1]

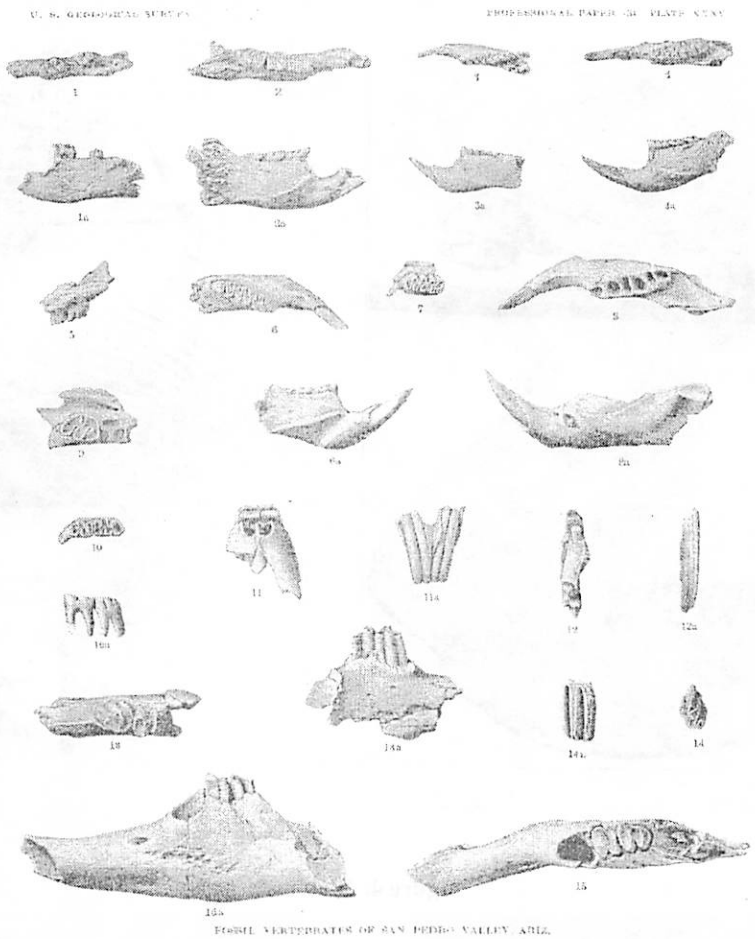

FOSSIL VERTEBRATES OF SAN PEDRO VALLEY, ARIZ.

PLATE XXXV.

[All figures about twice natural size.]

Figure 3: Paleontological Reconstructions from Follow-Up Excavation (Gidley 1926)[1]

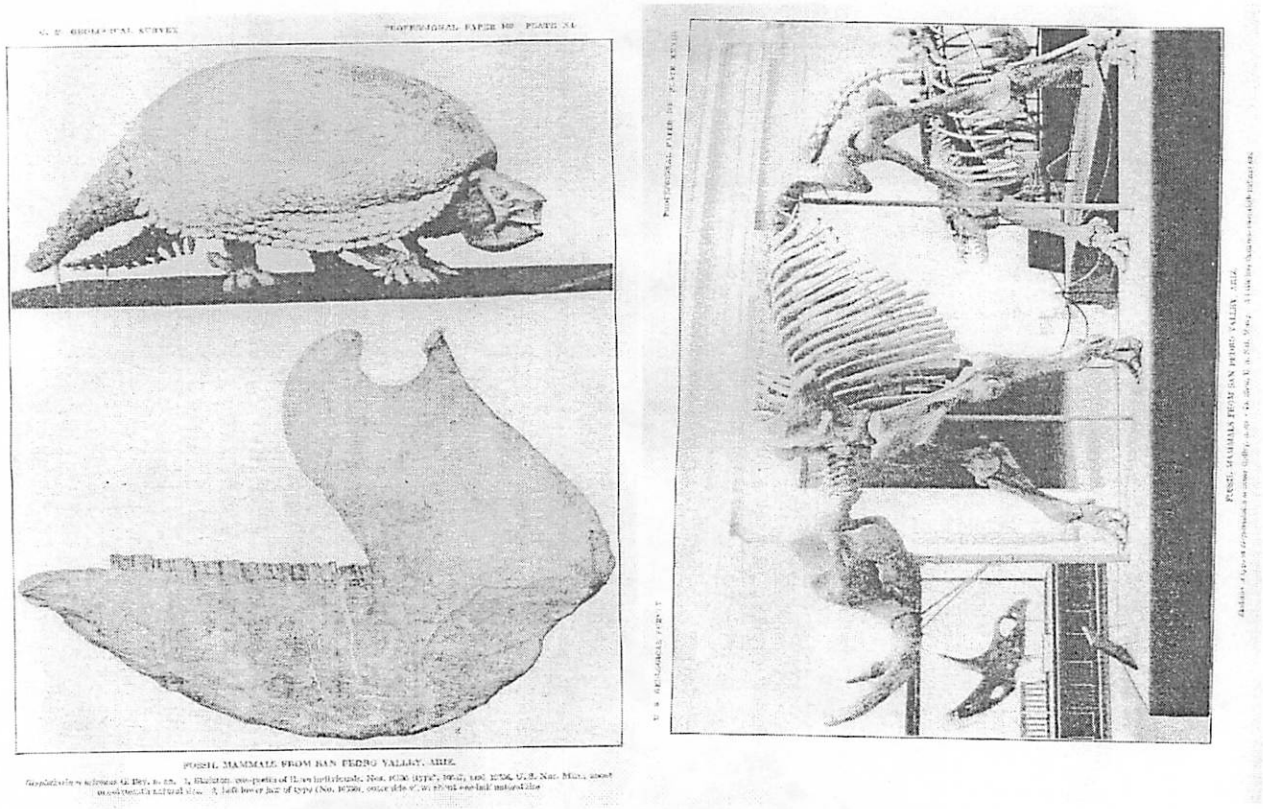

Figure 4: Diatoms[6]